Improvement of optical planar oxygen sensors and application in marine environments

Bettina König

Improvement of optical planar oxygen sensors and application in marine environments

Dissertation
zur Erlangung des Grades eines
Doktors der Naturwissenschaften
- Dr. rer. nat.-

dem Fachbreich 2 (Biologie/Chemie) der
Universität Bremen
vorgelegt von

Bettina König
aus Kronstadt

Mai 2007

Die vorliegende Arbeit wurde in der Zeit von Juni 1998 bis Mai 2007 am Max-Planck-Institut für Marine Mikrobiologie in Bremen angefertigt.

1. Gutachter: Prof. Dr. Bo Barker Jørgensen
2. Gutachter: Prof. Dr. Kai Bischof

Tag des Promotionskolloquiums: 13.07.2007

Table of content

Chapter 1

1. Introduction

1.1. Overview

This thesis deals with the improvement of optical planar sensors and their application in marine biological environments. Chapter one gives the scientific background of this thesis demonstrating also the reason for the scientific interest in the presented measuring principle as well as the experiment results. Chapter two summarizes the first results of two-dimensional optical oxygen measurements at benthic interfaces. Chapter three provides a detailed analysis of the properties of sol-gel based planar oxygen optodes with respect to application in marine sediments. A first set of test results gained by 2D oxygen measurements around worm burrows is presented. Chapter four describes in detail the applied measuring principle with respect to the technical and mathematical aspects. Chapter five presents the results of the study the behavior of *Hediste diversicolor* and the oxygen dynamics around its natural and artificial burrows with planar optodes. A summary of the thesis results is given in chapter six. Finally, chapter seven contains the list of publications.

1.2. The role of oxygen in the degradation process of organic matter

Oxygen is the most important element of the world and mandatory for the existence of higher life forms. The global oxygen cycle is backed by photosynthesis and aerobic organic carbon degradation which is a strong indication of the biological activity of an environment. Coastal marine sediments are a main location for the global oxygen cycling (Jørgensen 1983). From measuring the total benthic oxygen

uptake it is possible to estimate the carbon mineralization (Canfield et al. 1993). For typical benthic systems the ratio between measured O_2 exchange rates and CO_2 exchange ranges from 1.0 to 1.3 (Hammond et al 1996, Roden and Wetzel 1996).

Marine sediments represent a reducing environment covered with a thin oxic layer, only. The thickness of the oxic layer varies from millimeter in coastal areas to centimeter and decimeter in deeper oceanic areas (Reimers et al. 1986, Glud et al. 1994). Oxygen penetration depth in the sediment is controlled by O_2 uptake from the water column and O_2 consumption in the sediment. Molecular diffusion, advection, and bioirrigation dominate the supply of O_2 uptake of the sediment-water interface. In none permeable sediments the diffusive O_2 uptake is controlled by the development of a diffusive boundary layer at the sediment surface (Jørgensen and Revsbech 1985). Oxygen consumption is the result of microbial oxidation of organic matter and reduced inorganic metabolites (Jørgensen 1983). In phototrophic sediments re-oxidation of e.g. H_2S can account for up to 50% of the O_2 consumption and occurs direct (chemical reaction) or indirect via bacteria (e.g. *Beggiatoa* ssp., Jørgensen and Revsbech 1983) or via intermediates (e.g. pyrite, Howarth 1984). In macrofauna predominated sediments fauna respiration and faunal-mediated O_2 uptake dominated the O_2 consumption (Kristensen 1988. Banta et al. 1995, Glud and Wenzhöfer 2004).

1.2.1. Organic matter degradation

The degradation of organic matter can be divided into aerobic and anaerobic processes. In the upper layer of the sediment (oxic zone) O_2 is available and aerobic mineralization of the organic matter takes place whereas in deeper sediment zones anaerobic processes occur. Oxygen is the most favored electron acceptor for microbial respiration (Fenchel et al.1998) and thus its availability has a strong

implication on the degradation rates of organic matter (Kristensen et el. 1995, Fenchel 1996). As far as high oxygen concentrations result in high degradation rates. Only aerobic bacteria are capable of a complete degradation of organic carbon to H_2O and CO_2 according to the following equation:

$$(CH_2O)_x(NH_3)_y(H_3PO_4)_z + xO_2 \rightarrow xCO_2 + yNH_3 + zH_3PO_4 + xH_2O$$

The degradation rates decrease in with sediment depth (Canfield 1994) which has two main reasons. First, anoxic areas provide less efficient electron acceptors compared to oxygen. And anaerobic degradation becomes a stepwise process using a sequence of electron acceptors: Mn^{4+}, NO^{3-}, Fe^{3+}, SO_4^{2-}, and CO_2. The "quality" of the electron acceptors decreases in the given sequence (Figure 1-1) and the reaction process is more difficult and results in less energy output for the organisms. Several groups of bacteria are involved in anaerobic mineralization because no group seem to be able to perform the complete degradation process.

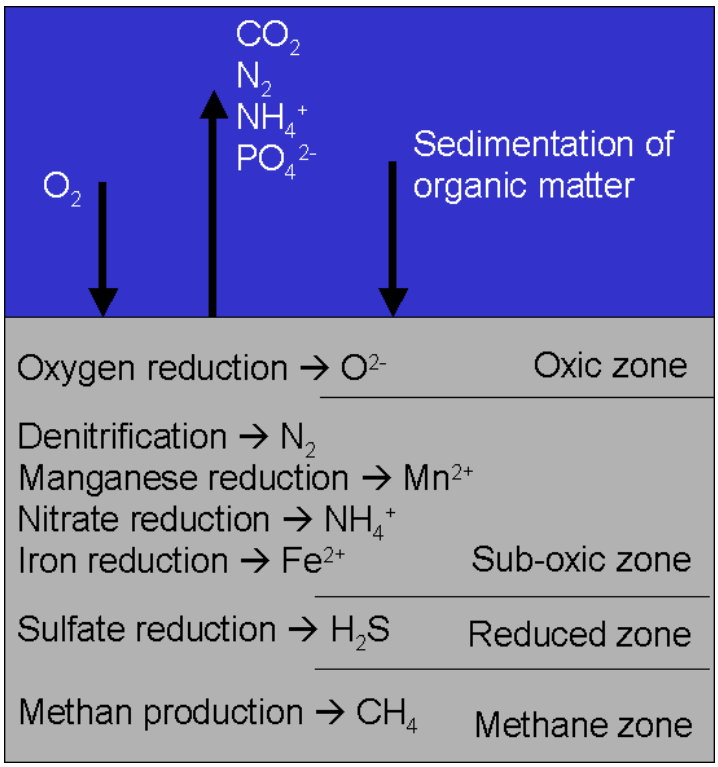

Figure 1-1. Redox cascade with the main electron acceptors relevant for the degradation of organic matter in sediments.

Second, the type of organic matter with respect to its degradability (e.g. lignin is more difficult to degrade) provide low degradation rates.

1.2.2. Impact of environmental conditions

Environmental conditions like temperature, light, and water current dominate to a large extent the rates of aerobic degradation of organic carbon. Additional, the diffusive boundary layer may limit the availability of oxygen at the benthic interface and thus may alter the aerobic degradation process. However, the DBL is also affected by water current and temperature. How this factors affect the mineralization processes at the oxic / anoxic boundary in marine sediments briefly summarized below:

- Temperature is a core factor controlling rates of chemical and biological processes. The temperature dependence can be quantified via the activation energy, according to the Arrhenius Equation, or via the quotient of rate increase following a 10° increase in temperature. Several studies on marine sediments revealed a high temperature dependency in O_2 consumption (e.g. Banta et al. 1995, Thamdrup et al. 1998) which is mainly due to acceleration of microbial processes. Chemical processes instead show only minor impacts. Molecular diffusion increases about 30–40% at an 10°C increase of temperature (between 0 and 30°C), whereas the O_2 solubility decreases about 17–23%. Experiments showed that oxygen penetration depth and concentration is lower during warm periods than cold, whereas the gradient driving the diffusive uptake at the sediment-water interface is steeper during warm periods (Rasmusen and Jørgensen 1992, Kristensen 2000) (Figure 1-2).

- The quality of organic matter the main factor determining the O_2 consumption in the sediment exceeding the availability and concentration of organic matter. TOC can be separated in degradable organic compounds with varying reactivity and in almost non-metabolizable organic compounds. A direct correlation between TOC and O_2 penetration depth was not found, because the relation between the different types of organic matter is unpredictable and consequently the amount of oxygen required for the degradation process (Kristensen and Hansen 1995).

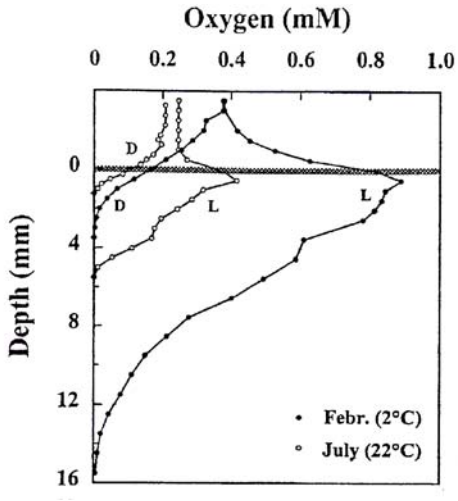

Figure 1-2. Oxygen profiles in a sandy coastal sediment (1m water depth) measured in daylight (L) and in darkness (D) during winter (February) and summer (July) (Kristensen 2000).

- Light is relevant in shallow areas, where sufficient light is available for photosynthetic activity of benthic primary producers. These sediments are often inhabited by microalgae or cyanobacterial mats. The resulting photosynthetic layer might have more impact on shallow sediments because of the chemical microenvironment they create than because of their primary production. This microenvironment at the sediment surface holds extreme physicochemical conditions (O_2 and pH) which may vary in seasonal and diurnal cycles (Revsbech

et al. 1983). Although the light penetration is not very deep (Kühl and Jørgensen 1994, Kristensen 2000) the O_2 concentration in the sediment can rise several fold to the normal water saturation, whereas during night the O_2 concentration can decreases to zero (Figure 1-2). As a consequence the penetration depth of oxygen can vary in a centimeter range and special adaptation is required for microorganisms living at or in the photic zone of the sediment.

- Water current above cohesive sediments determines the thickness of the diffusive boundary layer (DBL). The DBL acts as barrier for solute transport which is mediated by molecular diffusion. Thus the O_2 availability can be limited by the mass transport across the typically 0.5-1.0 mm thick DBL (Boudreau and Scott 1978, Thibodeaux at el. 1980, Santschi 1983). A higher flow velocity results in a reduced DBL thickness and consequently in an increased O_2 penetration depth (Jørgensen and Revsbech 1985). Changes in flow regime and temperature and consequently in the DBL on tidal, diurnal, and seasonal level make it difficult to extrapolate experimental data. Nevertheless, simulations revealed that on average over a year the diffusive oxygen uptake is not significantly influenced by the variability of the DBL. However, short term effects (eg. Storms, high sedimentation rates after bloom) may have a great impact on the O_2 uptake rate (Glud et al 2007). Another actor in the sizing of the DBL is the surface structure (roughness) of the sediment where an increasing particle size increases the thickness of the DBL. In permeable sediments advective pore water flow dominates the diffusive solute transport, induced by small-scale pressure gradients generated by water flowing around biogenic structures (e.g. burrow chimneys, fecal pallets) (Huettel and Gust 1992).

- Bioturbation has a major impact on marine sediments covered with oxic water conditions. The importance of fauna related O_2 uptake is highest in coastal sediments where very active irrigating species live and the oxic zone is small and thus the impact of irrigation high (Pfannkuche 2005). The faunal mediated oxygen uptake is the sum of faunal respiration and oxygen depletion due to expose of O_2 to anoxic sediment. With their high abundance sediment dwelling polychaetes play a quantitative role in the faunal meditated O_2 uptake. They enhance the sediment water interface significantly and thus create additional oxidized sediment in normally anoxic areas (Fenchel 1996, Kristensen 2000, Wenzhöfer and Glud 2004). To quantify the effect is a difficult task as 3-dimensional insight in the sediment is required.

1.2.3. Bioturbated Sediments

The idealized stratification of the sediment is disturbed by bottom-dwelling animals (e.g. polychaetes, crustaceans, bivalves), creating microenvironments in the range of millimeter to meter deep into the sediment (Figure 1-3). One advantage of a burrow is less predating pressure. In addition it is relative easy to establish a water circulation within a cylindrical burrow. The produced velocity allows burrowers to live at high oxygen levels in environments with otherwise low oxygen concentration. Some animals use these burrows also for gathering suspended food particles. However, even more animals are deposit feeders, feeding on the deposited particles thereby altering the sediment texture. Thus, different species create various amounts of sediment disturbance. The main impacts of macro benthos on the sediment can be summarized as the following:

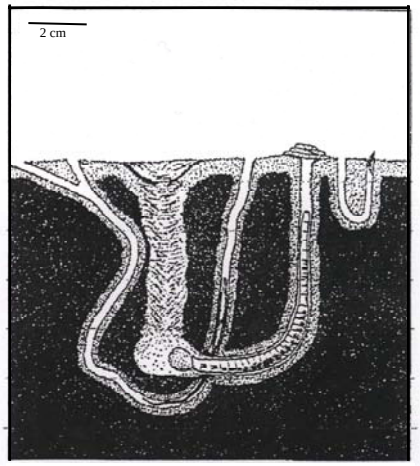

Figure 1-3. Schematic drawing of a bioturbated shallow coastal sediment. The light part of the sediment is oxidized and the dark part reduced sediment (Kristensen 2000).

- Material is trans located continuously between chemical reaction zones during feeding, burrowing, and the construction of tubes.
- Ventilation activities of the tube inhabitants create new oxic surfaces in deeper, normally anoxic sediment regions.
- New reactive organic mater also in the form of metabolic products, such as mucous secretions and dead organisms, are introduced into the sediment.
- The created biological niches inhabit conditions that promote activity of some species and at the same time exclude other species depending on the former conditions. This can result is an “unusual” composition of the biological community.

The implication on the O_2 exchange rates in the sediment depends on many factors. First, on the animal abundance, size of the individuals (millimeter to centimeter), and on the functional group of the species, e.g. feeding type, life habit, and mobility. Second, on the burrow structure varying in size, appearance, and

composition according to the inhabiting species. Finally, the effect depends on the wall lining, consisting of secretions mixed with sand or shell debris (Kristensen et al. 1991). The lining is highly enriched with organic matter compared to the surrounding sediment. However, degradability depends on the kind of secretion typical for the species. The solute permeability of the lining has also a strong impact on the chemical surrounding of the burrow (e.g. diffusivity of O_2: 10–40% of the free solution (Aller 1983), and as well as ventilation activities. The ventilation of burrows results on one side in a regular renewal of O_2-rich water and in a supply with electron acceptors normally not available at that sediment depth. On the other side, metabolites such as H_2S and Ammonia are removed (Kristensen 1988, Aller and Aller 1998).

Studies on polychaete ventilation patterns (Kristensen 1989, Riisgård 1991, Forster and Graf 1995) reported an intermittent pumping activity, interrupted by more or less rhythmical periods of rest. Pumping rates are strongly dependent on species and create unpredictable O_2 conditions for organisms living in the burrow environment. During periods of rest oxygen decreases fast by radial diffusion form the burrow into the sediment and due to degradation of the organic matter enriched along the burrow walls. Due to the difficulty of investigating this high spatial and temporal dynamics a radial distribution model has been developed (Fenchel 1996, Aller and Aller 1998). Assuming similar oxygen conditions and diffusive O_2 uptake rates at the primary sediment surface and in the burrow, the thickness of the oxic zone around burrow (L_B) walls resulted in smaller values than for the sediment surface (L_S), but the difference decreases with increasing burrow radius and increases with increasing L_S (Fenchel 1996). But detailed O_2 studies revealed that burrow walls may evolve to areas of intensified O_2 uptake with significantly higher O_2 uptake than at the primary interface (Wenzhöfer and Glud 2004, Jørgensen et al. 2005, König et al. Chapter 4 of this thesis).

Extrapolation from *in-situ* and laboratory experiments estimated for coastal sediments that the faunal-mediated oxygen uptake and the faunal respiration account for more than 50% of the total oxygen demand and that the faunal-mediated oxygen uptake exceeds the respiration (Forster and Graf 1995, Hansen et al. 1998, Hansen and Kristensen 1997, Glud et al. 2003, Vopel 2003).

To elaborate detailed mass-balances for burrow systems additional information on the geometry and increase of the sediment-water area is required. Once this data and the local volumetric O_2 uptake rates available one can estimate the oxidized volume around the burrow and the corresponding total O_2 uptake of the burrow (e.g. Aller 1982, 2001, Furukawa et al. 2001).

1.3. Hediste diversicolor, a brief summary

Among the various species *H. diversicolor* was chosen for this thesis as representative example for a burrow dwelling polychaete in marine shallow sediments. *Hediste* spp. (Figure 1-4) are typically used in laboratories because of their comparative high stress resistance and ease of availability.

The high abundant *H. diversicolor* is found in coastal areas with rough to fine sand as well as in muddy and fouling sediments. In the North Sea it lives in detritus rich areas and soft bottoms with H_2S production. The polychaete is mainly insensible versus temperature changes and lack of oxygen or present of H_2S, respectively. The salinity tolerance ranges from a minimum of 4 ‰ up to hypersaline water of 134 ‰ (Hartmann-Schröder 1996), however, for short time periods, only. It growths to a

length of up to 20 cm with a thick, cylindrical body. The color may range from yellowish to green, orange or red-brown with two dark length strips.

Figure 1-4. Example of a typical *Hediste* species

The polychaete digs mainly U-shaped, vertical burrows extending 2-8 cm into the sediment. However, much more complex systems have been documented (Rhoads and Germano 1982, Nilsson and Rosenberg 2000). The burrows reach a diameter of 2–7 mm depending on individual size with stable walls covered with a mucous secretion. It has been reported that the burrow surface area exceeds the sediment surface area by a factor of 1.3–5 (Hylleberg and Henriksen 1980, Kristensen 1984, Davey 1994, Fenchel 1996) mainly depending on the population density and size of the polychaete. The average population densitiy is 600 specimens m^{-2} in temperate coastal and estuarine sediments (Miron & Kristensen 1993, Riisgaard et al. 1996). Seasonal variations have been observed with high population densities of juvenile spp. in spring and lower densities of adult spp. in autum (Rysgaard et al. 1995, Wenzhöfer & Glud 2004).

H. diversicolor obtains nourishment by swallowing the uppermost layer with its content of detritus and microbenthic algae or use their jaws as predator (Goerke 1971). The ability of facultative filter-feeding enables *H. diversicolor* to live on a diet of phytoplankton. If the concentration of phytoplankton is high enough the polychaete shifts from predatory / surface deposit feeding to suspension feeding. A funnel-shaped mucous net collects particles which are pumped through the net by vigorously undulating body movements. After a period of pumping the polychaete swallows the net-bag with the entrapped particles (Riisgård 1994).

1.4. Oxygen optodes

1.4.1. Background

The established and widely used oxygen microsensor is a Clarke-type electrode with internal reference (Ag / AgCl) and an O_2 permeable silicone membrane at the sensor tip (Figure 1-5A). The electrode reactions are as follows:

Cathode: $O_2 + 2\ H_2O + 4e^- \rightarrow 4\ OH^-$

Anode: $4\ Ag + 4Cl^- \rightarrow 4\ AgCl + 4\ e^-$

The oxygen diffusion through the silicone membrane forces the reduction of the cathode and implies a current proportional to the O_2 concentration. Microelectrodes are characterized by perfectly linear calibration curves, response times around 0.1 s for very thin sensor tips, and low stirring sensitivity. The first microsensor (Figure 1-5B) optimized for application in marine biology was introduced by Revsbech in 1980. Microsensors are applied, for example, for fine-scale measurements of O_2 profiles in marine ecosystems (e.g. Revsbech 1989, and Revsbech et al. 1989, Kühl

and Revsbech 1999) and studies on photosynthesis and respiration. However, microelectrodes have some disadvantages:

- expensive and time consuming preparation
- insufficient long-term stability
- very fragile
- affected by electromagnetic fields
- pressure sensitive
- oxygen consumption during measurements
- limited to a one-dimensional approach

Some of these problems were overcome by applying an optochemical measuring principle (Wolfbeiss 1991): where an analyte interacts with an indicator resulting in a change of the optical properties (e.g. intensity, polarization, spectral distribution). The indicators are often immobilized in analyte permeable matrices, insoluble for water.

Several O_2-quenchable luminophores are reported in literature e.g. ruthenium-complexes, platin- and palladium-porphyrines (Wolfbeiss 1991, Papkovsky et al. 1991, Wilson et al. 1993, Klimant et al. 1995, 1997, Gouterman 1997). They can be excited with light in the range of 435 to 570 nm and emit red light (630-770 nm) showing an O_2 dependent change of luminescent intensity or lifetime (theory explained below). The first O_2 micro-optode (Figure 1-2B) for application in marine biology was introduced by Klimant et al. (1995, 1997). The luminescent dye is immobilized in polystyrene or organically modified sol-gel and is applied to the sensor tip by dip-coating. The excitation and emission light is guided through optical fibers and the sensor itself. Optodes are not influenced by electromagnetic fields, do not consume oxygen, and show a sufficient long-term stability. However, they still represent an one-dimensional approach. Describing two- and three-dimensional O_2

dynamics in heterogeneous environments (e.g. bioturbated sediments) remains a difficult and time consuming task.

Medicine was among the first disciplines to use optodes (Lübbers er al. 1975, Wilson et al. 1993). Some years later planar optodes were introduced as new and powerful tool to marine biology (e.g. Glud et al. 1996, 1998). Working on a similar measuring principle as micro-optodes, planar optodes overcome some of the problems of the micro-sensors as they allow two-dimensional studies and provide better results for temporal and fine-scale heterogeneity e.g. in sediments, biofilms, microbial mats, and plant roots (Glud et al. 1999, 2005, Wenzhöfer and Glud 2004, Frederiksen and Glud 2006, Oguri 2006, Precht et al. 2004, Franke et al. 2006).

To apply planar optode (PO) one has to be aware that the PO is an impermeable wall disturbing the natural 3-dimensional geometry. Especially in cases of radial oxygen diffusion limits the PO barrier the possible volume of oxidation (Figure 1-6). A model has been presented to quantify this effect, but it requires the knowledge of the burrow geometry and its relative location to the PO (Polerecky et al. 2006).

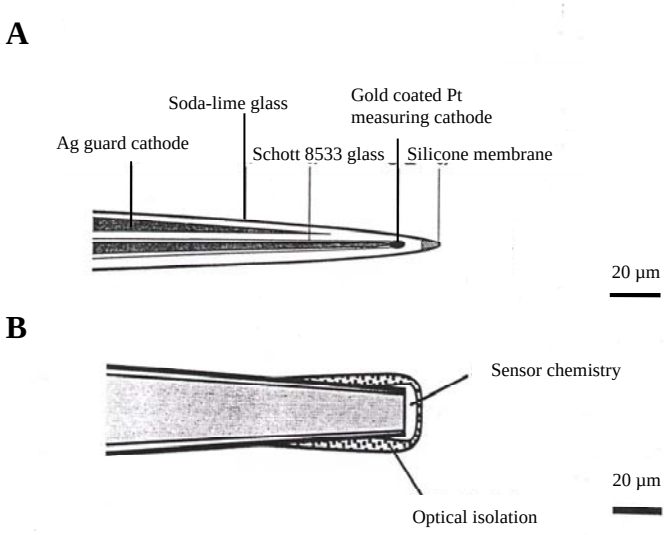

Figure 1-5. Design of the sensor tips of (A) an oxygen microelectrode (Kühl and Revsbech 1999) and (B) an O_2 microoptode (Klimant et al. 1995).

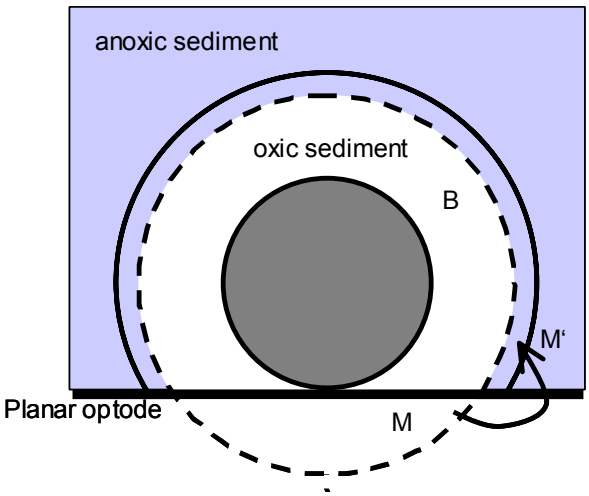

Figure 1-6. Distortion of the radial diffusion by the planar optode wall

Further the flow regime is affected by the presence of the PO reducing the flow in the corner of PO and sediment surface. Consequently the DBL is “creeping” up along the PO wall (Glud et al. 1996). Calculating the diffusive oxygen uptake at the sediment surface form planar optode images should rather be done by the oxygen gradient into the sediment (Bouldin 1968).

Another aspect in applying the PO technique is given by the light guidance effect also referred to as cross-talk effect (Franke, 2005). This effect causes the observed oxygen gradients to appear smaller than they are in reality. Furthermore, the absolute oxygen values in oxic regions can be (significantly) underestimated, particularly if these regions are close to anoxic areas. The light guidance probably results in an underestimation of the oxygen concentrations inside the burrows. According to Franke (2005) the effect of the spatial cross-talk effect is due to the different refraction indices of the aquarium wall, silicon glue, and support layer of the optode. The effect is minimized with increased wall thickness of the aquarium.

Sometimes species are attracted or disturbed by the presence of a wall so one has to check if the species behave naturally under experiment conditions. Altogether the constraints of the planar optode technique can be solved by a carefully and well customized experiment set-up. Combining PO measurements with micro-sensor measurement will provide the best insight on the dynamics of benthic systems.

1.4.2. Luminescence quenching

The absorption of electromagnetic radiation with a wavelength in the UV/VIS range rises a molecule to a higher energetic state. Once the activation stops there are several possible processes back to the energetic ground state of the molecule. The overall name for events including the emission of radiation is luminescence, which can be separated in fluorescence and phosphorescence. Additionally, several processes without emission of radiation occur (relaxation oscillations). Luminescence is mainly observed on aromatic and heterocyclic molecules, especially on condensed cycles. These molecules are known as fluorophores.

Fluorescence occurs during transition from the lowest level of the first excited (singlet-) state S_1 to ground (singlet-) state S_0 (Figure 1-7). The average lifetime of fluorescence is in the range of 10^{-9} – 10^{-6} s whereas phosphorescence lasts for 10^{-3} – 1 s or even longer. The prolonged lifetime of phosphorescence is due to the forbidden quantum mechanic transition (Pauli-Principle) from singlet to triplet state (intersystem crossing). The first step occurs radiation free followed by the radial transition (phosphorescence) to the ground state.

The lifetime of a fluorescent molecule can be significantly decreased in the presence of a quencher, reducing the fluorescence quantum yield of the fluorophore.

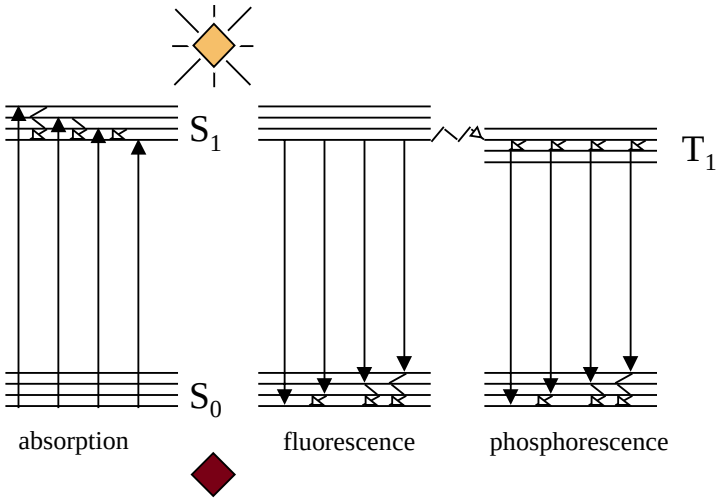

Figure 1-7. Energetic states of a luminophore (♦) drawn in a Jablonski-Diagram. Processes for absorption and deactivation of the excite molecule are sketched. Emission transitions are marked with → and radiation free relaxation oscillations are marked with ~>.

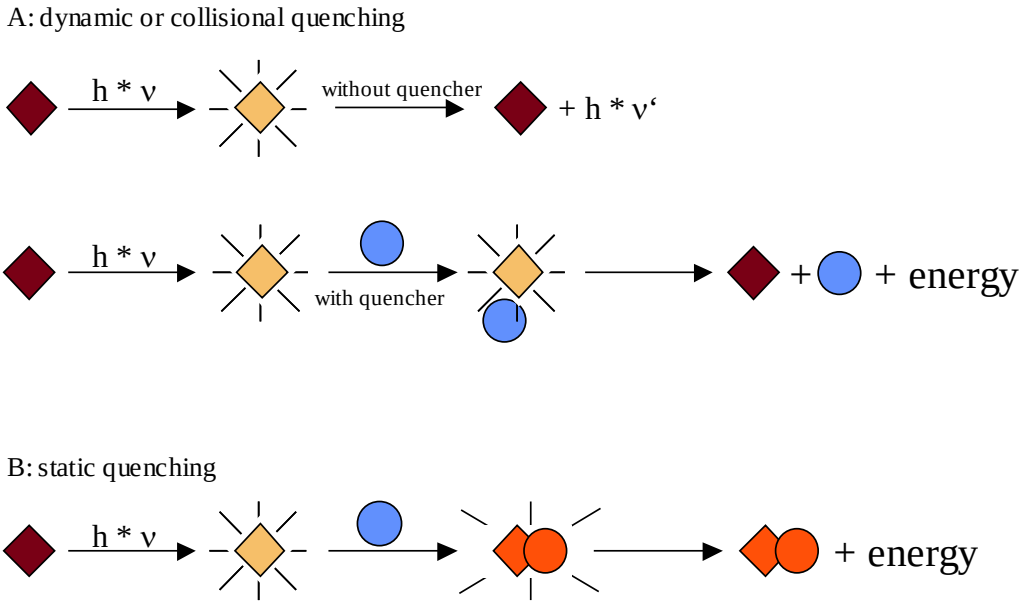

Figure 1-8. A: Scheme of dynamic quenching of a fluorophore (♦) without and with quencher (•). B: Scheme of static quenching of a fluorophore by complex formation.

This process does not affect the absorption of the molecule but the energy of the activation state is passed radiation free to the quencher molecule (Figure 1-8). The quenching process is separated in two types:

1. Dynamic fluorescence quenching due to collisional processes.
2. Static fluorescence quenching due to complex formation.

The main difference between the two processes is the lifetime of the formed complex in the intermediate step. During the dynamic quenching process the lifetime of the complex is significantly shorter than the lifetime τ_0 of the excited fluorophore. In contrary to the static quenching process where the complex lifetime is much longer.

Oxygen is one of the most famous fluorescence quenchers. The lifetime of the fluorescence (also referred to as decay time of the fluorescence) and with that the fluorescence intensity is decreased in presence of oxygen. The relation between oxygen concentration (cO_2) and fluorescence intensity (I) respectively lifetime (τ) is described by the Stern-Volmer-Equation:

$$\frac{I_0}{I} = \frac{\tau_0}{\tau} = 1 - K_{SV} * cO_2 \qquad (1)$$

where I_0 and τ_0 represent the fluorescence intensity and lifetime at zero oxygen. The quenching efficiency is quantified by K_{SV}, the bimolecular quenching coefficient (Stern Volmer constant). This equation is valid for ideal systems, only where all molecules follow the same reaction. Having a close look on the calibration curves of many optodes one finds a nonlinear shape when plotting I/I_0 versus cO_2. These nonlinear curves of oxygen optodes are better described by a two-component model of the Stern-Volmer-Equation (Bacon and Demas 1987, Klimant et al. 1995):

$$\frac{I_0}{I} = \frac{\tau_0}{\tau} = \frac{a}{1 + K_{SV} * cO_2} + (1 - a) \qquad (2)$$

where a is the fraction of quenchable fluorophore and K_{SV} is the bimolecular Stern-Volmer constant. Fraction a is an optode type specific value which has to be

determined experimentally. It can then be applied for all optodes prepared in a similar way. Finally, in Eq. 2 there are only two parameters left that have to be determined by a simple two-point calibration.

1.5. Outline of this thesis

The theme of this work can be separated into two aspects:

1. the improvement and detailed characterization of planar oxygen optodes and optimization of the measuring technique
2. the application of the planar oxygen optodes in a marine biological environment to study the behavior and associated benthic O_2 dynamics in burrow systems of *Hediste diversicolor*

In the frame of the first aspect special emphasis was drawn on the properties of the sensor matrix. The preparation of a modified sol-gel allowed tailoring of the matrix properties like oxygen solubility, stability, homogeneous distribution and good adhesion on the support foil. Several series of sol-gels were prepared and tested with respect to the mentioned parameters.

In a first approach planar O_2 optodes were applied using an intensity based measuring system. A preliminary study on a shallow marine sediment covered with a microbial mat gave an indication of the potential of the new optode. The high O_2 dynamic in the sediment was investigated under a natural light regime.

Parallel improvements on the measuring technique and the planar optode finally lead to a lifetime based imaging system which was applied in a marine sediment inhabited by *H. diversicolor*. The temporal and spatial O_2 dynamics were studied

around the polychaete burrow and at the sediment surface in natural and artificial burrow systems. Measurements with planar optodes were complemented by measurements with a flow sensor to investigate the behavior of H. diversicolor under experimental conditions. O_2 micsosensors were applied for incubation measurements. Based on theses data a total O_2 consumption budget was calculated for *H. diversicolor* and its burrow system.

1.6. References

Aller, R. C., 1982. The effects of macrobenthos on chemical properties of marine sediment and overlying water. In McCall P. L., Tevesz M. J. S. (eds) Animal-sediment relations. Plenum, p 53-102.

Aller, R. C., 1983. The importance of the diffusive permeability of animal burrow linings in determining marine sediment chemistry. J. Mar. Res. 41:299-322.

Aller, R. C., 2001. Transport and reactions in the bioirrigated zone. In Boudreau B. P., Jørgensen B. B. (eds) The Benthic Boundary Layer: Transport processes and biogeochemistry. Oxford, p.269-301.

Aller, R. C. and J. Y. Aller, 1998. The effect of biogenic irrigation intensity and solute exchange on diagenetic reaction rates in marine sediments. J. Mar. Res. 56:905-936.

Bacon, J. R., J. N. Demas, 1987. Determination of oxygen concentrations by luminescence quenching of a polymer immobilized transition-metal complex. Anal. Chem. 59:2780-2785.

Banta, G. T., A. E. Giblin, J. E. Hobbie, J. Tucker, 1995. Benthic respiration and nitrogen release in Buzzards Bay, Massachusetts. J. Mar. Res. 53:107-135.

Boudreau, B. P., M. R. Scott, 1978. A model for diffusion controlled growth of deep-sea managnese nodules. Amer. J. Sci. 278: 903-929.

Bouldin D. R., 1968. Models for describting the diffusion of oxygen and other mobile constituents across the mud-water interface. J. Ecol. 56: 77-87.

Canfield, D. E., B. B. Jørgensen, H. Fossing, R. Glud, J. Gundersen, N. B. Ramsing, B. Thamdrup, J. W. Hansen, L. P. Nielsen, O.J. Hall, 1993. Pathways of organic carbon oxidation in three continental margin sediments. Mar. Geol. 113:27-40.

Canfield, D. E., 1994. Factors influencing organic carbon preservation in marine sediments. Chem. Geol. 114:315-329.

Davey, J. T., 1994. The architecture of the burrow of Nereis diversicolor and its quantification in relation to sediment-water exchange. J. mar. Biol. Ecol. 179:115-129.

Fenchel, T., 1996. Worm burrows and oxic microniches in marine sediments. 1. Spatial and temporal scales. Mar. Biol. 127:289-295.

Fenchel, T., G. M. King, T. H. Blackburn, 1998. Bacterial biogeochemistry: the ecophysiology of mineral cycling. Academic Press, San Diego: 307 pp.

Franke, U., 2005. Application of planar optodes in biological acquatic systems. PH.D.-Thesis, Fachbereich Biologie/Chemie, University of Bremen, Germany.

Franke, U., L. Polerecky, E. Precht, M. Hüttel, 2006. Wave tank study of particulate organic matter degradation in permeable sediments. Limnol. Oceanogr. 51: 1084-1096.

Forster, S., G. Graf, 1995. Impact of irrigation on oxygen flux into the sediment: intermittent pumping by Callianassa subteranea and 'piston pumping' by Lanice conchilega. Mar. Biol. 123:335-346.

Frederiksen, M., R. N. Glud, 2006. Oxygen dynamics in the rhizosphere of Zostera marina: A two-dimensional planar optode study. Limnol. Oceanogr. 51.1072-1083.

Furukawa, Y., S. J. Bentley, D. L. Lavoie, 2001. Bioirrigation modeling in experimental benthic mesocosms. J Mar Res 59: 417-452.

Glud, R. N., J. K. Gundersen, B. B. Jørgensen, N. P. Revsbech, H. D. Schulz, 1994. Diffusive and total oxygen uptake of deep-sea sediments in the eastern South Atlantic Ocean: in situ and laboratory sediments. Deep Sea Res. 141:1767-1788.

Glud, R. N., N. B. Ramsing, J. K. Gundersen, I. Klimant, 1996. Planar optodes: a new tool for fine scale measurements of two-dimensional O2 distribution in benthic communities. Mar. Ecol. Prog. Ser. 140:217-226.

Glud, R. N., C. M. Santegoeds, D. de Beer, O. Kohls, N. B. Ramsing, 1998. Oxygen dynamics at the base of a biofilm studied with planar optodes. Aquat. Microb. Ecol. 14:223-233.

Glud, R. N, M. Kühl, O. Khols, N. B. Ramsing, 1999. Heterogenity of oxygen production and consumption in a photosynthetic microbial mat as studied by planar optodes. J. Phycol. 35: 270-279.

Glud, R. N., J. K. Gundersen, H. Røy, B. B. Jørgensen, 2003. Seasonal dynamics of benthic O2 uptake in a semienclosed bay: Importance of diffusion and faunal activitiy. Limnol Oceanogr 41: 1265-1276.

Glud, R. N., F. Wenzhöfer, A. Tengberg, M. Middelboe, K. Oguri, H. Kitasato, 2005. Distribution of oxygen in surface sediments from central Sagami Bay, Japan: In situ measurements by microelectrodes and planar optodes. Deep-Sea Res. I 52: 1974-1987.

Glud, R. N., P. Berg, H. Fossing, B. B. Jørgensen, 2007. Effect of the diffusive boundary layer on the benthic mineralization and O2 distribution: A theoretical model analysis. Limnol. Oceanogr. 52: 547-557.

Goerke, H., 1971. Die Ernährungsweisen der Nereis-Arten (Polychaeta, Nereidae) der deutschen Küsten. Veröff. Inst. Meeresforsch. Bremerh. 13: 1-50.

Gouterman, M., 1997. Oxygen quenching of luminescence of pressure sensitive paint for wind tunnel research, J. Chem. Educ. 74: 697–702.

Hammond, D. E., Cummins K. M. McManus, W. M. Berelson, G. Smith, F. Spagnoli, 2004. Methods for measuring benthic nutrient flux on the Californian margin: Comparing shipboard core incubations to in situ lander results. Limnol. Oceanogr. Meth. 2: 146-159.

Hansen, K., E. Kristensen, 1997. Impact of macrofaunal recolonization on benthic metabolism and nutrient fluxes in a shallow marine sediment previously overgrown with macroalgal mats. Estuar Coas. Shelf Science 45: 613-628.

Hansen K., S. Mouritsen, E. Kristensen, 1998. The impact of Chrionomus plumosus larvae on organic matter decay and nutrient (N,P) exchange in a shallow eutrophic lake sediment following a phytoplankton sedimentation. Hydrobiol. 364: 65-74.

Hartmann-Schröder, G. 1996. Annelida, Borstenwürmer, Polychaeta. Gustav Fischer Verlag, Jena: 201 pp.

Howarth, R. W., 1984. The ecological significance of sulfur in the energy dynamics of salt marsh and coastal marine sediments. Biogeochemistry. 1: 5-27.

Hüttel, M., G. Gust, 1992. Impact of bioroughness in interfacial solute exchange in permeable sediments. Mar. Ecol. Prog. Ser. 89: 253-267.

Hylleberg, J., K. Henriksen, 1980. The central role of bioturbation in sediment mineralization and element re-cycling. Ophelia, Suppl. 1: 1-16.

Jørgensen, B. B., N. P. Revsbech, 1983. Colorless sulfur bacteria Beggiatoa spp. and Thiovulum spp. in O2 and H2S microgradients. Appl. envir. Microbiol. 45:1261-1270.

Jørgensen, B. B., N. P. Revsbech, 1985. Diffusive boundary layers and the oxygen uptake of sediments and detritus. Limnol. Oceanogr. 30:111-122.

Jørgensen, B. B., R. N. Glud, O. Holby, 2005. Oxygen distribution and bioirrigation in Arctic fjord sediments (Svalbard, Barents Sea). Mar. Ecol. Prog. Ser. 292: 85-95.

Klimant, I., V. Meyer, M. Kühl, 1995. Fiber-optic oxygen microsensors, a new tool in aquatic biology. Limnol. Oceanogr. 40:1159-1165.

Klimant, I., M. Kühl, R. N. Glud, G. Holst, 1997. Optical measurements of oxygen and temperature in microscale: strategies and biological applications. Sensors and Actuators B 38-39:29-37.

Kristensen, E., 1984. Effect of natural concentrations on exchange of nutrients between a polychaete burrow in estuarine sediment and overlying water. J. exp. mar. Ecol. 75:171:190.

Kristensen, E., 1988. Benthic fauna and biogeochemical processes in marine sediments: microbial activities and fluxes. In Blackburn, T. H. and J. Søresnsen (eds), Nitrogen cycling in coastal marine environments. John Wiley & Sons Ltd., Chichester: 275-299.

Kristensen, E., 1989. Oxygen carbon dioxide exchange in the polychaete Nereis virens: influence of ventilation activity and starvation. Mar. Biol. 101: 381-388.

Kristensen, E., 2000. Organic matter diagenesis at the oxic/anoxic interface in coastal marine sediments, with emphasis on the role of burrowing animals. Hydrobiologica. 426: 1-24.

Kristensen, E., S. I. Ahmed, A. H. Devol, 1995. Aerobic and anaerobic decomposition of organic matter in marine sediment: which is faster? Limnol. Oceanogr. 40: 1430-1437.

Kristensen, E., R. C. Aller, J. Y. Aller, 1991. Oxic and anoxic decomposition of tubes from the burrowing sea-anemone Ceriantheopsis americanus: implications for sediment carbon and niotrogen dynamics. J. mar. Res. 49:589-617.

Kristensen, E., K. Hansen, 1995. Decay of plant detritus in organic-poor marine sediment: production rates and stoichiometry of dissolved C and N compounds. J. mar. Res. 53:675-702.

Kühl, M. and B. B. Jørgensen, 1994. The light field of microbenthic communities: radiance distribution and microscale optics of sandy coastal sediments. Limnol. Oceanogr. 39:1368-1398.

Kühl, M and N. P. Revsbech, 1999. Microsensor for the study of interfacial biogeochemical processes. In Boudreau, B. P., B. B. Jørgensen (eds.): The Benthic Boundary Layer. Oxford University Press, Oxford.

Lübbers, D.W., N. Opitz, 1975. The pCO2:pO2 optrode: a new probe for measuring pCO2 and pO2 of gases and liquids, Z. Naturforsch. 30C:532–533.

Miron, G., E. Kristensen, 1993. Factors influencing the distribution of Nereid polychaetes: the sulfide aspect. Mar Ecol Prog Ser 93:143-153.

Nilsson, H.C., R. Rosenberg, 2000. Succession in marine benthic habitats and fauna in response to oxygen deficiency: analyzed by sediment profiling-imaging and grab samples. Mar Ecol Progr Ser 197: 139-149.

Oguri, K., Kitazato, R. N. Glud, 2006. Platinum octaetylporphyrin based planar optodes combined with UV-LED excitation light source: An ideal tool for high resolution O2 imaging in O2 depleted environments. Mar. Chem 100: 95-107.

Papkovsky, D. B., J. Olah, I. V. Troyanovsky, N. A. Sadovsky, V. D. Rumyantseva, A. F. Mironov, A. I. Yaropolov, A. P. Savitsky, 1991. Phosphorescent polymer films for optical oxygen sensors. Biosensors & Bioelectronics. 7:199-206.

Pfannkuche, O., 2005. Allothonous deep-sea benthic communities: Functioning and forcing. In interactions between macro- and microorganisms in marine sediments. Kristensen E., R. R. Haese, J. E. Kostka (eds) Coastal Estuarine Studies. American geophysica Union, Washington.

Polerecky L., N. Volkenborn, P. Stief, 2006. High temporal resolution oxygen imaging in bioirrigated sediments. Environ. Sci. & Technol. 40: 5763-5769.

Precht, E., U. Franke, L. Polerecky, M. Hüttel, 2004. Oxygen dynamics in permeable sediments with a wave-driven pore water exchange. Limnol. Oceanogr. 49: 693-705.

Rasmusen, H., B. B. Jørgensen, 1992. Microelectrode studies of seasonal oxygen uptake in a coastal sediment: role of molecular diffusion. Mar. Ecol. Prog. Ser. 81:289-303.

Reimers, C. E., K. M. Fischer, R. Meerwether, K. L. Smith Jr., R. A. Jahnke, 1986. Oxygen microprofiles measured in situ in deep ocean sediments. Nature. 320:741-744.

Revsbech, N. P., 1989. An oxygen microelectrode with a guard cathode. Limnol. Oceanogr. 34:2017-2035.

Revsbech, N. P., J. Sørensen, T. H. Blackburn, J. P. Lomholt, 1980. Distribution of oxygen in marine sediments measured with microelectrodes. Limnol. Oceanogr.25:403-411.

Revsbech, N. P., B. B. Jørgensen, T. H. Blackburn, Y. Cohen, 1983. Microlelectrode studies of the photosynthesis and O2, H2S and pH profiles of a microbial mat. Limnol. Oceanogr. 26:717-730.

Revsbech, N. P., B. B. Jørgensen, T. H. Blackburn, 1989. Oxygen in the sea bottom measured with a microelectrode. Science. 207:1355-1356.

Riisgård, H. U., 1991. Suspension feeding in the polychaete Nereis diversicolor. Mar. Ecol. Prog. Ser. 70:29-37.

Riisgård, H. U., 1994. Filter-feeding in the polychaete Nereis diversicolor: a review. Neth. J. Aquat. Ecol. 28:453-458.

Riisgaard, H.U., L. Poulsen, P. S. Larsen, 1996. Phytoplankton reduction in near-bottom water caused by filter-feeding Hediste diversicolor: implications for worm growth and population grazing impact. Mar Ecol Progr Ser 141: 47-54.

Roden, E. E., R. G. Wetzel, 1996. Organic carbon oxidation and supression of methane production by microbial Fe(III) oxide reduction in vegetated an unvegetated freshwater wetland sediments. Limnol. Oceanogr. 41: 1733-1748.

Rhoads, D.C., J. D. Germano, 1982. Characterization of organism-sediment relations using sediment profile imaging: an efficient method of remote ecological monitoring of the seafloor (RemotsTM systems). Mar Ecol Progr Ser 8: 115-128.

Rysgaard, S., P. B. Christensen, L. P. Nielsen, 1995. Seasonal variation in nitrification and denitrification in estuarine sediment colonized by benthic microalgae and bioturbation infauna. Mar Ecol Progr Ser 126: 11-21.

Santschi, P. H., P. Bower, U. P. Nyffeler, A. Azevedo, W.S. Broecker, 1983. Estimates of the resistance to chemical transport posed by the deep sea boundary layer. Limnol. Oceanogr. 28: 899-912.

Thamdrup, B., J. W. Hansen, B. B. Jørgensen, 1998. Temperature dependence of aerobic respiration in coastal sediments. FEMS Microbiol. Ecol. 25:189-200.

Thibodeaux, L. J., L. K. Chang, D. J. Lewis, 1980. Dissolation rates of organic contaminants located at the sediment water interface of rivers, streams and tidal zones. In Baker R. A. (ed) Contaminants and sediments, Vol 1. Ann. Arbor Science, Ann Arbor, Mich.

Vopel, K., D. Thistle, R. Rosenberg, 2003. Effect of the brittle star Amphiura filiformis (Amphiuridae, Echinodermata) on oxygen flux into sediments. Limnol-Oceanogr. 48: 2034-2045.

Wenzhöfer, F, R. N. Glud, 2004. Small-scale spatial and temporal variability in coastal benthic O2 dynamics: Effects of fauna activity. Limnol Oceanogr 49: 1471-1481.

Wilson, D.F., S. Gomi, A. Pastuszko, J.H. Greenberg, 1993. Microvascular damage in the cortex of cat brain from middle cerebral artery occlusion and reperfusion, J. Appl. Physiol. 74:580–589.

Wolfbeiss, O. S. (ed.).1991. Fiber optic sensors and biosensors. CRC Press, Ann Harbor.

Chapter 2

Imaging of oxygen distributions at benthic interfaces: A brief review

Published in Organsim-Sediment Interactions,

edited by Joesphine Y. Aller, Sarah A. Woodin, and Robert C. Aller,

South Carolina, 2001

2. Imaging of oxygen distributions at benthic interfaces: A brief review

Bettina Koenig[1], Gerhard Holst[1], Ronnie N. Glud[2], Michael Kühl[2,*]

[1]Max-Planck-Institute for Marine Microbiology, Celsiusstr. 1, D-28359 Bremen, Germany

[2]Marine Biological Laboratory, University of Copenhagen, Strandpromenaden 5, DK-3000 Helsingør, Denmark

*corresponding author, Fax: +45 3532 1950, e-mail: mkuhl@bi.ku.dk

Abstract

Recently, new experimental techniques to map two-dimensional oxygen distributions in benthic communities have been developed. The oxygen distributions are visualized by the use of planar sensor foils with an oxygen sensitive fluorophore layer, containing a photostable ruthenium complex, that is reversibly quenched by oxygen. Recording the fluorescence intensity from the sensor foil by a light sensitive digital camera system allows the two-dimensional oxygen distribution to be quantified over an area of several cm^{+2} at a spatial resolution better than 50 µm. Larger areas can be covered by changing the optics of the system, however, the spatial resolution decreases. Since the first more primitive approaches, more sophisticated systems have been developed, in which both fluorescence intensity and fluorescence lifetime imaging is possible in one as well as two dimensions (planar optodes). We have applied planar optodes for mapping the oxygen dynamics in benthic systems exhibiting various degrees of heterogeneity (e.g. biofilms, microbial mats, and sediments with and without significant faunal activity). In the following, the technical developments of sensors, camera systems and applications of the imaging techniques are reviewed here.

2.1. Introduction

The benthic sediment-water interface is an important and active horizon of the marine environment. Intense production and degradation of organic matter takes place within a narrow zone leading to a dynamic exchange of solutes between the benthic community and the overlying water as well as with the sediment below this dynamic layer. However, the interface is not a flat horizon but is typically characterized by an extensive heterogeneity, both at micro (Jørgensen and Des Marais 1990) and macro scales (Aller et al. 1998; Glud et al. 1998a). For example, the heterogeneity is related to variability in settling rates of organic carbon, temperature, microbial and macrofaunal activity. In order to study the millimeter-to-centimeter-thick oxic zone of benthic communities, measuring techniques with a high spatial and temporal resolution are required. Oxygen microelectrodes were introduced to aquatic biology by Revsbech et al. 1980, and they for the first time enabled detailed studies at a sub-mm resolution of surface sediments.

Recently, a new optical microsensor (microoptode) was introduced to marine ecology (Klimant et al. 1995). Compared to microelectrodes, microoptodes have the main advantages of cheap and easy construction, and superior long-term stability. They now represent a realistic alternative to microelectrodes even on *in-situ* measuring platforms (Glud et al. in press a). The measuring principle of O_2 microoptodes is based on dynamic fluorescence quenching by oxygen. The fluorescence dye tris (4,7-diphenyl-1,10-phenantrolin)-ruthenium(II) perchlorate (Ru-DPP) is immobilized in a polymer matrix and coated on a thin fiber optic tip. However, even though both microelectrode and microoptode techniques offer high spatial and temporal resolutions, microprofiles only represent a one-dimensional approach, measuring oxygen concentration at a single point in a three-dimensional heterogeneous sample. The difficult task of describing or overcoming heterogeneity

of benthic communities has been performed by multiprofiling (Jørgensen and Des Marais 1990) or the use of sensor arrays (Holst et al. 1997). Often, this is time consuming, requires large and sophisticated set-ups, complicates many *in-situ* applications, and is in many instances almost impossible. For this reason, and to obtain solute distributions in two dimensions, oxygen planar optodes have been developed.

The technique of the oxygen planar sensor is based on the same principle as for oxygen microoptodes. However, instead of fixing the sensor matrix, incorporating the luminescence dye, on an optical fiber tip, the sensor matrix is immobilized on transparent support foils (Glud et al. 1996). The foils can, in combination with CCD cameras and imaging techniques, resolve O_2 gradients in two dimensions. Here, we present a brief review of planar optodes, and their applications to marine science, as well as results from the first measurements obtained by a newly developed camera measuring system that enables both luminescence intensity and luminescence life-time (rate of luminescence decay) based measurements.

2.2. Theory

Both the new and the old imaging systems for high resolution O_2 distributions in one and two dimensions, discussed below are based on the commonly known effect of dynamic quenching of luminescent indicators by oxygen (Stern and Volmer 1919; Kautsky 1939). Oxygen molecules diffuse into a sensor matrix where they react reversibly with a fluorescent dye (Ru-DPP) described as dynamic fluorescence quenching. The effect of this reaction is a measurable decrease in fluorescence

intensity with rising oxygen concentrations. The CCD camera monitors the emitted fluorescence intensity signal. According to the timing scheme (Figure 2-1) and the imaging processing, the resulting image either corresponds to the fluorescence intensity or the fluorescence lifetime (rate of fluorescence decay) (Holst et al. 1998). Lifetime imaging is based on the fact that the oxygen concentration is related to the rate of the fluorescence decay. The relation between oxygen concentration (c) and the fluorescence intensity (I) and the time decay rate (τ), respectively is given by the modified Stern-Volmer equation (Bacon and Demas 1987)

$$\frac{I}{I_0} = \frac{\tau}{\tau_0} = \left[\frac{a}{(1 + Ksv * c)} + (1 - a) \right]$$

where, c = oxygen concentration,

I = the luminescence intensity, I_0 in absence of O_2 ,

τ = the time decay rate, τ_0 in absence of O_2,

K_{SV} = the coefficient expressing the quenching efficiency of the fluorophore,

a = the non-quenchable fraction of the luminescence.

The parameter (a) is related to the type of matrix used and has to be determined before sensor application. To evaluate oxygen concentrations from fluorescence the value of K_{SV} has to be determined first, via a simple two-point calibration (Glud et al. 1996).

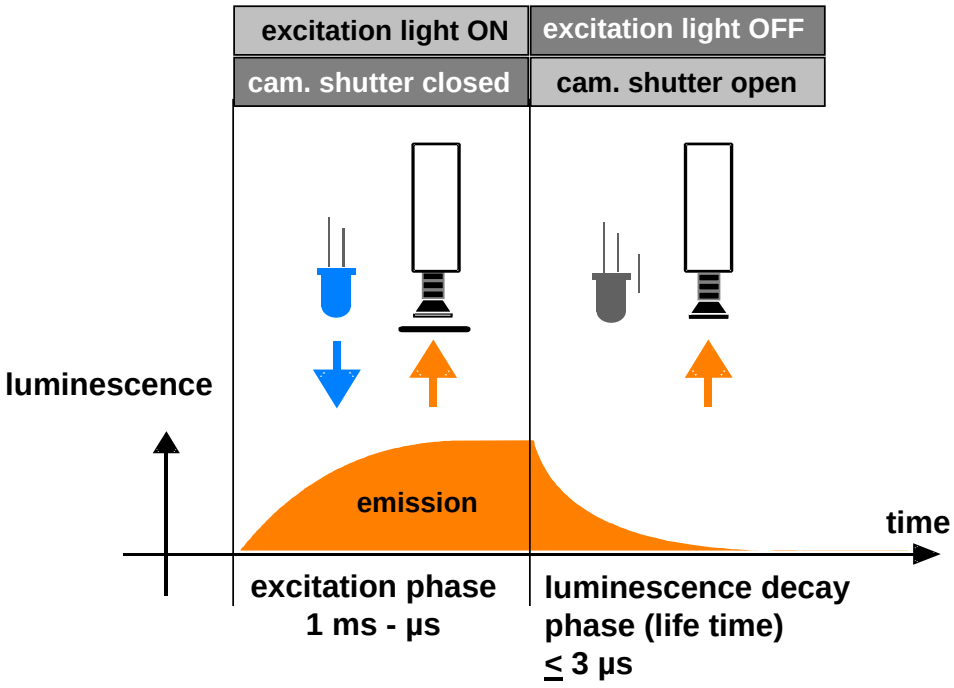

Figure 2-1. Principle for image acquisition of fluorescence life time imaging. The timing (range of ms to µs) starts with excitation light ON and the camera shutter closed. The excitation light is then switched OFF and the camera shutter is opened with a possible delay.

2.3. Applications with the old planar optode system

2.3.1 Materials and Methods

The imaging system described by Glud et. al (1996) for oxygen measurements was based on intensity measurements. As an oxygen quenchable fluorophore, the dye tris (4,7-diphenyl-1,10-phenantrolin)-ruthenium(II) perchlorate (Ru-DPP) was applied (Bacon and Demas 1987; Klimant and Wolfbeis 1995; Hartmann and Ziegler 1996). The fluorescence dye was dissolved together with scattering particles in plasticized PVC (Preininger et. al 1994). This solution was spread on a 175-µm thick polyester

foil (© Mylar, Du Pont, Germany). The thickness of the sensing layer was approximately 10 µm, and was covered by a second black silicon layer (20 µm) for optical insulation. This was necessary in order to avoid scattering effects of the biological sample and a potential stimulation of photosynthesis. Silicon was used because it is highly permeable to oxygen.

The planar optode was glued to the inside of a small Plexiglas frame (Figure 2-2). To excite the fluorophore, light from a halogen lamp filtered with a blue glass filter (450 nm) was used. After passing through an emission filter, the emitted fluorescence light was collected by a CCD camera. Camera timing and data acquisition were controlled via a Macintosh Computer. A spatial resolution of approximately 26 µm was achieved with the system. The initial calibration measurements were performed using sea water flushed with defined gas mixtures of oxygen and nitrogen.

Correlation between averaged fluorescence intensity and O_2 saturation of the water is shown in Figure 2-3A. The intensity decline with rising oxygen saturation resulted in a hyperbolic curve, which could be described by the modified Stern-Volmer equation. The standard deviation of the fluorescence intensity varied between 5 and 8% of the average signal of all pixels. This signal to noise ratio is mainly influenced by heterogeneity in the sensor layer, due to uneven distribution of the fluorophore, agglutination of scattering

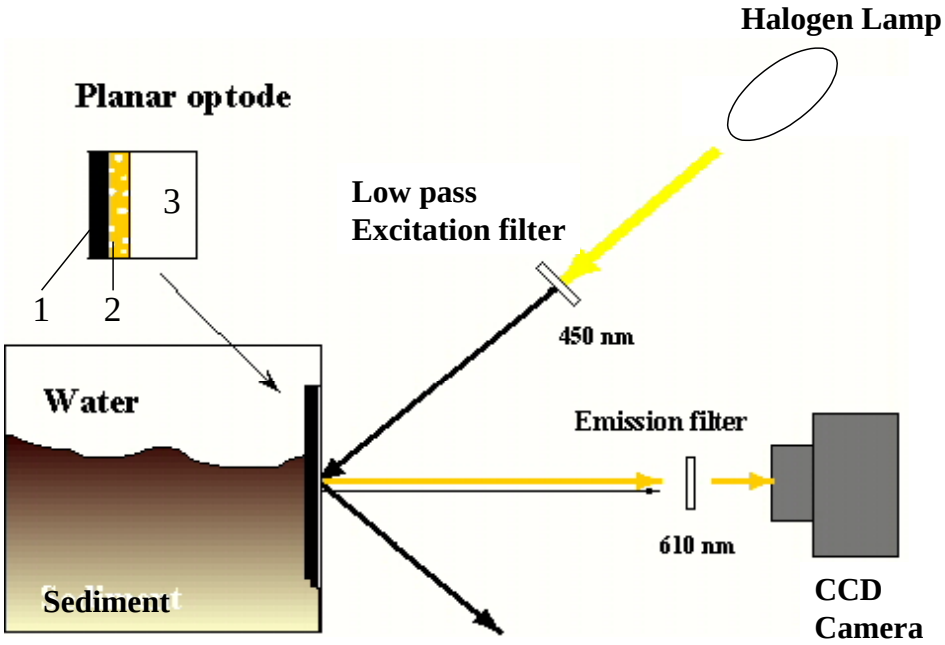

Figure 2-2. Schematic illustration of the experimental set-up (Glud et al, 1996). An enlargement of the three-layered planar optode is shown in the upper left corner: supporter foil (3), sensing layer (2), optical insulation (1).

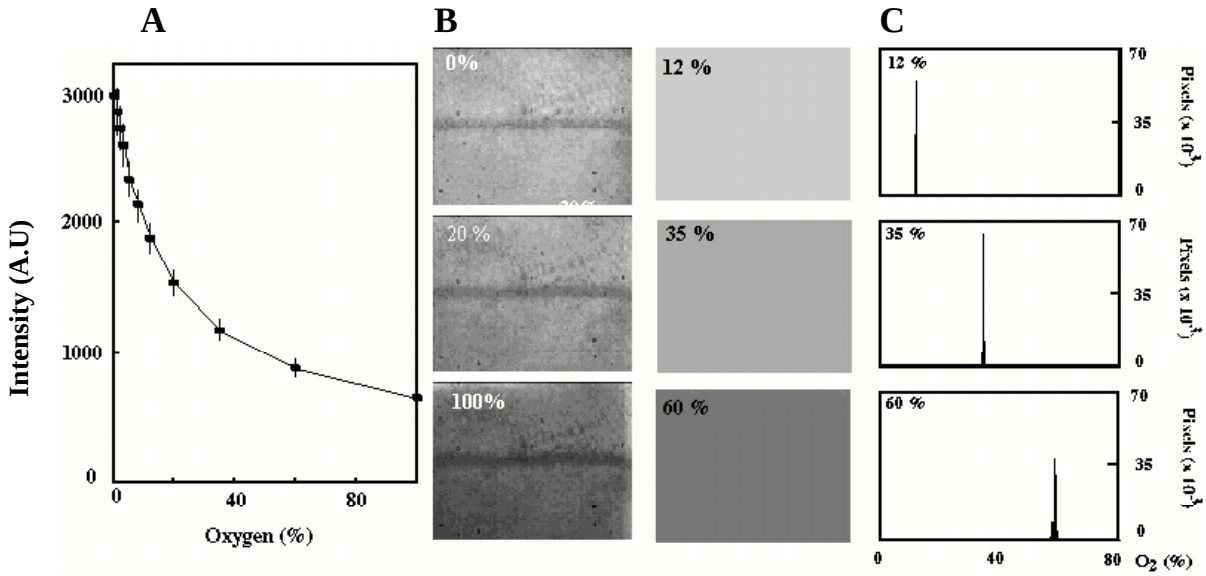

Figure 2-3. (A) Average fluorescence intensity as a function of O_2 saturation in water; standard deviation shown as error bars. (B) Three original images obtained at different O_2 saturation. The darker line is caused due to sensor heterogeneity. (C) Three examples of pixel by pixel calculated images at different O_2 saturation expressed on an linear gray scale from 0 to 255. (D) The average O_2 concentration measured by the planar optode as a function of the actual O_2 concentration.

particles, and an uneven field of excitation light. A further source of measured heterogeneities could be caused by an unevenly distributed clear silicon used to glue the optode to the aquarium wall (Figure 2-3B). Every pixel of the image can be treated as a single one-dimensional optical sensor. As a consequence pixel by pixel calibration was performed to reduce the influence of the aspects mentioned above. The result of a pixel to pixel calibration is demonstrated by Figure 2-3C and 3D.

2.3.2 Application to Marine Sediments

The first planar optode measurements in aquatic sediments were performed in an intertidal sediment (Glud et al. 1996). The overlying water was flushed with 12 and 24% oxygen saturated water, and after equilibration was established, a series of images were taken (Figure 2-4). To determine the position of the sediment surface, sodium dithionite grains were deposited on the sediment surface. Due to reduction of any O_2 in their immediate vicinity, the grains appeared as single blue dots on the image. The sediment-water interface was estimated by the dots on subsequent images (thick black line in the images of Figure 2-4A and 4B). Oxygen penetration varied between 0.54 and 2.62 mm at 12% O_2 saturation, and between 1.8 and 3.5 mm at 24% O_2 saturation.

2.3.3 Measurements on a Biofilm

As an example of a complex benthic community a biofilm developing from an inoculated waste water treatment plant was examined. Planar optodes were fixed in a flume and as biofilms gradually developed, the two-dimensional O_2 distribution at the base of the biofilms was investigated (Glud et al. 1998b). The O_2 distribution of a

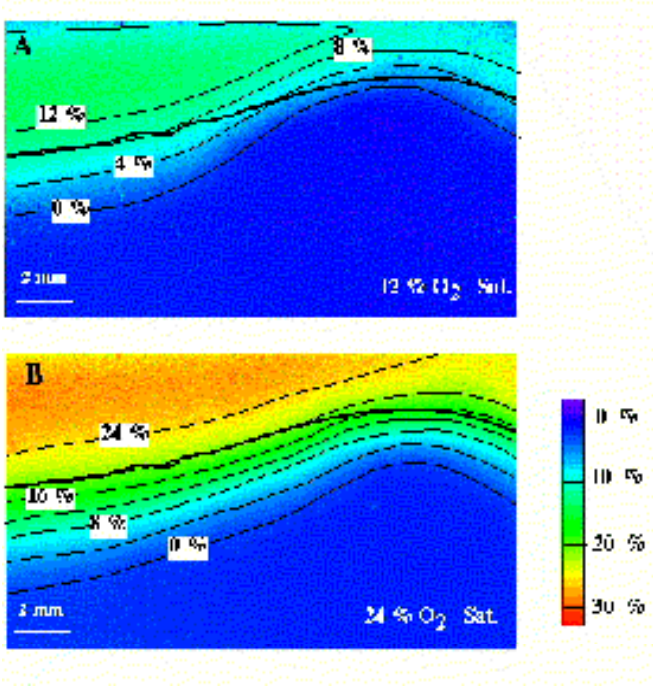

Figure 2-4. Calibrated images of the O_2 distribution at the sediment-water interface with 12% (A) and 24% (B) O_2 saturation in the overlying water. The images represent an area of 17.0 x 10.2 mm. The surface is denoted with a fat, black line. The O_2 concentration is expressed on a linear color scale with 256 colors.

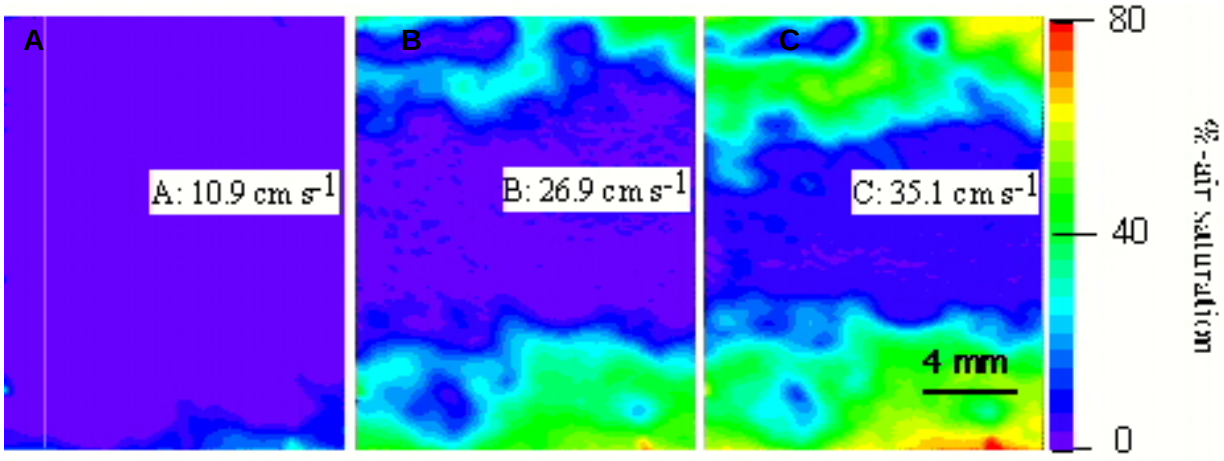

Figure 2-5. Oxygen images at the base of a 13 days old biofilm (growing on the bottom of a flow chamber) at flow velocities of 10.9 cm s^{-1} (A), 26.9 cm s^{-1} (B), and 35.1 cm s^{-1} (C). The oxygen concentration is expressed on a linear color scale of 256 colors.

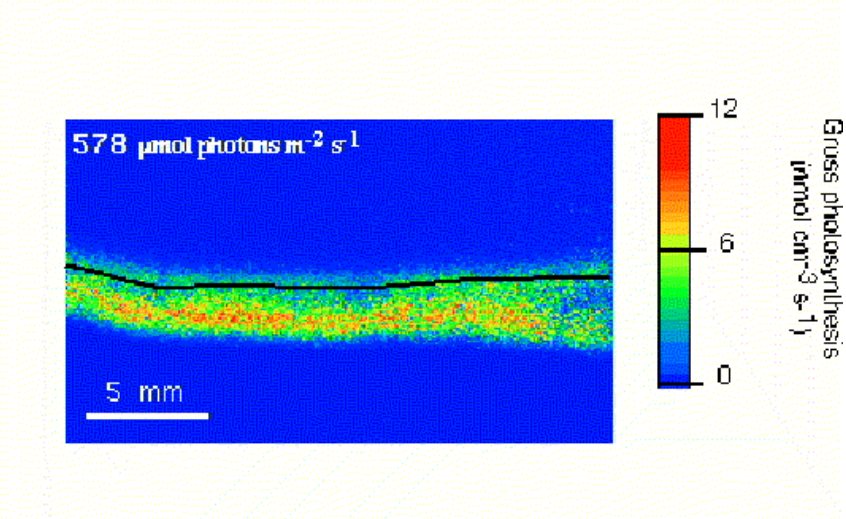

Figure 2-6. Gross photosynthetic rates determined by the light-dark shift technique (Revsbech and Jørgensen ,1983) at irradiance of 578 µmol photon m^{-2} s^{-1}. The thick horizontal line indicates the position of the mat surface.

400-µm thick, 13-d-old biofilm is shown in Figure 2-5. As flow increased from 6.2 to 35.1 cm s^{-1}, the average O_2 saturation increased from 0 to 23.1%.

Some areas of the biofilm were more sensitive to changes in flow velocities than others (Figure 2-5). Flow-sensitive sites coincided with voids of anoxic 'islands' cell clusters as observed through a stereomicroscope. The complex structure ensured efficient nutrition to the base of the film and the community as such (Costerton et al. 1994, de Beer at al. 1994). Due to the high spatial heterogeneity of biofilms it is normally not appropriate to study them with microsenors. One alternative is to use planar optodes.

Very recently Glud et al. (in press b) applied planar oxygen optodes in a comparable experimental set-up to study gross and net photosynthesis in a heterogeneous cyanobacterial mat. The gross photosynthetic rates of the mat were determined by applying the light-dark-shift technique to the mat (Revsbech and Jørgensen 1983; Glud et al. 1992). The gross rates showed a surface layer with low

activity and a deeper horizon dominated by micro colors with a relatively high activity (Figure 2-6).

2.4. The new System

2.4.1. Materials and Methods

To overcome heterogeneity in sensors and light field, a pixel by pixel calibration was also applied in this set-up. In case of lifetime imaging, intensity variations due to photobleaching or variable indicator concentrations is negligible since the decay rate of fluorescence is independent of, for example, fluorochrome concentrations (Holst et al. 1998). This new system, still under development, consists of a fast-gated CCD camera (SensiMod PCO) with an electronic-operated on-chip shutter and a blue excitation light source (Figure 2-7).

Two different light sources have been used, a combination of 8 blue-light emitting diodes (LED, BP280CWPB1K, DCL Components Limited) or a Xenon flashlamp (A0021F, Oxygen Enterprise) combined with a blue bandpass filter. A close to homogeneous light field was created by a fiberoptic ring light (light spot of 50 mm diameter at a distance of 50 mm from the ring light, Schölly Fiberoptic GmbH). The ring was mounted in a light tight housing in front of the camera and connected to the light source (Holst et al. 1998). The area covered by one image is approximately 32 mm x 24 mm and corresponds to a theoretical spatial resolution of 50 μm^2 per pixel. As for the old system, applying other optics can change both the covered area and the spatial resolution.

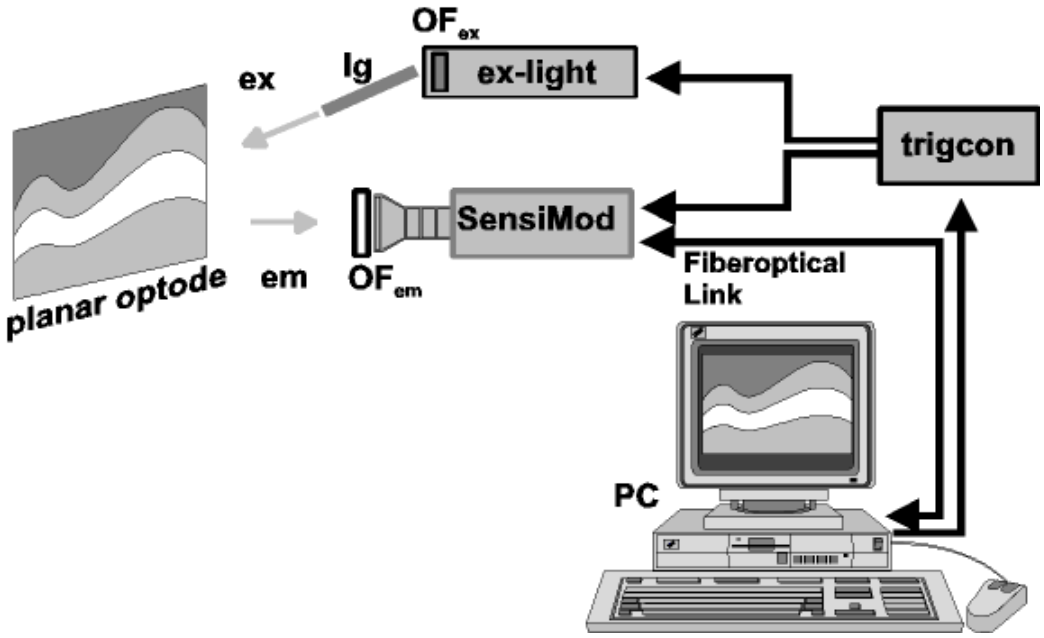

Figure 2-7. Schematic drawing of the imaging system combined with a planar optode. The imaging system consists of a CCD camera, a PC, and a trigger control unit working together with an excitation light source, optical filters (OF), and a ring light as light guide (lg).

The camera is connected to a PC, which is the controlling unit for image acquisition, storage, display and timing. To ensure a precise timing of excitation light source switching and image acquisition, essential for accurate lifetime measurements, the PC adjusts the necessary timing signals via a connected pulse-delay generator (DG535, SRS Stanford Research Systems) as described in detail by Holst et al. (1998). A schematic drawing of the set-up is shown in Figure 2-7.

Concurrent with the improvement of the technical part of the system, the matrix of the planar oxygen optode has been improved. An organically modified sol-gel matrix is in part characterized by the pore size and its water insolubility (Hoshino and Mackenzie 1995; McEvoy, McDonagh and Mc Craith 1996). During the sol-gel process, hydrolysis and polycondensation reactions of silica alkoxides take place,

allowing the preparation of a unique, noncrystalline material with tunable properties. Matrices with high oxygen permeability and a hydrophobic character can be obtained by varying the sol-gel process.

Adding substituted organic precursors induce flexibility and lower brittleness of the matrix. The preparation of the organically modified sol-gel was further improved to achieve a long term stability and foil homogeneity, overcoming the main problems of plasticized PVC-based sensors.

For preparation of the planar optode, the fluorescence dye Ru-DPP (1% wt) was dissolved with scattering particles (33% wt) in the sol-gel matrix (66% wt) and spread as a thin layer (~10 µm after solvent evaporation) on a polyester foil (125 µm) as described by Glud et al. (1996). In contrast to Glud et al., this oxygen sensor has been applied without optical insulation. Because of the milky appearance of the sensor, caused by the scattering particles, the measurements are not affected by scattering from sediment particles (data not shown). While taking an intensity image, the excitation light is switched on for < 1 ms. During such short exposure, it is unlikely for photosynthetic oxygen stimulation within the sample to occur (Holst et al. 1995).

2.4.2. Measurements in bioirrigated sediments

The newly developed imaging system was applied in the intensity mode and calibrated as described above. The very first data of the new measuring device was obtained from a microbial mat sampled at shallow water depth at Gullmars Fjord (Sweden). At the sampling location the bottom water was practically stagnant. The sample, taken by a core with a flat glass window, was kept at *in-situ* conditions. Two-dimensional oxygen distributions were measured during a 24-h cycle. During

recording, the core and the measuring set-up was maintained outside the laboratory so that the sample was exposed to natural irradiance.

Oxygen distributions within the mat at 1:00 p.m. and at 1:00 a.m., respectively are shown in Figure 2-8. The original size of the observed area is 12.5 mm x 18.5 mm, and the surface is approximately at the level of 14 mm (Figure 2-8). The different oxygen penetration depths of the two mats reflected the effect of the two light extremes. In daylight, high levels of oxygen super saturation were observed in the mat at a depth of approximately 4 mm. The overlying water was supersaturated. At night, high O_2 values were only observed closed to the mat surface, while the

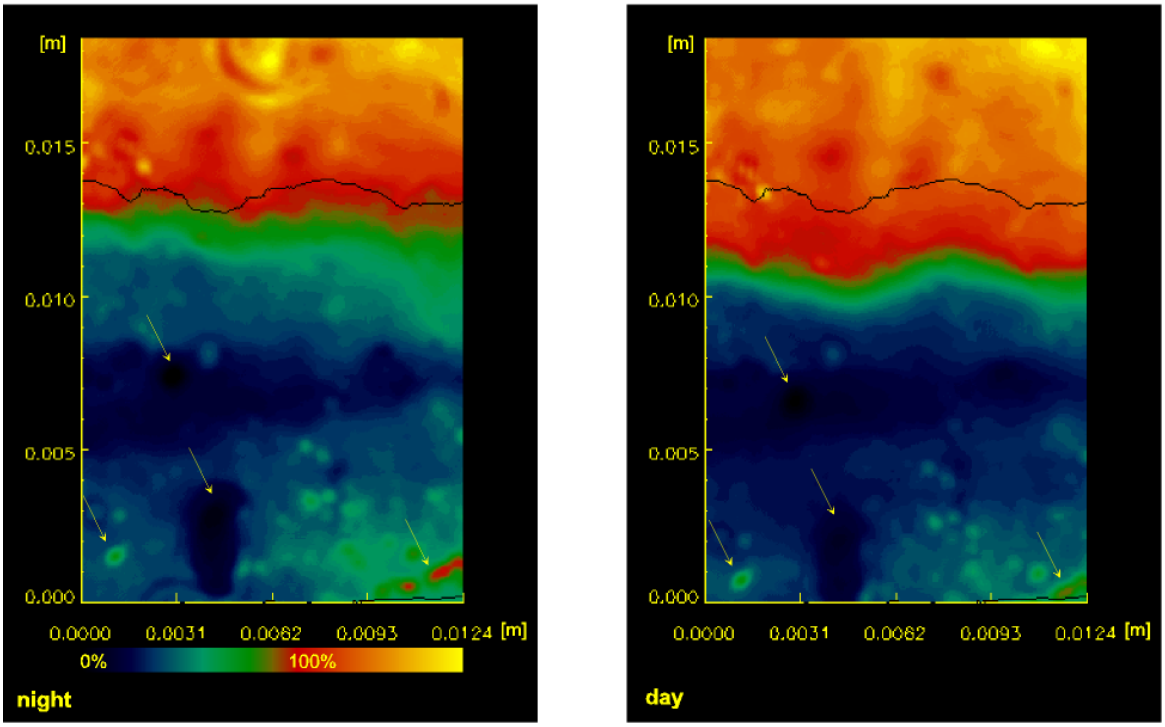

Figure 2-8. Images of the oxygen distribution in the fjord mat during a 24 h cycle at 1:00 a.m. (day) and 1:00 p.m. (night). The image represents an area of 12.5 x 18.5 mm with a spatial resolution of 50 µm. The surface is denoted as thick, black line and the O_2 concentration is expressed in a linear color scale of 256 colors. The dots marked with arrows are insensitive spots or sand grains between sensor foil and glass window.

overlying water was still supersaturated. In contrast to Glud et al (1996), a relief picture (in the way of a contrast picture of the surface) was taken to detect the surface of the mat.

Non-sensitive spots in the planar optode or sand grains between the sensor and the core wall most likely caused the small dots (marked with arrows) that were visible in the images. Non-sensitive sites could result from evaporation of the solvent out of the sensing matrix. In the future, applying other solvent mixtures and a more homogeneous spreading of the matrix-dye mixture will minimize this effect.

2.5. Future plans

In the near future, we will optimize measurements in a luminescence decay-rate based mode. Further plans are to develop planar sensors for other chemical variables, for example, pH and CO_2 and to combine several fluorochromes in one sensor for fast detection of multiple chemical parameters. A pH planar optode could work based on a fluorescence indicator with a pH-sensitive adsorption maximum in the visible part of the spectrum and a nearby pH-independent wavelength. The second wavelength can be used as referencing system (Kohls et al. 1997). Developments at modular and flexible *in-situ* use (for example, benthic landers) will be initiated.

There are also plans to detect concentration changes continuously over time as has been done by Glud et al. (1998b).

2.6. Acknowledgments

We acknowledge the financial support from the European Commission (Microflow CT 970078) and the Max-Planck Society.

2.7. Literature Cited

Aller, R. C., P. O. J. Hall, P. D. Rude, J. Y. Aller, 1998. Biogeochemical heterogeneity and suboxic diagenesis in hemipelagic sediments of the Panama Basin, *Deep Sea Research*, 45: 133-165.

Bacon, J. R. and J. N. Demas, 1987. Determination of Oxygen Concentrations by Luminescence Quenching of Polymer Immobilised Transition-Metal Complex, Analytical Chemistry, 59: 2780-2785.

Costerton, J. W., Z. Lewandowski, D. de Beer, D. Caldwell, D. Korber and G. James, 1994. Biofilm the Customised Microniche, Journal of Bacteriology, 176: 2137-2142.

De Beer, D., P. Stoodley, F. Roe and Z. Lewandowski, 1994. Effects of biofilm Structures on Oxygen Distribution and Mass Transport, Biotechnology and Bioengineering, 43: 1131-1138.

Glud, R. N., N. B. Ramsing and N. P. Revsbech, 1992. Photosynthesis and Photosynthesis Coupled Respiration in Natural Biofilms Quantified with Oxygen Microsensors, Journal of Phycology, 28: 51-60.

Glud, R. N., N. B. Ramsing, J. K. Gundersen and I. Klimant, 1996. Planar Optodes: a New Tool for Fine Scale Measurements of Two-dimensional O2 Distribution in Benthic Communities, Marine Ecology Progress Series, 140: 217-226.

Glud, R. N., O. Holby, F. Hofmann, D. E. Canfield, 1998a. Benthic Mineralisation in Arctic Sediments (Svalbard), Marine Ecology Progress Series, 173: 237-251.

Glud, R. N., C. M. Santegoeds, D. de Beer, O. Kohls and N. P. Ramsing, 1998b. Oxygen Dynamics at the Base of a Biofilm Studied with Planar Optodes, Aquatic Microbial Ecology, 14: 223-233.

Glud, R. N., I. Klimant, G. Holst, O. Kohls, V. Meyer, M. Kuehl, J. K. Gundersen, in press a. Adaptation, Test and In Situ Measurements with O2 Microoptodes on Benthic Landers, Deep Sea Research.

Glud, R. N., M. Kuehl, O. Kohls, N. B. Ramsing, in press b. Heterogeneity of Oxygen Production and Consumption in a Photosynthetic Microbial Mat as Studied by Planar Optodes, Journal of Phycology.

Hartmann, P. and W. Ziegler, 1996. Lifetime Imaging of Luminescent Oxygen Sensors Based an All-Solid-State Technology, Analytical Chemistry, 68: 4512-4514.

Holst, G., M. Kühl and I. Klimant, 1995. A novel Measuring System for Oxygen Microoptodes based on a Phase Modulation Technique, SPIE Proceedings, 2508:387-398.

Holst, G., R. N. Glud, M. Kuehl, I. Klimant, 1997. A microoptode array for fine-scale measurements of oxygen distribution, Sensors and Actuators B, 38-39: 122-129.

Holst, G., O. Kohls, I. Klimant, B. Koenig, M. Kuehl and T. Richter, 1998. A Modular Luminescence Lifetime Imaging System for Mapping Oxygen Distribution in Biological Samples, Sensors and Actuators B, 51/1-3: 163-170.

Hoshino, Y. and J. D. Mackenzie, 1995. Viscosity and Structure of Ormosil Solutions, Journal of Sol-Gel Science and Technology, 5: 83-92

Jørgensen, B. B., D. Des Marais, 1990. The Diffusive Boundary Layer of Sediments: Oxygen Microgradients over a Microbial Mat, Limnological Oceanography, 35: 1353-1355.

Kautsky, H., 1939. Quenching of luminescent by oxygen, Faraday Society, 35: 216-219.

Klimant, I., V. Meyer and M. Kuehl, 1995. Fibre-optic Microsensors, a new Tool in Aquatic Biology, Limnological Oceanography, 40: 1159-1165.

Kohls, O., I. Klimant, G. Holst and M. Kühl, 1997. Development and Comparison of pH Microoptodes for Use in Marine Systems, SPIE Conference on Progress in Biomedical Optics, 2978: 82-91.

Kuehl, M., Y. Cohen, T. Dalsgraad, B. B. Jørgensen and N. P. Revsbech, 1995 Microenvironment and Photosynthesis of Zooxanthellae in Scleractinian Corals Studied with Microsensors for O2 pH and Light, Marine Ecology Progress Series, 117: 159-172.

McEvoy, A. K., C. M. McDonagh and B. D. MacCraith, 1996. Dissolved Oxygen Sensor Based on Fluorescence Quenching of Oxygen-Sensitive Ruthenium Complexes Immobilised in Sol-Gel-derived Porous Silica Coatings, Analyst, 121: 785-788.

Preininger, C., I. Klimant and O. S. Wolfbeis, 1994. An Optical Fibre Sensor for Biological Oxygen Demand, Analytical Chemistry, 66: 1841-1846.

Revsbech, N. P., J. Sørensen, T. H. Blackburn and J. P. Lomholt, 1980. Distribution of Oxygen in Marine Sediments Measured with Microelectrodes, Limnological Oceanography, 25: 403-411.

Revsbech, N. P. and B. B. Jørgensen, 1983. Photosynthesis of Benthic Microflora Measured by the Oxygen Microprofile Method: Capabilities and Limitations of the Method, Limnological Oceanography, 28: 749-756.

Stern, O. and M. Volmer, 1919. Ueber die Abklingzeit der Fluoreszenz, Physikalische Zeitschrift, 20: 183-188.

Chapter 3

Published in Marine Chemistry

November 2005

3. Fabrication and test of sol-gel based planar oxygen optodes for use in aquatic sediments

Bettina Koenig[1], Oliver Kohls[1], Gerhard Holst[1], Ronnie N. Glud[2], Michael Kühl[2,*]

[1]Max-Planck-Institute for Marine Microbiology, Celsiusstr. 1, D-28359 Bremen, Germany

[2]Marine Biological Laboratory, University of Copenhagen, Strandpromenaden 5, DK-3000 Helsingør, Denmark

*corresponding author, Fax: +45 3532 1950, e-mail: mkuhl@bi.ku.dk

Abstract

We describe the fabrication of organically modified sol-gel (ORMOSIL) planar optodes for mapping the two-dimensional oxygen distribution in sediments. All sensor foils were based on the use of ruthenium(II)-tris-(4,7-diphenyl-1,10-phenantrolin)-perchlorate, which is a fluorescent dye quenched dynamically by oxygen. Sensors made with different sol-gel immobilisation matrices, different concentrations of precursors and indicator dye, as well as different types of scattering particles co-immobilized in the sensor foil were investigated systematically. Optimal sensor performance was obtained with dye concentrations of 2-10 mmol/kg in an immobilisation matrix made of diphenyldiethoxy-silan and phenyltriethoxy-silan precursors with addition of organically coated TiO_2 particles. The sensors exhibited a good mechanical stability and a high sensitivity from 0 to 100% oxygen, which remained constant over at least 36 days. The planar optodes were used with a fluorescent lifetime imaging system for direct mapping of the spatio-temporal variation in oxygen distribution within marine sediment inhabited by the polychaete *Hediste diversicolor*. The measurements demonstrated the spatio-temporal heterogeneity of the oxygen distribution in bioturbated sediments due to burrow structures and non-constant irrigation activity of the polychaete, which is difficult to resolve with microsensors or with traditional biogeochemical techniques.

3.1. Introduction

Optical sensors for oxygen, pH and CO_2 measurements in aquatic environments have been developed over the past 5-10 years and represent a good alternative to electrochemical sensors (Holst et al. 2000). In particular fiber-optic microsensors (microoptodes) for oxygen (Klimant et al. 1995) have been applied in biogeochemical studies for both laboratory and *in-situ* measurements (e.g. Glud et al. 1999a, Wenzhöfer et al. 2000, Mock et al. 2002). However, microsensors allow only for a limited amount of point measurements that cannot fully resolve the inherent spatiotemporal heterogeneity in sediment structure and oxygen distribution, especially in bioturbated sediment. The recent development and application of optical sensor foils (planar optodes) and imaging systems now enable microscale measurements of oxygen distribution in two-dimensions (Glud et al. 1996, Holst et al. 1998, 1999, Liebsch et al. 1999). However, a detailed description of the production and evaluation of planar oxygen optodes is still lacking.

Optical oxygen sensors can be made with different oxygen sensitive dyes and immobilisation matrices causing differences in e.g. sensor response time, oxygen sensitivity, and photostability. Important design criteria for planar optodes to be used in environmental applications are 1) good hydrophobicity, 2) solid adhesion to the supporting foil, 3) homogeneity of the sensor foil, and 4) long term stability against bleaching, ageing and biodegradation. Furthermore, the oxygen permeability of the applied immobilisation polymer is of major concern for the development of planar oxygen optodes.

Organically modified sol-gels (so-called *ORMOSILs*) are transparent, tolerate high temperatures, and are not biodegraded. *ORMOSILs* have previously been used as immobilization matrix for various optical sensors (Iwamoto and Mackenzie 1995, Lev et al 1995, Shahriari et al 1997), including well-functioning oxygen microsensors

(Klimant et al. 1999). The sol-gel formation is based on i) hydrolysis of the precursors, ii) condensation and densification of the hydrolysed precursors, and iii) drying of the matrix material. The properties of the resulting polymers are highly sensitive to environmental conditions like pH and temperature as well as the applied solvent. Furthermore, the choice of precursor affects the properties of the resulting sol-gels and numerous different types of organically modified sol-gels have been described in the literature (e. g. Liu et al 1992, McEvoy et al 1996). Phenyl-substituted precursors generally result in sensor foils with good hydrophobicity and a high photostability of the incorporated dye. The O_2 sensitivity of the sensor foils is mainly influenced by the hydrophobicity and the pore size of the matrix, both of which can be adjusted by varying the ratio of alkoxy- and phenyl-substituted groups of the precursors.

The measuring principle used with planar optodes is based on the dynamic quenching (Stern and Volmer 1919, Kautsky 1939) of ruthenium(II) 4,7-diphenyl-1,10- phenantroline (Ru-DPP) fluorescence by oxygen (Hartmann and Leiner 1995). The oxygen dependent quenching can be quantified by a modified Stern-Volmer-Equation (Bacon and Damas 1987, Carraway et al 1991):

$$\frac{I}{I_0} = \frac{\tau}{\tau_0} = \left[\frac{a}{(1 + Ksv * c)} + (1 - a) \right] \quad (1)$$

The equation shows the relation between oxygen concentration, *c*, the fluorescence intensity, *I*, and the lifetime, τ, respectively. The lifetime is defined as the average fluorescence lifetime of the excited state of the dye assuming mono-exponential decay. I_0 is the maximal fluorescence and τ_0 the lifetime in the absence of oxygen, K_{sv} is a constant expressing the quenching efficiency of the fluorophore, and *a* is the non-quenchable fraction of the fluorescence. Both K_{sv} and *a* are affected

by the choice of the immobilisation polymer. The non-quenchable fraction can be considered constant for similar *ORMOSIL*s with similar dye concentration (Klimant et al. 1999). Once the calibration curves are obtained the parameter *a* in Eq. (1) can thus be determined for a calibration curves are obtained the parameter a in Eq. (1) can thus be determined for particular *ORMOSIL*/dye mixture. Thereafter, two variable parameters remain in Eq. (1), i.e. K_{SV} and I_0 (or τ_0), and these can be determined from a simple two-point calibration (see details in Holst et al. 1998).

According to Eq. (1), optical oxygen measurements can be based on either fluorescence intensity or lifetime measurements. First applications of planar oxygen optodes were based on fluorescence intensity imaging (Glud et al. 1996). Fluorescence lifetime is, however, a more robust parameter for optical quantification of oxygen, as the measuring signal is independent of the absolute fluorescence intensity. Therefore some potential artefacts can be avoided (see also Holst et al. 1995, 1998) and transparent or semi-transparent planar optodes can be used (Holst and Grunwald 2000). Fluorescence intensity based sensing often appears to have a better signal to noise ratio, but such measurements require a sensor layer that is oxygen permeable and optically dense (e.g. made of black silicone) leading to a slower response time and elimination of the possibility to observe the sample through the optode. However, the preferred measuring scheme depends on the given application (e.g. Glud et al. 1999b). Fluorescent lifetimes can be determined by phase-modulation techniques (Holst et al. 1995) or by direct determination of the fluorescence lifetime by measuring fluorescence in defined time windows after an excitation light pulse (Holst et al. 1998). The lifetime imaging system used in this study uses the latter approach.

The goals of this study were i) to develop and optimise planar optodes for oxygen, which are well suited for application in sediments, and ii) to demonstrate the potential

of the new planar optodes for studies in bioturbated marine sediments. We present detailed fabrication details and a systematic investigation of optodes made with various sol-gels materials. Optimised planar optodes were used for measurements of oxygen dynamics around a *Hediste diversicolor* burrow in coastal marine sediment.

3.2. Material and methods

3.2.1. Synthesis of the ORMOSILs

Three different *ORMOSIL* matrices were fabricated from silicon alkoxide- and organylalkoxy-silanes precursors with one to three oxide-bound functional groups. The precursors were converted to *ORMOSILs* via acid catalyzed hydrolysis and poly-condensation reactions (Figure 3-1), followed by a temperature controlled densification process (Brinker 1988).

The first series of *ORMOSILs* were prepared from the precursors diphenyldiethoxy-silan (DDOS; Merck, Germany) and trimethoxymethyl-silan (denoted as TOMS; Merck, Germany) with an increasing concentration of TOMS versus DDOS (Table 1). A known amount of DDOS (denoted *m* in Table 1) was added to 6.42 ml Ethanol (0.11 mol) and 2.1 ml 0.1N Hydrochloric Acid (0.21 mmol) (Merck, Germany), which acted as a catalyst (Liu et al 1992, Klimant et al 1999). In all experiments, the solution became turbid upon catalyst addition but then turned transparent after a few minutes. Subsequently, the solution was quickly heated to 60°C under reflux condensation for 120 min. The temperature stabilized at 60°C ± 3° C within 5 min after the reflux was started. Special care was taken to obtain homogeneous solutions by applying rigorous stirring. After the heating was stopped

various amounts of TOMS (denoted *x* in Table 1) were added followed by further stirring at room temperature for 30 min. The solution was then poured into de-ionized water and left for phase separation at room temperature over night. The following day, the viscous polymer oil was separated and dried at 200°C. The drying process was stopped after 24 hours, and the cold sol-gel was pulverized before further use.

A second series of *ORMOSILs* was made with phenyltriethoxysilan (PTS; Merck, Germany) and methoxytrimethysilan (MOTS; Merck, Germany) under identical experimental conditions concerning amount of solvent, catalyst, heating and drying conditions, as used in the first series (Table 2). Additionally, the effect of using different reflux times, i.e. 30, 60 or 90 minutes, was studied.

Table 1. Composition of the *ORMOSIL* series 1 matrices. The precursors diphenyldiethoxysilane (DDOS) and trimethoxysilan (TOMS) were used to synthesize the organically modified sol-gel series 1 (OMS 1). In the second and third columns the experimental concentrations are given while the last column contains the TOMS:DDOS molar ratio.

OMS	DDOS	TOMS	TOMS/DDOS
type no.	Mass		Molar ratio (mol TOMS/mol DDOS)
	m (mmol)	*x* (mmol)	$\underline{x}$
1.1	25.3	0	0
1.2	25.0	0.6	0.02
1.3	25.0	1.0	0.04
1.4	28.4	3.1	0.11
1.5	28.4	5.0	0.18
1.6	16.7	3.4	0.20
1.7	25.0	7.0	0.28
1.8	25.0	9.6	0.38

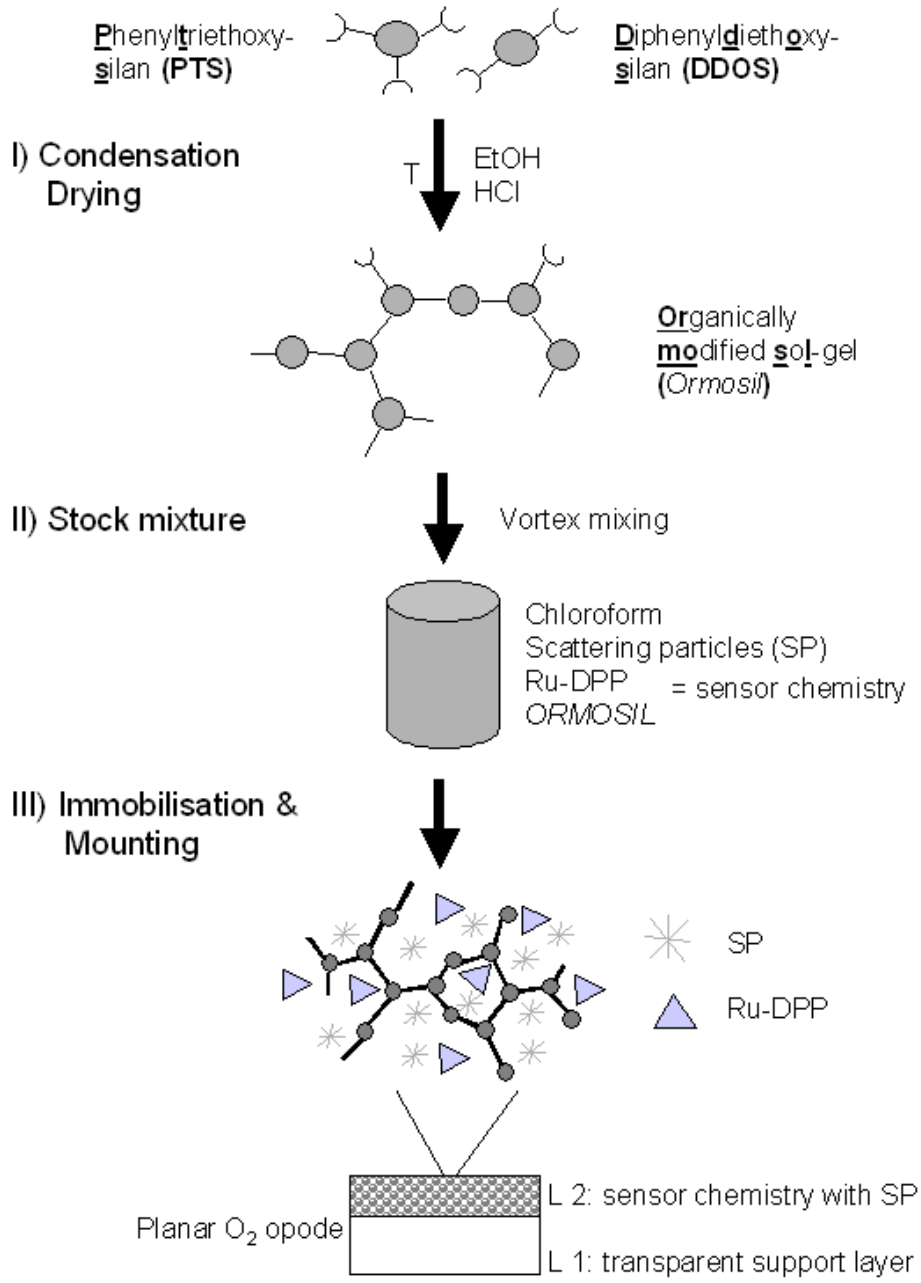

Figure 3-1. Scheme for the synthesis of *ORMOSIL* based planar O_2 optodes: I) Condensation and drying of the precursors PTS and DDOS. II) Stock mixture preparation consisting of the solvent chloroform, scattering particles (SP), the fluorescence dye (Ru-DPP), and the *ORMOSIL.* III) Immobilisation of the sensor chemistry (=L2; final thickness after hardening ~10 µm), and mounting on a transparent support layer (=L1; thickness ~100 µm).

Table 2. Composition of the ORMOSIL series 2 matrices. The second series of ORMOSILs (OMS 2) were prepared from phenyltriethoxysilan (PTS) and methoxytrimethylsilan (MOTS). The reflux time was varied for the fabrication of OMS 2.2. In the second and third columns the experimental concentrations are given while the last column contains the MOTS:PTS molar ratio.

OMS	PTS	MOTS	MOTS/PTS	Reflux time
type no.	Mass		Molar ratio (mol MOTS/mol PTS)	
	m (mmol)	*x* (mmol)	$\underline{x}$	
2.1	25.0	0	0	
2.2 a	26.0	1.8	0.07	30 min
2.2 b	26.0	1.8	0.07	60 min
2.2 c	26.0	1.8	0.07	90 min
2.2 d	26.0	1.8	0.07	120 min
2.3	25.0	2.5	0.10	
2.4	26.0	3.6	0.14	
2.5	25.0	5.0	0.20	
2.6	26.0	7.3	0.28	

Finally, a third series of *ORMOSIL* matrices were made from the two components DDOS and PTS with increasing ratios of PTS to DDOS (Table 3). In this case the two precursors were added at once and dissolved in 5.83 ml ethanol (0.1 mol). Thereafter, 2.3 ml 0.1N HCl (0.23 mmol) was added under vigorous stirring. The reflux time and temperature were the same as in series one. Although nothing was added to the solution after the heating was stopped, the solution was stirred for 20 min at room temperature. The final steps were undertaken under identical conditions as in series one.

Table 3. Composition of the *ORMOSIL* series 3 matrices. The third series of *ORMOSIL*s (OMS 3) were fabricated from the two components diphenyldiethoxysilan (DDOS) and phenyltriethoxysilan (PTS). In the second and third columns the experimental concentrations are given while the last column contains the molar ratio of PTS to the base of the molar sum of DDOS and PTS. The DDOS ratio is given by one minus the PTS ratio.

OMS	PTS	DDOS	PTS
type no.	Mass		Molar ratio (mol DDOS/ mol DDOS+PTS)
	m (mol)	*x* (mol)	$\underline{m}$
3.1	25.0	0	1
3.2	22.6	2.5	0.9
3.3	20.0	5.0	0.8
3.4	17.6	7.5	0.7
3.5	15.1	10.0	0.6
3.6	12.5	12.5	0.5
3.7	9.9	14.9	0.4
3.8	7.5	17.6	0.3
3.9	5.0	20.0	0.2
3.10	2.5	22.7	0.1
3.11	0	25.3	0

3.2.2. Synthesis of the fluorescence dye

225.9 mg $RuCl_3*H_20$ (Fluka, Germany) were diluted in 5 ml ethylene-glycol (Fluka, Germany) and 0.5 ml de-ionized water, and then heated to 160° C under reflux condensation. At 120° C 1.06 g of the ligand 4,7-diphenyl-1,10-phenantrolin (also known as batho-phenantrolin; Fluka, Germany) was added. The mixture was heated for another 45 minutes, cooled, and then 50 ml acetone (Fluka, Germany) was poured into the cold solution. The mixture was filtered through a G4 glass filter and the filtrate then contained the ligand-substituted ruthenium complex. To precipitate the ruthenium complex as a perchlorate salt, 50 ml perchloric acid (1N; Fluka,

Germany) were added to 10 ml of the filtrate. Finally, the ruthenium complex salt was re-crystallized to gain pure ruthenium (II) tris (4,7-diphenyl-1,10-phenantrolin) perchlorate (denoted as Ru-DPP). A more detailed description of the synthesis is given elsewhere (Klimant 1993, Klimant et al. 1999).

3.2.3. Preparation of the planar oxygen optode

Planar optodes with and without light scattering particles (denoted as SP) incorporated in the dye-*ORMOSIL* matrix were fabricated. A stock sensor solution was prepared by dissolving varying amounts (0.4-16.5 mg) of Ru-DPP and 250 mg *ORMOSIL* in 1 ml chloroform (Merck, Germany). After addition of scattering particles, the mixture of sensor solution and scattering particles was homogenized by Vortex mixing for two hours (Klimant et al 1999).

Oxygen sensors based on *ORMOSIL* 3.2 were fabricated with dye concentrations of 1, 2, 5, 10, 20, and 50 mmol/kg, respectively, in order to identify the optimal dye concentration for planar optodes. Furthermore *ORMOSIL* 3.10-based planar optodes were fabricated with different types of scattering particles made of TiO_2 (Merck, Germany), $BaSO_4$ (Merck, Germany), lipophilized $BaSO_4$, Pigment A (coated TiO_2, Kronos, Germany), or Pigment B (coated TiO_2, Kronos, Germany) in order to find the optimal type of scattering material.

Planar optodes were fabricated by spreading the sensor cocktail on a 125 µm thick transparent polyester foil (Mylar, Goodfellow, Great Britain) (for a schematic drawing see Figure 3-1). For this, the polyester foil was fixed to a flat stainless steel plate by generating vacuum from below. The sensor cocktail was then applied to the foil and spread in a thin layer using a sharp knife-like metal device. The layer thickness was regulated with spacers so that the knife moved ~100 µm over the surface of the foil.

After evaporation of the solvent (at least 24 h at room temperature) the sensor layer had a final thickness of approximately 10 µm.

3.2.4. Characterization of planar oxygen optodes

Measuring characteristics of the planar optodes were determined by calibration measurements in water flushed with defined mixtures of nitrogen and oxygen. Two-point calibrations were performed from readings within air saturated water and N_2 flushed water. For first characterizations of the optodes, we used a fiber-optic instrument for measuring fluorescent lifetimes via the phase-modulation method (described in Holst et al. 1995). With this method, the dye in the planar optode is excited with sinusoidal modulated light and therefore emits sinusoidal modulated light with a certain delay. The delay causes a shift in the phase angle (ϑ) between excitation and emission allowing the determination of the lifetime (see below). The applied setup consisted of a two-phase lock-in amplifier (Stanford Research Instruments, SR 830, USA), which controlled both the excitation source (a 470 nm LED, Nichia, Japan, equipped with a Schott BG12 glass filter) and the detector (a photodiode, Hamamatsu/S5821-01 equipped with a Schott OG590 glass filter). Light was guided to and from the planar optode via a bifurcated optical fiber (AMS Optotech, Germany). The emitted fluorescence signal was referenced to a red-colored foil (fire red, Conrad Electronics, Germany). After analogue and digital signal processing, the oxygen dependent fluorescence signal was recorded as a phase angle, i.e. the phase shift between the two sinusoidal signals. From this phase angle, ϑ, and the modulation frequency, *f* (here 45kHz), the fluorescence life time, τ, was calculated according to

$$\tau = \frac{\tan(\vartheta * \pi / 180)}{2 * \pi * f} \qquad \text{(Eq. 2)}$$

A more detailed characterization of sensor foils was done with a modular luminescence lifetime imaging system (described in Holst et al. 1998). The experimental set-up (Figure 3-2) consisted of a fast gate-able CCD camera (SensiMod VGA, PCO, Germany) and a blue excitation light source, which was either an array of 8 blue light emitting diodes (470 nm LED, DCL Components Ltd., UK) or a Xenon flash lamp (Oxygen Enterprises, USA). Homogeneous illumination of the planar optode was realized with a fiber optic ring light (Schölly Fiberoptic GmbH; Germany) coupled to the excitation light source. The ring light was mounted in a light-tight housing in front of the camera and connected to the light source via a fiber-optic cable (Hartmann and Ziegler 1996, Holst et al. 1998).

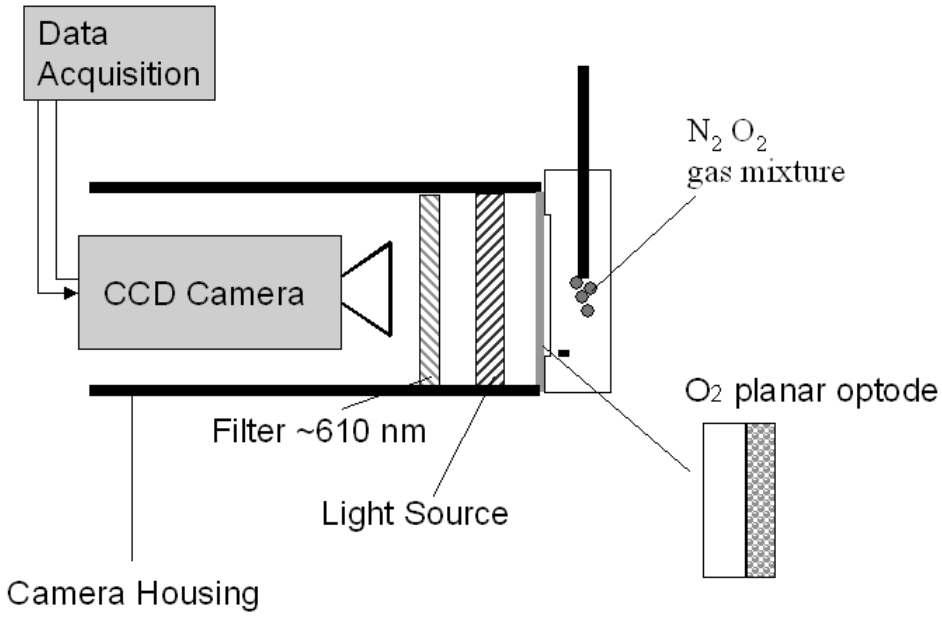

Figure 3-2. Schematic drawing of the imaging system with camera housing, filter, light source and data acquisition device. The experimental chamber equipped with an O_2 planar optode was flushed with defined mixtures of N_2 and O_2. The walls of the chamber were darkened.

In this study, the images covered an area of 2.6 x 2.5 cm^2, corresponding to a spatial resolution of 50 x 50 μm^2 per pixel. However, the spatial resolution can easily be changed by modification of the optical configuration in front of the CCD camera. A pulse-delay generator (SRS-DG535, Stanford Research, USA) controlled the triggering of excitation light and image acquisition. All instruments were controlled by custom-made software (see Holst and Grunwald 2000). Image analysis and calibration were done with self-made programs in the software package IDL (Research Systems Inc., USA). A detailed description of the data acquisition and post-processing procedures are presented elsewhere (Holst and Grunwald, 2000).

3.2.5. Measurements of O_2 distribution around worm burrows

The planar optodes with the best measuring characteristics were used to make measurements of O_2 distribution in sediment surrounding burrows of the polychaete *Hediste diversicolor*. The sediment and small specimens of *H. diversicolor* were retrieved from Helsingør Harbour, Denmark. The sediment was sieved and transferred to a self-made flow chamber (4 x 100 x 40 mm) equipped with a planar oxygen optode (Figure 3-3). The planar optode covered an area of 2.6 x 2.5 cm^2 yielding a pixel resolution of approximately 50 x 50 μm^2. The flow chamber was mounted in front of the camera housing and was shielded against ambient light on all other sides in order to prevent stimulation of photosynthetic oxygen production and optical interferences. Aerated water kept at constant salinity (30) and temperature (23ºC), was circulated at constant flow velocity through the flow chamber during the experiments. One specimen of *H. diversicolor* was added to the flow chamber and the polychaete was allowed to establish a burrow and to acclimate to the

experimental conditions overnight before pictures of the oxygen distribution were recorded.

The experiments were performed with 3 different specimens of *H. diversicolor.* The polychaetes were kept for 2 – 3 days in the chambers without feeding in order to limit bacterial growth within the chamber and tubing, which would affect the O_2 measurements. With every specimen up to 10 trials were performed with intervals of 1 min, 2 min, 3 min, and 10 min between the images. The trials lasted from 10 min to 3 hours. The images presented here show the most spectacular events.

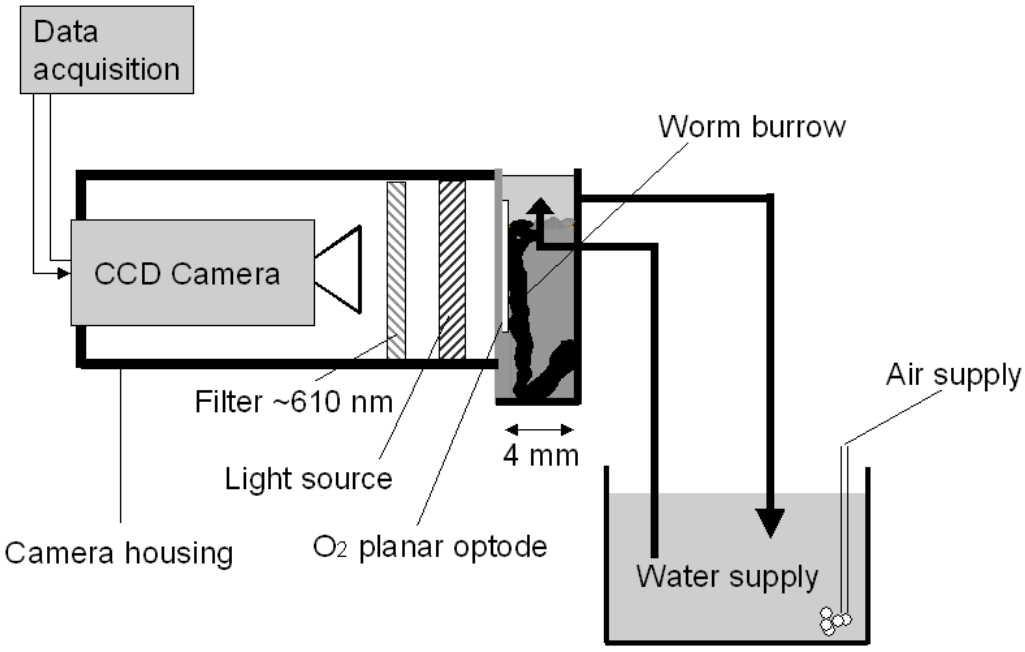

Figure 3-3. Schematic drawing of the imaging system with camera housing, filter, light source and data acquisition device. The experiment chamber equipped with an O_2 planar optode was filled with sediment inhabited by one specimen of *H. diversicolor*. The chamber was constantly supplied with fresh aerated seawater at constant temperature and salinity. The walls of the chamber were darkened.

The diffusive oxygen uptake (DOU) was calculated from O_2 images by Fick's first law of diffusion. According to Fick's first law of diffusion the vertical flux of O_2 through the sediment surface, J_V can be calculated as

$$J_V = -\phi * D_S * \left(\frac{\partial C(z)}{\partial z} \right) \quad \text{(Eq.3)}$$

where ϕ is the porosity (here 0.34 vol/vol) of the sediment, D_S is the tortuosity, temperature and salinity corrected diffusion coefficient for O_2 in the sediment (Ullman and Aller 1982, Broecker and Peng 1974, Li and Gregory 1974), and ($\partial C/\partial z$) is the vertical gradient of O_2 just below the sediment surface. Equation 3 was also used to estimate the horizontal O_2-flux through the burrow wall (J_H) from horizontal oxygen gradients. These calculations assume steady state conditions around the burrow walls for the moment images were taken.

3.3. Results and discussion

3.3.1. Influence of precursor concentration on quenching and mechanical properties of optodes

Precursors and reaction conditions were partly chosen based on the findings of Carraway et al. (1991) and Murtagh et al. (1998). Their studies demonstrated that Ru-DPP exhibits improved quenching by oxygen when immobilised in materials of increasing hydrophobicity and oxygen permeability. Additionally, the increase of methyl groups in the *ORMOSIL*s lead to a better O_2 sensitivity at lower O_2 concentrations. Nevertheless, it was difficult to foresee the final polymerisation products. In case of the *ORMOSIL* series 1-3, the solvent concentration was high compared to the precursor concentration promoting intra-molecular reactions leading

to cyclic and short molecule chains (Hoshino and Mackenzie 1995). Furthermore, aromatic-groups can improve the photostability of oxygen-sensing materials and phenyl-substituted *ORMOSILs* enhance the solubility of the Ru-DPP dye in the matrix (Klimant et al 1999). Phenyl groups do not participate in the polymerisation process and they need more steric space than alkoxy groups leading to a less dense network formation in the *ORMOSIL* matrix.

We took advantage of these effects in our fabrication of optimised planar O_2 optode with high sensitivity. One measure of O_2 sensitivity is the signal width, i.e. the difference between $\tau(0)$ and $\tau(\text{air})$, of a planar oxygen optode, where $\tau(0)$ and $\tau(\text{air})$ denote the luminescence lifetime in oxygen free and fully aerated water, respectively. The signal width depends on the O_2 permeability of the polymer matrix and a steep slope in the calibration curve indicates a high O_2 permeability (Liu et al 1992). The O_2 signal width is also reflected in the lifetime ratio, $R = \tau(0) / \tau(\text{air})$, (Figure 3-4). For every stock solution of sensor material (see § 2.4) two similar planar optodes were prepared and characterised and each of these optode represent a single data point in Figure 3-4.

In the *ORMOSIL* series 1 material, DDOS had two hydroxy-groups capable of polymerisation. This promoted the formation of linear chains and the addition of a 'cross-linker' such as TOMS caused the formation of larger interconnected structures resulting in weak glass like polymers exhibiting a low O_2 sensitivity. Increasing the amount of interconnections (by increasing amounts of TOMS) yielded a harder polymer matrix but did not increase the O_2 sensitivity. No significant change in R was observed with O_2 sensors prepared from the *ORMOSIL* series 1 with varying molar ratios of the precursors (Figure 3-4A; Table 1). The R-values varied only between 1.1 and 1.2 although the amount of the 'cross-linker' TOMS was increased from 0 to 0.4 mol TMOS/mol DDOS. However, the optodes with high amounts of TOMS became

more brittle and less adhesive to the supporting foil. One reason for this could be the progressed self-condensation of DDOS, which reduces the chance for TOMS to form interlinks between the DDOS polymers. Thus the resulting molecule and matrix structures were not changed in their basic appearance. It is also likely that TOMS reacted with itself and formed its own dense structure, which fills in the larger structure of the DDOS polymers. This could also explain the low O_2 sensitivity.

The O_2 optodes prepared from the *ORMOSIL* series 2 were expected to show a decrease in their O_2 sensitivity with increasing molar ratio of MOTS yet were also expected to have a less brittle structure and show better adhesion to the support foil. Indeed, the optodes changed from a hard glassy consistency to a soft polymer structure with increasing amounts of MOTS. The results presented in Figure 3-4B show a minor decrease of R (and thus in the O_2 permeability) from 2.2 to 1.7 with this increase in the amount of MOTS. MOTS functions as 'end-cap' (Liu et al 1992, Klimant et al 1999) for the self-condensation of PTS and interrupts the polymerisation. The relatively low amounts (Table 2) of MOTS used here (Table 2) lead to an enhanced number of free alkoxyl groups, allowing for continued condensation reactions in the planar oxygen optodes. This then causes drift of the calibration curve over time after fabrication (data not shown).

Table 4. The role of reflux time for OMS 2.2 performance. Planar oxygen optodes were fabricated on the base of OMS 2.2, prepared under different reflux times, and characterized by their decay-time ratio, R.

OMS type no.	t (min)	R
2.2 a	30	1.41
2.2 b	60	1.54
2.2 c	90	1.68
2.2 d	120	1.80

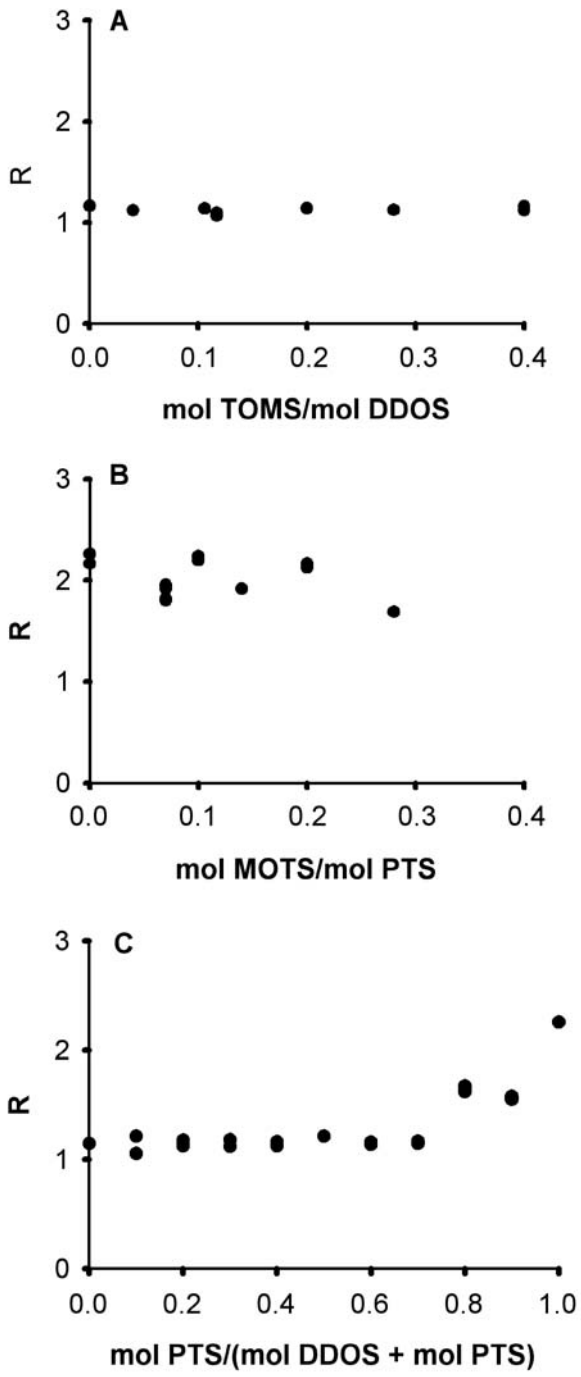

Figure 3-4. Impact of the precursor molar ratio on R-values of the ORMOSILS 1-3: (A) precursor TOMS relative to DDOS molar ratio prepared as presented in Table 1 , (B) precursor MOTS relative to PTS molar ratio prepared as presented in Table 2, (C) precursor PTS relative to DDOS molar ratio as presented in Table 3. The R-values were measured with a decay time based imaging technique.

We studied the impact of varying reflux time on the measuring characteristics of O_2 optodes made of the OMS 2.2 matrix. It was observed that R increased from 1.4 to 1.8 with increasing reflux time (30–120 min) during the sol-gel preparation (Table 4). The short reflux time of 30 min resulted in a soft polymer with a poor oxygen solubility. Longer reflux times (60-120 min) increased the formation of cross-links during the polymerisation resulting in a more open net-like structure with improved oxygen solubility. A reflux time of 120 min resulted in planar optodes with good R-values and this timing was used for all further *ORMOSIL* preparations. Although the optodes of *ORMOSIL* series 2 exhibited a much better oxygen permeability (R > 1.7) than those made of the *ORMOSIL* series 1 (R < 1.2), the solubility of *ORMOSIL* 2 in chloroform was poor, and the manufactured planar optodes suffered from a poor mechanical stability.

Another approach was to moderate the *ORMOSIL* properties via mixing the precursors DDOS and PTS without later supply of an ‘end-cap’ or ‘cross-linker’ (*ORMOSIL* 3 material). Previous studies showed that pure DDOS forms weak polymers with a low O_2 sensitivity, whereas pure PTS forms a brittle glass with a good O_2 sensitivity. By using a mixture of the two precursors we could fabricate planar oxygen sensors with both a high O_2 sensitivity and a stable polymer matrix. The optodes prepared from the *ORMOSIL* series 3 (Figure 3-4C) exhibited a significant increase of R at > 0.7 mol fractions PTS. With pure PTS, the value of R almost doubled from 1.2 to 2.2. The *ORMOSIL* 3 materials generally had a good solubility in chloroform and exhibited a good mechanical stability. Based on the mentioned observations, the *ORMOSIL* 3.2 (R=1.6) (see Table 3) was selected as the most promising matrix material for planar optodes. Tests of planar optodes made of this *ORMOSIL* showed very good sensor performance for > 36 days (see below).

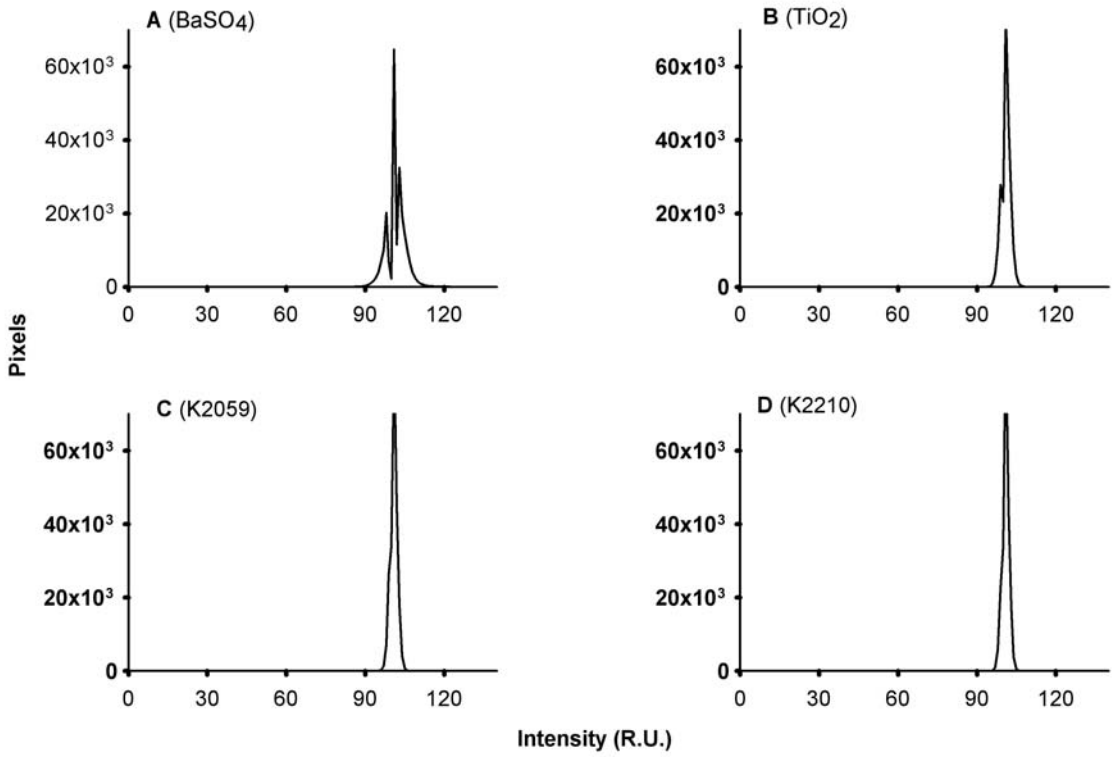

Figure 3-5. Histograms of pixel intensity values as a measure of sensor homogeneity. The applied ORMOSIL was 3.2 with a dye concentration of 5 mmol/kg. Results from planar optodes prepared with different types of scattering particles: (A) BaSO4, (B) TiO2, (C) K2059 and (D) K2210. The mean intensity of each image was set to 100%.

3.3.2. Role of scattering particles for planar optode performance

The addition of scattering particles to the sensing layer can enhance the signal intensity of planar optodes, as the fluorescent indicator is excited more efficiently due to increased scattering in the matrix. Furthermore, scattering particles can facilitate a more even excitation of the foil if the particles are dispersed homogeneously in the sensor material. However, too large amounts of TiO_2 in the sensor matrix can cause significant fluorescence quenching due to a charge transfer process between Ru-DPP and TiO_2 (Matthew et al. 1997). Four different types of scattering particles were

investigated with respect to their dispersion in *ORMOSIL* 3.2 and the homogeneity of the final oxygen optode (Figure 3-5). As a measure of homogeneity, we calculated the mean and standard deviation of the fluorescent intensity values of all pixels in images recorded with the optode in air-saturated water (Figure 3-5). The most homogeneous sensors were manufactured with the Kronos pigments A and B yielding a symmetrical peak with a low standard deviation of 1.3 (Figure 3-5C + D). It was not possible to detect a significant difference in performance between the two pigments. In comparison, the optodes prepared with uncoated $BaSO_4$ (Figure 3-5A) and TiO_2 (Figure 3-5B) exhibited non-symmetrical distributions of fluorescence intensity with a standard deviation of 3.7 and 1.7, respectively. Besides facilitating good dispersion and homogeneous sensor foils, the organic coating of the Kronos pigments apparently also minimized the quenching effect of TiO_2 mentioned above. Although a high homogeneity was reached, it was not possible to use average calibration values for the entire planar optode, and it was still necessary to perform a pixel-by-pixel calibration, when the planar optodes were applied with the imaging system. This means that every pixel of the O_2 concentration image corresponds to a specific area (here approximately 50 x 50 μm^2) of the planar optode, which must be regarded as a local sensor with its corresponding calibration values. Consequently, the experimental setup must not be modified after calibration or, alternatively, precise position markers have to be set on the optodes to enable re-adjustment of the images during data processing.

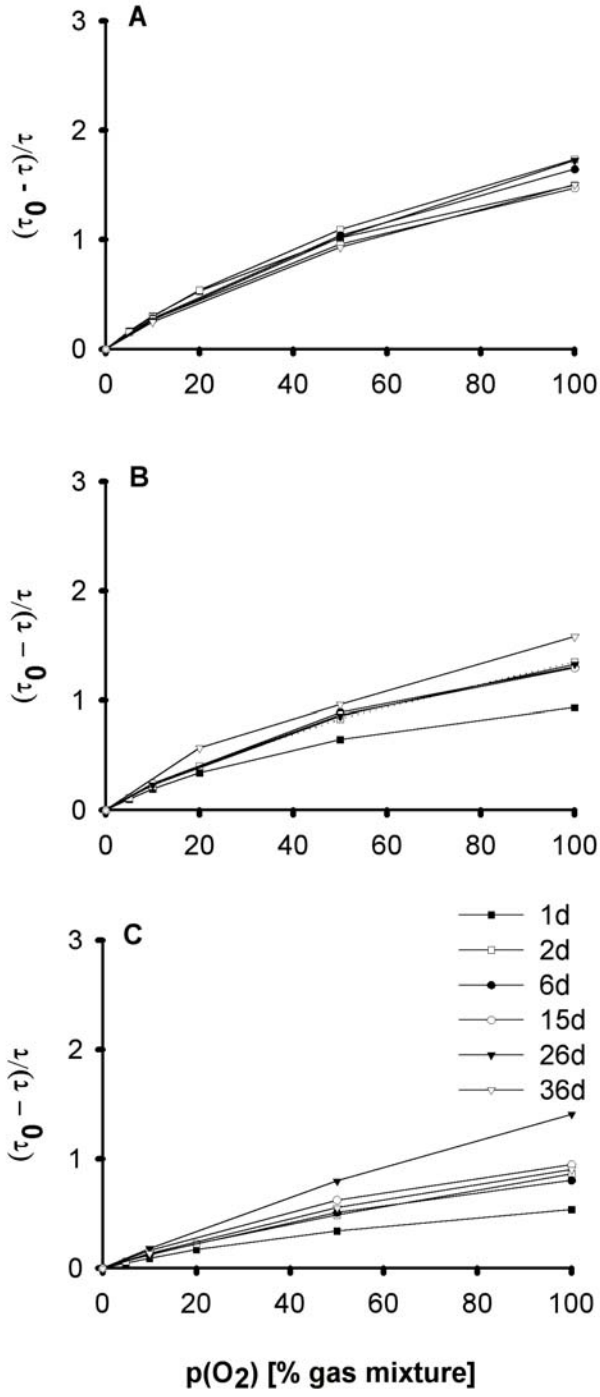

Figure 3-6. Calibration curves from planar oxygen prepared of *ORMOSIL* 3.2 with dye concentrations of (A) 2mmol /kg, (B) 10 mmol/kg and (C) 50 mmol/kg at varying ageing stages. The calibration curve is given as ratio of τ_0/τ normalized to zero versus the O_2 concentration.

3.3.3. Dye concentration and ageing of planar optodes

The performance of 3 sensors made with *ORMOSIL* 3.2 and (Ru-DPP) concentrations of 2, 10 and 50 mmol per kilogram matrix polymer, respectively, was investigated over 36 days (Figure 3-6). The best performance with respect to both O_2 sensitivity and long-term stability of the sensor was observed with planar optodes containing a low indicator concentration of 2 mmol per kg matrix material (Figure 3-6A). The calibration curves of the two other sensors showed less oxygen sensitivity and the curves changed significantly over time (Figure 3-6B, C). For long-term applications in sediments we thus found *ORMOSIL* 3.2-based sensors with Kronos pigment A scattering particles and a dye concentration of ~2-10 mmol per kg matrix material to be optimal. At higher dye concentrations photodegradation increases and products thereof can quench the fluorescence (Klimant et al. 1999).

3.3.4. Reproducibility of planar optode fabrication

Three sets of *ORMOSIL* 3.2-based planar optodes with Kronos pigment A were fabricated and calibrated under identical conditions (Figure 3-7). While properties like mechanical stability, long-term stability of calibration, and adhesion were indifferent between the foils, it was difficult to produce polymers with absolute identical physical properties with respect to O_2 permeability. Thus, it was not possible to obtain a large batch of sensor foils with identical calibration curves. This may, however be achieved by a more advanced setup for coating the carrier foil. Especially at high partial pressure of oxygen the calibration curves for different foils deviated from each other, while the performance in the range of 0 to 20% O_2 was relatively uniform. Overall, the reproducibility was sufficient for our needs but it is important to carefully calibrate

each individual sensor foil. All calibration curves showed an excellent correlation with the modified Stern-Volmer equation Eq. (1).

The main difference between our procedure and the *ORMOSIL* preparation process described by Klimant et al. (1999) was the use of a lower drying and curing temperature, which simplifies the preparation of the *ORMOSIL*s. Furthermore, our systematic investigation showed that reflux times of up to 120 min during fabrication resulted in *ORMOSIL* matrices with improved oxygen solubility and that addition of organically coated TiO_2 yielded more homogeneous planar optodes.

3.3.5. Mapping of the 2-dimensional O_2 distribution around a N. diversicolor burrow

A laboratory application of *ORMOSIL* 3.2-based planar optodes allowed direct mapping of the two-dimensional O_2 distribution around a worm burrow (Figure 3-8). We show here a time series of 4 images obtained with a time delay of 3 minutes between each image.

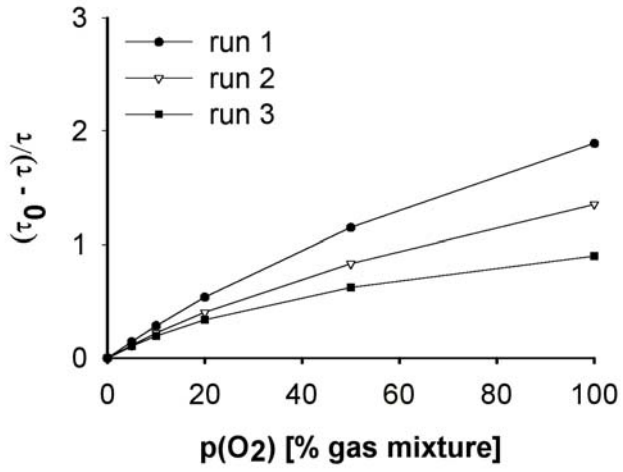

Figure 3-7. Calibration curves of planar oxygen optodes based on 3 preparation trials of *ORMOSIL* 3.2 with a dye concentration of 5 mmol/kg. The calibration curve is given as ration of τ_0/τ normalized to zero versus the O_2 concentration.

A more detailed study of oxygen dynamics around *H. diversicolor* burrows in natural and artificial sediments is presented elsewhere (König et al. in prep.). The images reflect the 2-dimensional oxygen distribution (expressed in a linear colour table) around the outlet branch of a U–shaped tube inhabited by one individual. Since the flow chamber was larger in width than the diameter of the worm burrow, part of the burrow was not build completely parallel to the measuring plane. The effect is visible in all images of Figure 3-8, where the burrow appears to be interrupted. Furthermore, the images showed no pronounced heterogeneity of oxygen in the sediment except around the worm burrow, as the sediment was sieved and homogenized before being introduced to the experimental chamber.

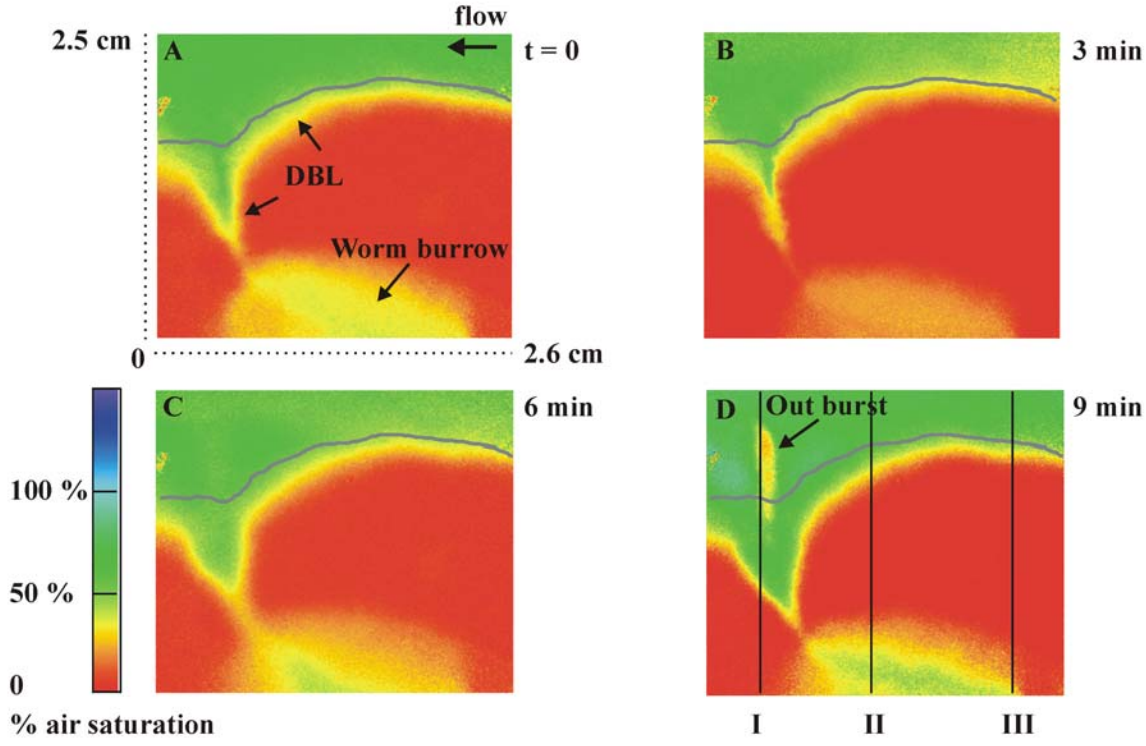

Figure 3-8. Time series (3 min intervals) recording of the oxygen distribution around a *Hediste diversicolor* burrow (presented in a linear color scale). They thick grey line indicates the sediment surface. The flow of the overlaying water was directed from the right to the left. The positions of the 3 profiles presented in Figure 3-9 are indicated in the last image.

The oxygen penetration depth at the primary sediment-water interface varied between 2 and 3.8 mm and was affected by the presence of a diffusive boundary layer (DBL) closely following the sediment surface. However, the polychaete frequently left its tube causing a rearrangement of the sediment surface. The outline of the burrow and the sediment surface could be traced by illuminating the flow chamber from the opposite side of the planar optode coated chamber causing a detectable shadow relief which could be detected by the camera system.

During the shown image sequence (Figure 3-8), the O_2 level inside the burrow and in the outlet oscillated between 60% and 5% air saturation. The last image of the sequence shows an outburst of water with low oxygen content from the burrow (see arrow in Figure 3-8D) after a period of less irrigation activity. The O_2 fluctuations over time in the burrow were due to variations in the pumping activity of the polychaete causing the oxygen concentration to vary from zero to 60% or even 90% (not shown) air saturation within a few minutes. Three characteristic oxygen profiles (Figure 3-9) were extracted from Figure 3-8D (as indicated by vertical lines). Profile I was strongly affected by an outburst of oxygen-depleted water (~19% air sat.), and by the presence of the burrow opening. Profiles II and III showed the diffusive oxygen uptake at the primary sediment-water interface and enhanced levels of oxygen deep in the sediment due to radial diffusion of oxygen from the burrow, i.e., the secondary sediment-water interface. Our data show that planar optodes have a large potential for resolving the oxygen dynamics in bioturbated sediments at a hitherto unreached spatio-temporal resolution (Kristensen 1988). With this technique it is possible to visualize the oxygen distribution and dynamics both at the primary sediment-water interface and at the secondary interface present around worm burrows, and to calculate fluxes and specific oxygen consumption activities at these interfaces.

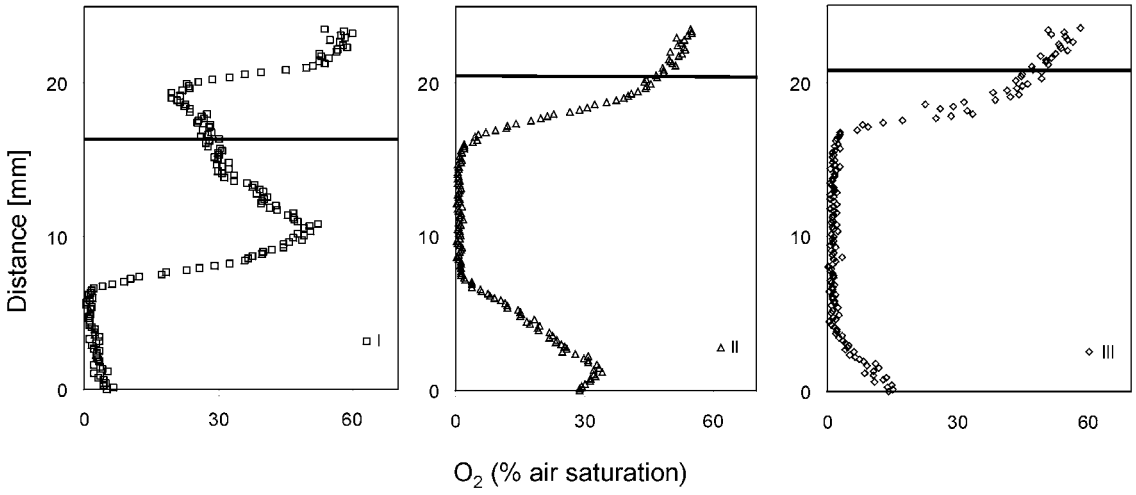

Figure 3-9. Concentration profiles extracted from Figure 3-8. The sediment surface is indicated with the black line. Profile I is dominated by the outburst of water with low oxygen content from the worm burrow. Profiles II and III both show evidence of O_2 diffusion across the sediment-water interface and radial diffusion from the burrows, although profile II clearly shows a stronger effect of radial diffusion.

Images of the vertical O_2 flux (Figure 3-10A & C) were obtained by applying Eq. (3) to the O_2 images of figure 8A and D making no differentiation in the flux directions. In order to increase the signal to noise ratio of the flux calculations 3 x 3 neighbouring pixels were averaged. Consequently, the spatial resolution of the calculated O_2 flux images was reduced to 150 µm per pixel. The DOU indicated by the vertical flux at the primary sediment surface reached at maximum of 4.7 mmol m^{-2} d^{-1}. Images of the horizontal oxygen flux were also calculated (Figure 3-10B & D). Maximal horizontal oxygen fluxes of up to 7.9 mmol m^{-2} d^{-1} were calculated at the burrow wall. At the primary sediment-water interface no significant horizontal flux was observed. These O_2 fluxes are relative low compared to the reported fluxes of 18-27 mmol m^{-2} d^{-1} (Fenchel 1996, Pelegri and Blackburn 1995) and 52.8 nmol m^{-2} d^{-1} (Banta et al. 1999) and this could be due to the manipulation of the sediment prior to experiments.

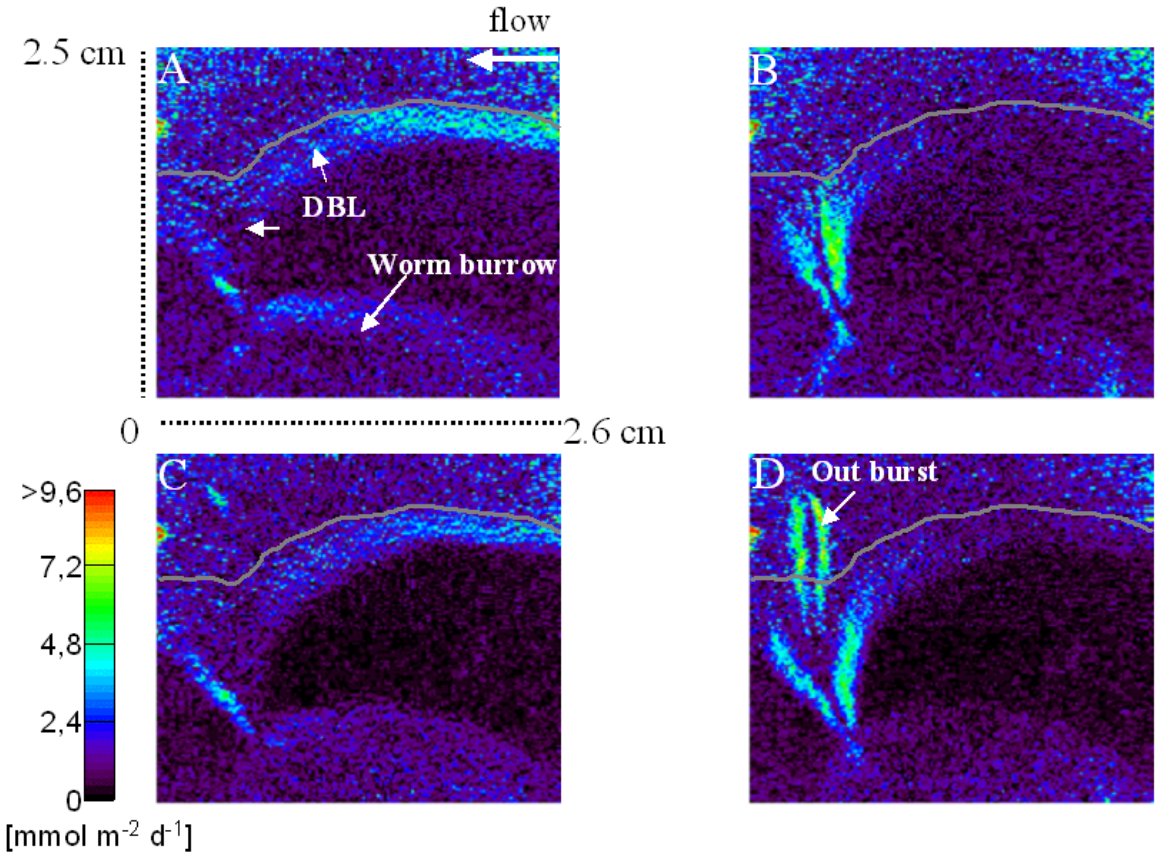

Figure 3-10. The vertical and horizontal distribution of O_2-flux expressed in a linear color scale. In order to increase the signal to noise ratio the spatial resolution was reduced to 150 µm. They thick grey line indicates the sediment surface. Panel A and C show the distribution of vertical O_2 flux (derived from Fig 8A and D), whereas panel B and D show the horizontal the O_2 flux. In all panels no indication on the direction of the fluxes is given.

The O_2 uptake of the primary and secondary sediment water interface were in the same order of magnitude as e.g. reported by Fenchel (1996). The oxygen flux images presented in Figure 3-10. 10 show highest O_2 fluxes along the primary and secondary sediment-water interfaces. Such data obtained in combination with other measures of the sediment biogeochemistry such as e.g. total oxygen uptake, oxygen microsensor measurements, measurements of polychaete biomass and irrigation activity, and precise determination of burrow geometry now enable the construction

of a precise oxygen budget for bioturbated sediments (see e.g. Wenzhöfer and Glud 2004). Here we have focussed on describing the fabrication and performance of planar optodes.

3.4. Summary

We developed planar oxygen indicator foils (planar optodes) well suited for environmental application in aquatic systems. This study is to our knowledge the first to present a detailed description of planar optode fabrication along with a more systematic investigation of important variables affecting planar optode performance. It is our hope that these details will help make the technique more accessible. We demonstrated the first use of planar oxygen optodes for investigating the oxygen dynamics around polychaete burrows in sediments. With planar oxygen optodes and the corresponding imaging system, the spatial and temporal O_2 dynamics in bioturbated marine systems can now be investigated at a hitherto unreached level of resolution in the laboratory and even *in situ* by use of a recently developed underwater instrument for planar optodes (Glud et al. 2001; Wenzhöfer and Glud, 2004).

3.5. Acknowledgements

This study was financed by the European Commission (MICROFLOW, CT970078; PHOBIA, QLK3-CT-2002-01938), the Max-Planck-Society (Germany), and the Danish Natural Science Research Council.

3.6. References

Bacon, J. R., and Demas, J. N. 1987. Determination of oxygen concentrations by luminescence quenching of a polymer-immobilized transition-metal complex. Anal. Chem. 59: 2780-2785.

Banta, G.T., Holmer, M., Jensen, M.H., and Kristensen, E. 1999. Effects of two polychaete worms, Hediste diversicolor and Arenicola marina, on aerobic and anaerobic decomposition in sandy marine sediment. Aquat. Microb. Ecol. 19: 189-204.

Brinker, C. J. 1988. Hydrolysis and condensation of silicates: Effects on structure. J. Non-Cryst. Solids. 100: 31-50.

Broecker, W. S., and Peng, T-H. 1974. Gas exchange rates between air and sea. Tellus. 26: 21-35.

Carraway, E.R., Demas, J.N., DeGreff, A., and Bacon, J. R. 1991. Photophysics and photochemistry of oxygen sensors based on luminescent transition-metal complexes. Anal Chem. 63: 337-342.

Fenchel, T. 1996. Worm burrows and oxic microniches in marine sediments. 1. Spatial and temporal scales. Mar. Biol. 127: 289-295.

Glud, R. N., Ramsing, N. B., Gundersen, J. K., and Klimant, I. 1996. Planar optrodes: A new tool for fine scale measurements of two-dimensional O2 distribution in benthic communities. Mar. Ecol. Prog. Ser. 140: 217-226.

Glud, R. N., Klimant, I., Holst, G., Kohls, O., Meyer, V., Kühl, M., and Gundersen, J. K. 1999a. Adaption, test and in situ measurements with O2 microopt(r)odes on benthic landers. Deep-Sea Res. I 46: 171-183.

Glud, R. N., Kühl, M., Kohls, O., Ramsing, N. B. 1999b. Heterogeneity of oxygen production and consumption in a photosynthetic microbial mat as studied by planar optodes. J Phycol. 35: 270-279.

Glud, R.N., Tengberg, A., Kühl, M., Hall, P., Klimant, I., and Holst, G. 2001. An in situ instrument for planar O2 optode measurements at benthic interfaces. Limnol. Oceanogr. 46: 2073-2080.

Hartmann, P., and Ziegler, W. 1996. Lifetime imaging of luminescent oxygen sensors based on all-solid-state technology. Anal. Chem. 68: 4512-4514.

Holst, G., Kühl, M., and Klimant, I. 1995. A novel measuring system for oxygen microoptodes based on a phase modulation technique. SPIE Proc. Conf. Chem., Biochem. and Enviro. Fibre Sensors, VII: 2508-2545.

Holst, G., Kohls, O., Klimant, I., König, B., Kühl, M., and Richter, T. 1998. A modular luminescent lifetime imaging system for mapping oxygen distribution in biological samples. Sens. Act. B 51: 163-170.

Holst, G., Grunwald, B., Klimant, I., and Kühl, M. 1999. A luminescent lifetime imaging system using imaging fibres to measure the 2D distribution of O2 in biological samples. Proc. SPIE 3860: 154-163

Holst, G., and Grunwald, B. 2000. Luminescence lifetime imaging with transparent oxygen optodes. Sens. Act. B 64: 1-13.

Hoshino, Y., and Mackenzie, J. D. 1995. Viscosity and structure of Ormosil solutions. J. of Sol-Gel Sci. Technol. 5: 83-92.

Iwamoto, T., and Mackenzie, J. D. 1995. Ormosil coatings of high hardness. J. Mat. Sci. 30: 2566-2570.

Kautsky, H., 1939. Quenching of luminescence by oxygen. Faraday Society 35: 216-219.

Klimant, I. 1993.Entwicklung optischer Sauerstoffsensoren auf der Basis luminiezierender Übergangsmetallkomplexe, Ph.D. thesis, Universitiy Graz, Austria,.

Klimant, I., Meyer, V., and Kühl, M. 1995. Fibre-optic oxygen microsensors, a new tool in aquatic biology. Limnol. Oceanogr. 40: 1159-1165.

Klimant, I., Ruckruh, F., Liebsch, G., Stangelmayer, A., and Wolfbeis, O. 1999. Fast response oxygen micro-optodes based on novel soluble ormosil glasses. Mikrochim. Acta 131: 35-46.

König, B., Glud, R. N., and Kühl, M. Oxygen Dynamics around Nereis diversicolor burrows as studied with planar optodes (in prep.).

Kristensen, E. 2000. Organic matter diagenesis at the oxic/anoxic interface in coastal marine sediments, with emphasis on the role of burrowing animals. Hydrobiologia 426: 1-24.

Lev, O., M. Tsionsky, M., Rabinovich, L., Glezer, V., Sampath, S., Pankratov, I., and Gun, J. 1995. Organically Modified Sol-Gel Sensors. Anal. Chem. 67: 22-30.

Li, Y-H. and Gregory, S. 1974. Diffusion of ions in sea water and in deep-sea sediments. Geochim. Cosmochim. Acta 38: 703-714.

Liebsch, G., Klimant, I., and Wolfbeis, O. S. 1999. Luminescent lifetime temperature sensing based on sol-gels and poly(acrylnitrile)s dyed with ruthenium metal-ligand complex. Adv. Mater. 11: 1296-1299.

Liu, H.-Y., Switlaski, S. C., Coltrain, B. K., and Merkel, P. B. 1992. Oxygen permeability of sol-gel coatings. Appl. Spectrosc. 46: 1266-1272.

Matthews, L. R., Avnir, A., Modestov, A. D., Sampath, S., and Lev, O. 1997. The incorporation of titania into modified silicates for solar photodegradation of aqueous species. J. Sol-Gel Sci. Technol. 8: 619-623.

McEvoy, A. K., McDonagh, C. M., and MacCraith, B. D. 1996. Dissolved oxygen sensor based on fluorescence quenching of oxygen-sensitive ruthenium complexes immobilized in sol-gel–derived porous silica coatings. Analyst 121:785-788.

Mock, T., Dieckmann, G., Haas, C., Krell, A., Tison, J.L., Belem, A., Papadimitriou, S., Thomas, D. N. 2002. Micro-optodes in sea ice: A new approach to

investigate oxygen dynamics during sea ice formation, Aq. Microb. Ecol. 29: 297-306.

Murtagh, M. T., Shahriari, M. R., and Krihak M. 1998. A study of the effects of organic modification and processing technique on the luminescence quenching behavior of sol-gel oxygen sensors based on a Ru(II) complex. Chem. Mater. 10:3862-3869.

Ullman, W. J., and Aller, R. C. 1982. Diffusion coeffiecients in nearshore marine sediments. Limnol Oceanogr. 27(3): 552-556.

Shahriari, M. R., Murtagh, M. T., and Kwon, H.C. 1997. Ormosil thin films for chemical sensing platforms. Proc. SPIE 3105: 40-51

Stern, O., and Volmer, M. 1919, Über die Abklingungszeit der Fluoreszenz. Physik. Zeitschr. 20: 183-188.

Wenzhöfer, F., Holby, O., Glud, R. N., Nielsen, H. K., and Gundersen, J. K. 2000. In situ microsensor studies of a shallow water hydrothermal vent at Milos. Mar. Chem. 69: 43-54.

Wenzhöfer, F., and Glud, R. N. 2004. Small-scale spatial and temporal variability in benthic O2 dynamics of coastal sediments: Impact of fauna activity Limnol. Oceanogr. 49: 1471–1481.

Chapter 4

A modular luminescent lifetime imaging system for mapping oxygen distribution in biological samples

Published in Sensors and Actuators B51

July 1998

4. A modular luminescent lifetime imaging system for mapping oxygen distribution in biological samples

Gerhard Holst[1*], Oliver Kohls[1], Ingo Klimant[3], Bettina Koenig[1], Michael Kühl[2], Thomas Richter[4]

[1]Max-Planck-Institute for Marine Microbiology, Celsiusstr. 1, D-28359 Bremen, Germany

[2]Marine Biological Laboratory, University of Copenhagen, Strandpromenaden 5, DK-3000 Helsingør, Denmark

[3]Institute for Analytical Chemistry, Chemo- and Bio-Sensors, University of Regensburg, D-93040 Regensburg, Germany

[4]Institute for Biology II, Schänzlestr. 1, D-79104, Freiburg, Germany

*corresponding author, Fax: +49 421 2028834, e-mail: gholst@mpi-bremen.de

Abstract

We developed a new modular luminescence lifetime imaging system (MOLLI), that enables the imaging of luminescence lifetimes in the range of 1 µs to 1 s. The system can easily be adapted to different experimental applications. The central parts of the system are a recently released CCD-camera with a fast electronic shutter and gated LED (light emitting diode) or Xe excitation light sources. A personal computer controls the gating and image acquisition via a pulse delay generator. Here we present the new imaging system and give examples of its performance when used for measuring two-dimensional oxygen distributions with planar optodes. Furthermore, future applications of the system in biology are discussed.

4.1. Introduction

Imaging of two-dimensional solute distributions with luminescent indicators has become an important tool in medicine, biology and physics. Most of the described image measuring systems and experimental setups were designed for specific applications like measurements of oxygen distribution in tissue [1–5], pH and Ca^{2+} distribution in cells [6,7], oxygen partial pressure on skin surfaces or oxygen flux into skin [8,9], oxygen distribution across the water-sediment interface [10] and in biofilms [11]. These setups were optimised for the corresponding experimental situation, but they lack versatility and many of them were e.g. confined to microscope setups [12–17]. Furthermore, imaging systems for time and frequency-domain measurements often consist of complicated and rather bulky setups, using lasers as light sources, optical modulators, and sensitive slow scan CCD-cameras combined with fast gatable image intensifiers.

New bright semiconductor light sources, light emitting diodes (LED), that emit in the blue and blue-green part of the spectrum, offer a much cheaper and simpler alternative for a fast modulated or gated light source as compared to lasers. Furthermore, a recently developed sensitive and fast gateable CCD-camera simplifies lifetime imaging as it allows fast gating directly on the photosensitive chip. The image is digitised in the camera, and can be read out with the camera control board. An additional frame grabber is thus obsolete. We combined these new technologies with a trigger controller and a personal computer (PC) to develop a modular imaging system, which can easily be adapted to various applications. Here we describe the new imaging system and show its performance in applications where two-dimensional O_2 distributions are mapped via lifetime imaging of planar O_2 optodes.

Table 1
Overview of different luminescence lifetime imaging methods

Lifetime detection	Procedure	+	–	Source
Frequency domain method	Sinusoidal modulation and phase angle shift	Better separation of different species with similar lifetimes	Complex setups (that need an image intensifier for sinusoidal modulation of gain), good optical filtering necessary	[26,25,28]
Ratioing method	Rectangular modulation and ratioing	Higher signal-to-noise ratio than time-domain and fast calculation	Background luminescence cannot be separated, good optical filtering necessary	[9]
Time-domain method	Pulse and gate	Simple separation of high background with short lifetimes, simple optical filtering	Species with similar lifetimes are difficult to separate, background with long lifetimes is difficult to separate	[15,3,5,27]

4.2. Theory

4.2.1. Oxygen sensing [2,6]

The dynamic quenching of luminescence by oxygen [1,7–10,3,4,18,5,19–24,11] is the basis for the measurement of oxygen distributions in various systems. The applied sensors have a planar structure with the luminescent indicator embedded in a polymer matrix that is spread on a transparent support foil. The sensor area is imaged through an optical emission filter in the case of intensity images or directly in the case of lifetime images by lenses or imaging fibres coupled to a photosensitive CCD-chip of the camera. Each pixel on the CCD now monitors the light intensity either as the absolute luminescence light emission, or, with proper timing, a part of the luminescence decay curve.

The oxygen optodes were calibrated with a two component model of the Stern–Volmer equation [22]:

$$\frac{\tau}{\tau_0} = \frac{I}{I_0} = \frac{\tan(\Phi)}{\tan(\Phi_0)} = \frac{frac}{(1 + K_{SV} * [O_2])} + (1 - frac) \qquad (1)$$

τ, I, Φ =decay time, intensity or measured phase angle in presence of oxygen, τ_0, I_0, Φ_0 = decay time, intensity or measured phase angle in absence of oxygen, frac = fraction of quenchable luminophore, K_{SV} = bimolecular quenching coefficient, $[O_2]$, oxygen concentration.

4.2.2. Image detection

Luminescence lifetime imaging has two major advantages over intensity based imaging. It allows a good contrast enhancement and background suppression of unwanted luminescence contributions in the image. If this background luminescence has a different decay time than the luminophore of interest it is possible to separate the two signals by lifetime imaging. Further, lifetime imaging does not depend on intensity variations due to photobleaching (if it does not take place faster than the image acquisition) or variable indicator concentrations, and calibration free sensing applications [5] are possible. Table 1 gives an overview of the different possible methods for lifetime imaging, their inherent advantages and disadvantages.

The presented camera can not be modulated sinusoidally for frequency-domain evaluation, which has an advantage if images of different luminophores with similar lifetimes should be separated [25,13,14]. The phase delay rationing method by Hartmann et al. [8,9] is possible with the new camera. However, it is not suitable for our applications because there can be an enormous background luminescence in the natural systems investigated with the new imaging system.

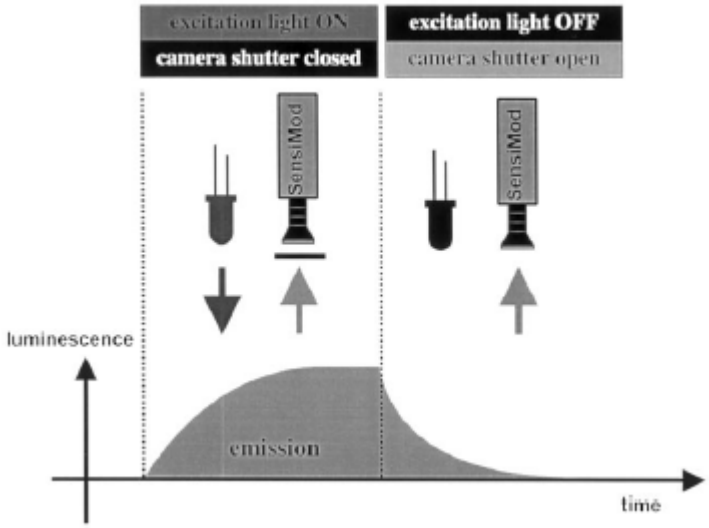

Figure 4-1. Principle image acquisition timing scheme for luminescence lifetime imaging. The luminescence signal vs. time corresponds to the light signal that is detected by each pixel of the CCD-chip. The timing starts with excitation light ‘on’ and the camera shutter closed, the luminophore absorbs light and luminescence is emitted. Then the excitation light is switched ‘off’ and the camera shutter is opened with a possible delay.

The new system, therefore, measures luminescence in the time-domain via a so called pulse-gate method [15,3–5]. Figure 4-1 shows the detection principle applied for each pixel. For excitation the light source is switched ‘on’ and illuminates the planar optode, the arriving luminescence intensity increases until an equilibrium between absorbed and emitted energy of the dye molecules is reached. Then the light source is switched ‘off’ and the camera shutter is opened allowing luminescence and ambient light to reach the CCD-chip. This is repeated for a number of times, while incident light during the shutter open time is integrated on the CCD-chip before being passed to the PC. This procedure is repeated a couple of times to average the images and improve the signal-to-noise-ratio. To evaluate the corresponding lifetime of the light information detected by each pixel, three sets of images are collected,

where each set is acquired with a different delay time t_i relative to the switch 'off' of the excitation light source.

The following image collection procedure is performed. Three sets of images (i= 1, 2, 3) are collected (see Figure 4-2), while each image detection with a time interval Δ_i has a certain delay t_i compared to the excitation light 'off'. To receive enough light intensity, each image represents the integral over a number, n_i, of illumination events. The measured images S_i are stored.

The intensity of one image is given by:

$$I_i = \frac{S_i}{n_i}, \qquad \text{i = 1, 2, 3} \tag{2}$$

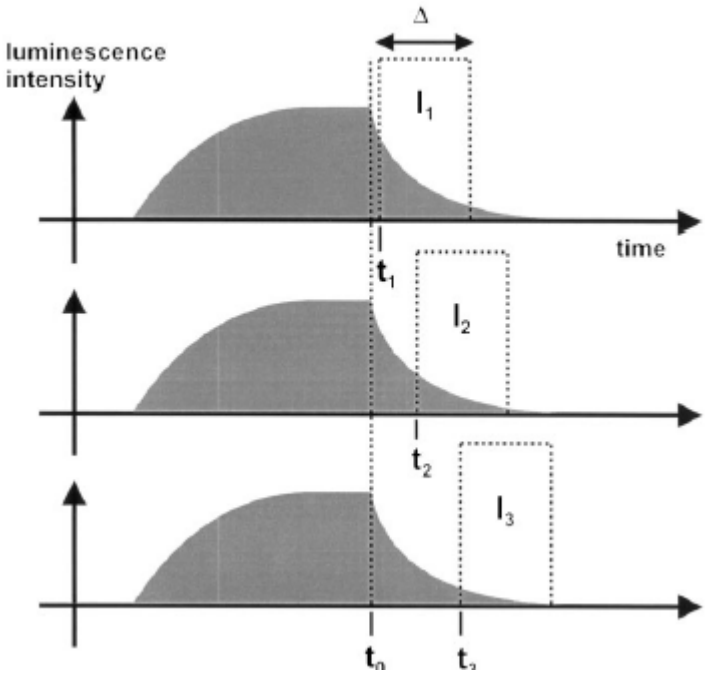

Figure 4-2. Timing scheme for recording of images to evaluate the luminescence lifetime to generate lifetime images. All detected images have time windows of the same width D and integrate the intensity Ii of the decay curve. Each window has a different delay t_i compared to the switch 'off' time of the excitation light. To collect enough light, this window 'open' operation for a certain delay t_i is performed several hundred times and the light information is integrated on the CCD-chip.

This intensity is, assuming a mono exponential decay curve with the apparent lifetime τ, described by the following equation:

$$I_i = I_o * \tau * \exp\left(\frac{t_i}{\tau}\right) * \left[1 - \exp\left(-\frac{\Delta_t}{\tau}\right)\right] \tag{3}$$

with the unknown intensity I_0 at time t_0 when the excitation light is switched 'off' (see Figure 4-2). Instead of fitting the Values I_i to I_0 and τ we generate the new values:

$$W_1 = -\ln\left(\frac{I_1}{I_2}\right) \tag{4}$$

$$W_2 = -\ln\left(\frac{I_3}{I_2}\right) \tag{5}$$

If the image collection happens with the condition:

$$\Delta_1 = \Delta_2 = \Delta_3 = \Delta = const. \tag{6}$$

the new values give the following relations:

$$W_1 = \frac{t_1 - t_2}{\tau} \tag{7}$$

$$W_2 = \frac{t_3 - t_1}{\tau} \tag{8}$$

Therefore the lifetime per pixel can be directly calculated with the known delay times t_i :

$$\tau = \frac{(t_1 - t_2)^2 + (t_3 - t_2)^2}{W_1 * (t_1 - t_2) + W_2 * (t_3 - t_2)} \tag{9}$$

This method is not limited compared to a general fit to all values I_i. The generation of each value W_i (Eqs. (7) and (8)) with subsequent fit (Eq. (9)) do not yield to a principal deviation from a general fit as long as Eq. (6) is valid.

The calculation of the values (Eqs. (7) and (8)) has, by division of the average values, the smallest error accumulation and is numerically stable. A variation of the

timing window interval Δ, that is constant for all images, principally gives the opportunity to detect a non-limited number, *n*, of values to evaluate τ and, therefore, an error degression in the size of $1/\sqrt{n}$. This can be an advantage in the case of very noisy signals.

4.3. Experimental

4.3.1. Planar optode

The sensing layers for the comparison of luminescence intensity versus lifetime images were made of three different luminophores. The background or 'noise' layer was a commercial luminescent paint (Feuerrot, Conrad Electronics, Hirschau, Germany) with a luminescence decay time <1 ns. This paint was spread on a microscope slide. The layers that should be identified were made of two different oxygen indicators. One indicator was a Tris (4,7-diphenyl-1,10-phenantrolin)-ruthenium(II) perchlorate [8,9,22–24], dissolved in an organically modified sol-gel (ormosil) with dispersed titanium dioxide scattering particles. The other example was a platinum-octaethyl-porphyrine (Porphyrin Products, Utah, USA), dissolved in polystyrene that also can be used for oxygen determination. Both oxygen indicators were spread on microscope slides. For the oxygen measurement the ruthenium based sensor was knife-coated on a polyester foil that was cut to a size of 28x40 mm^2 to fit into the test setup.

4.2.1. Imaging system and application

The imaging system (Figure 4-3) consists of an electrically cooled CCD-camera (SensiMod, PCO Computer Optics, Kehlheim, Germany) with a direct fast electronical shutter feature, due to a new and fast charge carrier transport from the light detection cell to the shift register, where the electrons can be accumulated until the picture frame is read out. Additionally, the camera has a special modulation input to control directly the fast shutter (t_{on}=500 ns and t_{off}=500 ns, maximum frequency=1 MHz). The camera (dynamic range=12 Bit, resolution=640x480 pixel) is connected via a serial fibre-optical link to a camera control PCI-board in a Pentium based PC. The PC controls image acquisition, storage, display and the timing. For the precise timing of the excitation light source switching and image acquisition, the PC is connected via a GPIB interface to a delay pulse generator (DG535, SRS Stanford Research Systems, Sunnyvale, USA). Timing control und primary image acquisition was programmed in C (Watcom C/C^{++}10 Compiler, Sybase, Emeryville, USA), while the image calculations and visualisation were programmed in a special software language made for the handling of large amounts of data (IDL 5.0, Research Systems, Boulder, USA).

For the experimental applications, the camera was equipped with a macro lens (Tevidon, F1.6/*f*=35 mm, PCO) that imaged an area of 28x40 mm^2 onto the CCD-chip. This corresponds to a theoretical resolution of 50 µm pixel^{-1}. Two different light sources were applied for illumination, respectively excitation of the planar optodes. For lifetimes >6 µs and luminophores with very low quantum efficiency, a Xenon flash lamp with adjustable output power and a maximum repetition rate of 30 Hz (A0021F, Oxygen Enterprises, Philadelphia, USA) was connected to a fibre-optical ring light, that was specially designed for the applications, i.e. a homogenous illumination of a

circle of 50 mm diameter in a distance of 50 mm (Schölly Fiberoptic, Denzlingen, Germany).

The second light source was developed for lifetime measurements from 100 ns upward and consists of up to 12 light emitting diodes (λ=470 nm, BP280CWPB1K, DCL Components, Hungerford, UK), that are coupled into the same fibreoptical ring light. To enable fast switching of the LEDs, a special driving circuit with adjustable current was designed. The camera and the ring light were fixed in a special light tight housing, that can easily be applied to a vertically mounted sensing layer.

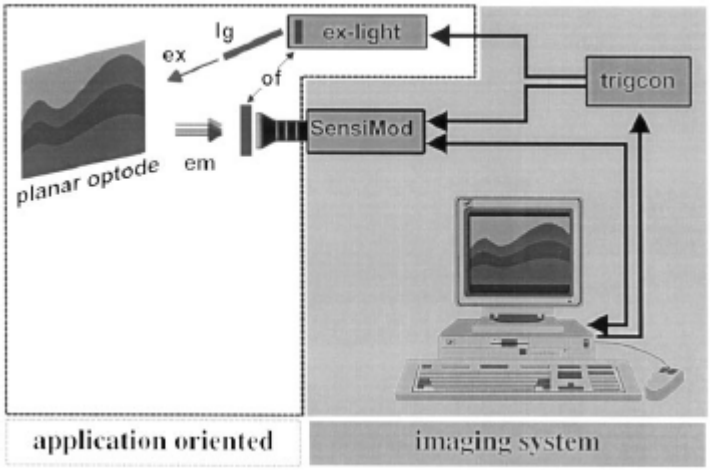

Figure 4-3. Schematic overview of the modular luminescence lifetime imaging system. The imaging system consists of a fast gateable CCD-camera, SensiMod, a Pentium based PC, and a trigger control unit, trigcon. The application oriented part consists of the imaging object, planar optode, the excitation light source, ex-light, an optional light guide (lg) to transport the light to the imaging object, if necessary, optical filters (of). The emitted luminescence (em) reaches the camera via a lens.

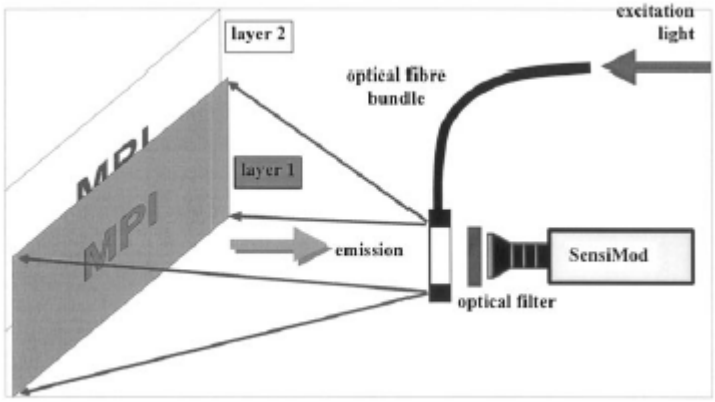

Figure 4-4. Schematic drawing of the experimental setup for demonstrating the background suppression feature of luminescence lifetime imaging. The excitation light is coupled via fibre-optical ring light onto two different luminescent layers on microscope slides. The emission passes through the hole of the ring light, an emission filter (for the intensity images) and the lens to the CCD-camera.

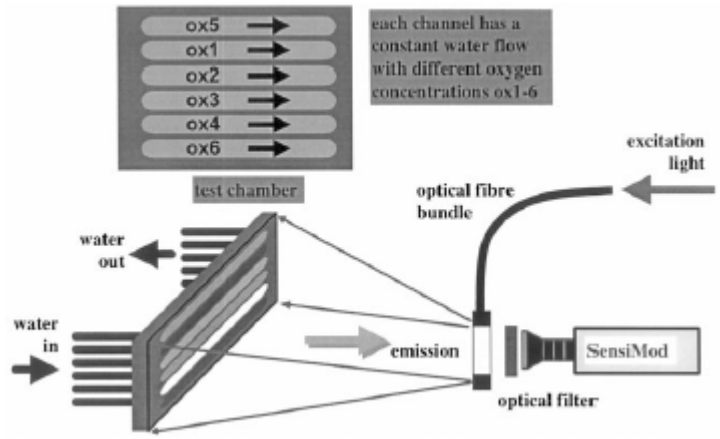

Figure 4-5. Schematic drawing of the experimental setup for the oxygen mapping with planar optodes. A thermo stated (not shown) test chamber with six perfusion channels was perfused separately by water with defined levels of dissolved oxygen (ox1–ox6). Towards the camera, the channel test chamber is closed with the planar optode pressed by a plastic window onto these channels. The chamber has a size of about 35x50 mm^2 to accept planar optodes of 28x40 mm^2. The excitation light again is coupled into a fibre-optical ring light as in Figure 4-4.

4.2.2. Experimental setups

For testing the luminescence background suppression, microscope slides were mounted in front of the camera setup (Figure 4-4). The first strongly luminescent layer was the slide with the commercial paint, followed by the slides with the two different oxygen indicators. To be able to compare the situations, the optical emission filter was kept at its position in front of the camera. The images were recorded with different timing between excitation light and camera.

For oxygen mapping, a special multi channel setup was designed with six different flow channels, that were connected to a peristaltic pump. Water with different oxygen concentrations can be guided through these channels, while the whole system is surrounded by a thermo stating housing to keep the temperature constant. The planar optodes were pressed by a plastic window onto these channels and an outer o-ring (Figure 4-5). Therefore, the system was closed towards the camera. Water was pumped from water bottles immersed in water with the same temperature as the test setup. The test water in the bottles was constantly flushed with nitrogen (Figure 4-5, ox4), oxygen (Figure 4-5, ox2) and room air (Figure 4-5, ox1, ox3), and while channels 5 and 6 were filled with tap water and closed. In the results channel 5 (Figure 4-5, ox5) cannot be seen because it was out of the camera field of view, which was adjusted for 50 µm pixel^{-1} resolution. Images were taken at 2 pixel vertical and horizontal binning, so the spatial image resolution was reduced to 100 µm pixel^{-1}.

4.4. Results and discussion

Figure 4-6 shows the advantage of luminescence lifetime imaging in general. The pure intensity images (Figure 4-6a, c) show a nearly constant grey distribution emphasising that the background luminescence is larger then the signal. Additionally, a lot of in-homogeneities can be seen (dark and white dots in Figure 4-6a, c), that are due to the applied spreading procedure of the luminescence paint and some dirt on the microscope slide. When now the images are delayed by a certain time, t_d, the fluorescence of the paint is decayed while the two stripes forming a ‘X’ of the

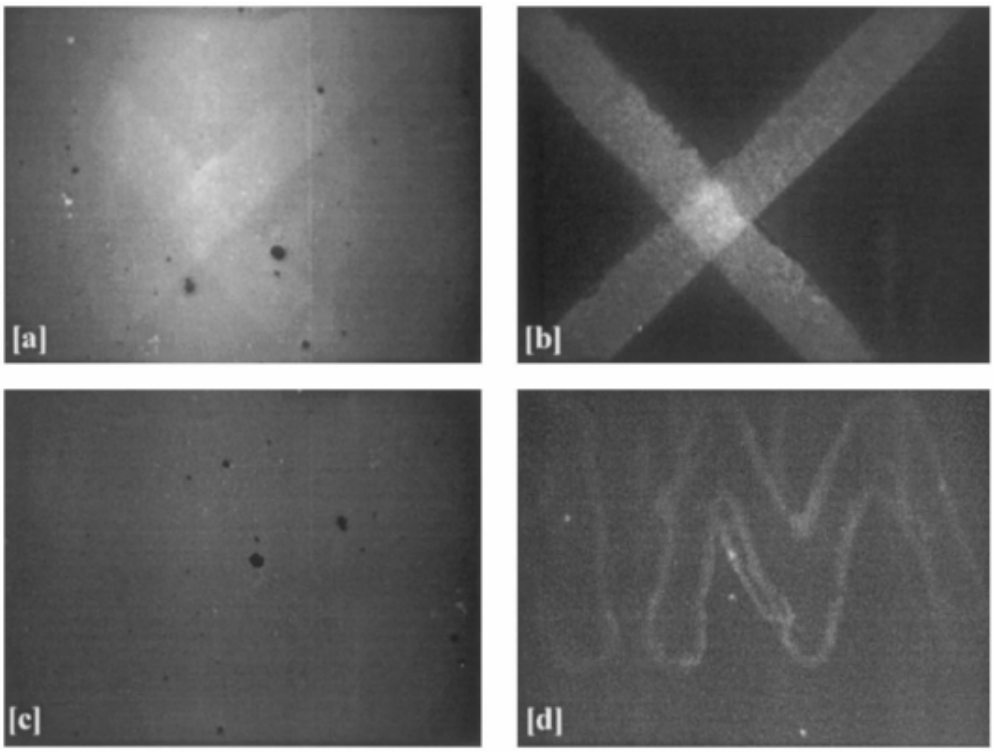

Figure 4-6. Images of the background suppression tests, (a) and (c) are luminescence intensity images and (b) and (d) are delayed, decay curve proportional images. Layer 1 was for all cases a microscope slide with a fluorescent paint and layer 2 was in the upper case, a letter ‘X’ made of a ruthenium oxygen indicator (see text) with a decay time of 2.8 µs and in the lower case, a letter ‘M’ made of a porphyrine oxygen indicator with a decay time of ≈30 µs. The time delay of (b) was 1 µs and the delay of (d) was 4 µs.

ruthenium indicator (Figure 4-6b) as well as the drawn ‘M’ of the porphyrine compound (Figure 4-6d) clearly can be detected.

The ruthenium based optode had a decay time at room air of about 2.8 µs, therefore, the delay of the image in Figure 4-6b was t_d=1 µs. The drawn ‘M’ with the porphyrine had a decay time of ≈30 µs, but the image taken with a delay time t_d=4 µs (Figure 4-6d) is not as high in contrast as the ‘X’. This is due to the fact that the porphyrine has a lower quantum efficiency, a higher quenching coefficient compared to the ruthenium, and the sensing layer did not contain any additional scattering particles.

The results with the oxygen mapping setup clearly demonstrated that the test chamber needs further improvement (Figure 4-7a to c). The images show no sharp channel structure. Obviously, oxygen diffused from the 100% channel (Figure 4-5 ox2, the black one in Figure 4-7a and b, the white one in Figure 4-7c) into neighbouring channels (flow direction in Figure 4-7 was from the left to the right), while the channel with zero oxygen (Figure 4-5 ox4, the white one in Figure 4-7a and b, the black one in Figure 4-7c) received oxygen from the channels above and below (Figure 4-5 ox3, ox6), respectively. Nevertheless, the lifetimes in the middle of the channels were in the same range as determined with single point measurements based on a phase modulation technique (i.e. τ_0=4.8$\pm$0.05 µs, τ_{20}=3.2$\pm$90.05 µs, τ_{100}=2.1$\pm$0.05 ms for oxygen saturation of 0, 20, 100%, respectively).

Figure 4-7 shows the luminescence intensity image with all associated imperfections, like texture within the sensing foil due to the knife coating process and the fast and difficult to control evaporation of the solvent of the ormosil. Additionally, some shadows can be seen, that are caused by water between the transparent

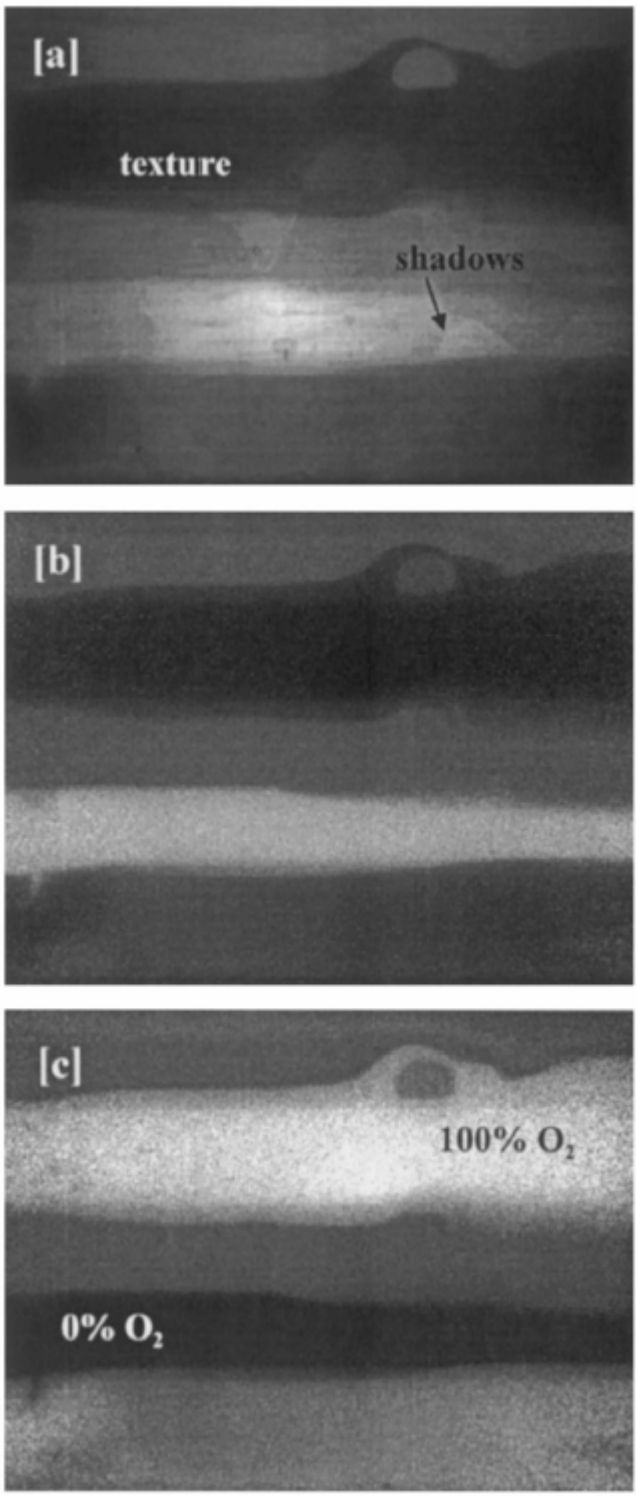

Figure 4-7. Images with the oxygen mapping setup. Image (a) is an luminescence intensity image of the planar optode in the test setup with a certain texture of the sensing foil and some shadows due to an additional liquid layer in the setup between polyester support foil and terminating window. Image (b) is a luminescence lifetime picture evaluated by the described timing and calculation scheme, and image [c] is the corresponding oxygen image, that demonstrates the unwanted diffusion between each perfusion channel of the test chamber (see Figure 4-5).

window and the polyester support foil of the optode. Both phenomena are gone in the lifetime image (Figure 4-7b), and the converted image of oxygen values (Figure 4-7c), which represents an inversion of Figure 4-7b because now the location of the most oxygen is white and the absence is black. The lifetime image was calculated both with a set of three delayed images and with four delayed images with a window at a width of Δ=2 ms and delay times of t_1=500 ns, t_2=1 µs, t_3=2 µs and t_4=3 µs, respectively. Additionally, a background blank image was subtracted with the same time window but with lights 'off', because the CCD-chip has a specific locally fixed noise distribution. Both fitting calculations resulted in the same lifetime distribution. This indicates the stability of the fitting procedure as well as the quality of the information gained within the images. A 2 pixel vertical and horizontal binning was used for the oxygen mapping to increase the absolute signal range. We also took images without binning at full spatial resolution of 50 µm pixel^{-1}. Here the calculations gave the same lifetimes but resulted in higher noise levels. The correspondence between the spatial image resolution per pixel, given by the camera chip and the lenses (either 50 or 100 µm pixel^{-1} in the demonstrated results), and the possible measuring resolution of the planar optodes has to be further investigated with specific test setups. This is necessary because of possible oxygen diffusion processes parallel to the optode surface, which could smear the spatial information.

4.5. Conclusion

A modular lifetime imaging system (MOLLI) based on a new, fast gateable CCD-camera was developed. This camera reduces the amount of equipment needed for

lifetime imaging systems and allows for an easy adaptation of the imaging system to different applications like optode based oxygen mapping in sediments and biofilms, around cells and aggregates. Although the test setup for application of defined oxygen concentrations to the planar oxygen optodes was not optimum, the imaging system demonstrated the advantages of luminescence lifetime imaging in background signal suppression and less noise sensitive signal readout of planar optodes. This combined with the possibility of the measurement of two-dimensional distributions of solutes at high spatial resolutions instead of single profiles with microsensors the new system is a powerful tool for the investigation of natural biological systems.

4.6. Acknowledgements

We gratefully acknowledge the technical support of PCO Computer Optics for modification of the camera and help in programming the interfaces. We acknowledge financial support from the European Commission via the EC MAST III project MICROMARE (950029).

4.7. References

[1] W.L. Rumsey, J.M. Vanderkooi, D.F. Wilson, Imaging of phosphorescence: a novel method for measuring oxygen distribution in perfused tissue, Science 241 (1988) 1649–1651.

[2] W.L. Rumsey, R. Iturriaga, D.F. Wilson, S. Lahiri, D. Spergel, Phosphorescence and Fluorescence Imaging: New Tools for the Study of Carotid Body Function, Chemoreceptors and Chemoreceptor Reflexes, Plenum Press, New York, 1990, pp. 73–79.

[3] R.D. Shonat, D.F. Wilson, C.E. Riva, M. Pawlowski, Oxygen distribution in the retinal and choroidal vessels in the cat as measured by a new phosphorescence imaging method, Appl. Opt. 31 (1992) 3711–3718.

[4] D.F. Wilson, S. Gomi, A. Pastuszko, J.H. Greenberg, Microvascular damage in the cortex of cat brain from middle cerebral artery occlusion and reperfusion, J. Appl. Physiol. 74 (1993) 580–589.

[5] S. Vinogradov, L.-W. Lo, W.T. Jenkins, S.M. Evans, C. Koch, D.F. Wilson, Noninvasive imaging of the distribution in oxygen in tissue in vivo using near-infrared phosphors, Biophys. J. 70 (1996) 1609–1617.

[6] J. Kavandi, J. Callis, M.P. Gouterman, et al., Luminescent barometry in wind tunnels, Rev. Sci. Instrum. 61 (1990) 3340–3347.

[7] M. Gouterman, Oyxgen quenching of luminescence of pressure sensitive paint for wind tunnel research, J. Chem. Educ. 74 (1997) 697–702.

[8] P. Hartmann, W. Ziegler, Lifetime imaging of luminescent oxygen sensors based on all-solid-state technology, Anal. Chem. 68 (1996) 4512–4514.

[9] P. Hartmann, W. Ziegler, G. Holst, D.W. Lübbers, Oxygen flux fluorescence lifetime imaging, Sensors and Actuators B 38–39 (1997) 110–115.

[10] R.N. Glud, N.B. Ramsing, J.K. Gundersen, I. Klimant, Planar optrodes: a new tool for fine scale measurements of two-dimensional O_2 distribution in benthic communities, Mar. Ecol. Prog. Ser. 140 (1996) 217–226.

[11] R.N. Glud, C.M. Santegoeds, D. DeBeer, O. Kohls, N.B. Ramsing, Oxygen dynamics at the base of a biofilm studied with planar optodes, Aquat. Microb. Ecol. 14 (1998) 223–233.

[12] J.R. Lakowicz, Fluorescence lifetime imaging sensing generates cellular images, Laser Focus World, 5 (1992).

[13] J.R. Lakowicz, H. Szmacinski, K. Nowaczyk, K.W. Berndt, M. Johnson, Fluorescence lifetime imaging, Anal. Biochem. 202 (1992) 316–330.

[14] H. Szmacinski, J.R. Lakowicz, M.L. Johnson, Fluorescence lifetime imaging microscopy: homodyne technique using high-speed gated image intensifier, Methods Enzymol. 240 (1994) 723–748.

[15] G. Marriott, R.M. Clegg, D.J. Arndt-Jovin, T.M. Jovin, Time resolved imaging microscopy, Biophys. J. 60 (1991) 1374–1387.

[16] R.M. Clegg, B. Feddersen, E. Gratton, T.M. Jovin, Time resolved imaging fluorescence microscopy, SPIE Conference on Time-Resolved Laser Spectroscopy in Biochemistry II (1990) 448–460.

[17] S. Nomura, M. Nakao, T. Nakanishi, S. Takamastu, K. Tomita, Real time imaging of microscopic pH distribution with a two-dimensional pH-imaging apparatus, Anal. Chem. 69 (1997) 977–981.

[18] R.L. Plant, D.H. Burns, Quantitative, depth-resolved imaging of oxygen concentration by phosphorescence lifetime measurement, Appl. Spec. 47 (1993) 1594–1599.

[19] H. Kautsky, Quenching of luminescence by oxygen, Trans. Faraday Soc. 35 (1939) 216–219.

[20] D.W. Lübbers, N. Opitz, The pCO_2:pO_2 optrode: a new probe for measuring pCO_2 and pO_2 of gases and liquids, Z. Naturforsch. 30C (1975) 532–533.

[21] I. Bergman, Rapid response atmospheric oxygen monitor based on fluorescence quenching, Nature 218 (1986) 396.

[22] J.R. Bacon, J.N. Demas, Determination of oxygen concentrations by luminescence quenching of a polymer immobilised transition-metal complex, Anal. Chem. 59 (1987) 2780–2785.

[23] I. Klimant, O.S. Wolfbeis, Oxygen sensitive luminescent materials based on silicone-soluble ruthenium dimiine complexes, Anal. Chem. 34 (1995) 3160–3166.

[24] I. Klimant, V. Meyer, M. Kühl, Fibre-optic oxygen microsensors, a new tool in aquatic biology, Limnol. Oceanogr. 40 (1995) 1159–1165.

[25] J.R. Lakowicz, K.W. Berndt, Lifetime-selective fluorescence imaging using a RF phase sensitive camera, Rev. Sci. Instrum.62 (1991) 1727–1734.

[26] C.G. Morgan, A.C. Mitchell, J.G. Murray, Fluorescence decay time imaging using an imaging photon detector with a radiofrequency photon correlation system, SPIE Conference on Time-Resolved Laser Spectroscopy in Biochemistry II (1990) 798–807.

[27] X.F. Wang, T. Uchida, D.M. Coleman, S. Minami, A two-dimensional fluorescence lifetime imaging system using a gated image intensifier, Appl. Spec. 45 (1991) 360–366.

[28] R.M. Clegg, B. Feddersen, E. Gratton, T.M. Jovin, Time-resolved imaging fluorescence microscopy, SPIE Conference on Time-Resolved Laser Spectroscopy in Biochemistry III 1640 (1992) 448–460.

Chapter 5

Behavior and associated benthic oxygen dynamics in artificial burrow systems of *Hediste diversicolor*

to be published

5. Behaviour and associated benthic oxygen dynamics in artificial burrow systems of Hediste diversicolor

Bettina Koenig[1], Michael Kühl[2], Ronnie N. Glud[2,*]

[1]Max-Planck-Institute for Marine Microbiology, Celsiusstr. 1, D-28359 Bremen, Germany

[2]Marine Biological Laboratory, University of Copenhagen, Strandpromenaden 5, DK-3000 Helsingør, Denmark

*corresponding author, Fax: +49 421 2020 700, e-mail: koenig@ohb-system.de

Abstract

Planar optodes were used to investigate 2-dimensional O_2 dynamics in burrow systems inhabited by *Hediste diversicolor.* Natural burrows often deviated from the classic U-shape and changed over time. This complicated quantitative assessment of the O_2 dynamics of the burrow. Therefore, we established a stable U-shaped burrow surrounded by agar-solidified sediment. Visual inspection and measured ventilation patterns indicated similar behavior of polychaetes in natural and artificial systems. The volume specific O_2 consumption, R_P, along the primary interface in the two systems were identical. Planar optode and microelectrode measurements gave similar results along the primary sediment-water interface. The radial diffusion of O_2 around a burrow was disturbed by the presence of the planar optode directly attached to the burrow wall causing an enhanced oxygen penetration depth compared to the undisturbed system. With the known geometry of the burrow system the effect could be corrected. Microbial colonization along the burrow lining increased the volume specific O_2 consumption, R_B, from 3.8 ± 0.5 to 13.7 ± 2.1 mol m^{-3} d^{-1} within two days reflecting that the burrow lining of *H. diversicolor* acts as a zone of intensified diagenetic activity. Extrapolated to natural densities in coastal sediments (600 m^{-2}) our findings indicate that 88% of the benthic O_2 uptake is associated to worm burrows and that the major fraction hereof (66%) is related to microbial activity in the burrow lining, while 22% can be ascribed to fauna respiration.

5.1. Introduction

Macrofauna is important for mass transfer and mineralization of organic matter in marine sediments (Aller 1988, Kristensen 2000). Bioturbation translocates organic matter between oxic and anoxic reaction zones, and enhances the area of the sediment-water interface by forming ventilated burrows and funnels (Yingst and Rhoads 1980, Aller 1982). Bioirrigation of burrows with oxic water enhances the sediment volume exposed to oxygen and leads to a constantly changing complex 3-dimensional pattern of oxic and anoxic environments in surface sediments (Fenchel 1996, Forster 1996, Kristensen 2000, Aller 2001, Wenzhöfer & Glud 2004). However, the burrow lining does not just represent an extension of the primary sediment-water interface, but is also a niche for microbial activity with it's own physical, chemical and biological microenvironment linked to the animal behavior (Aller 2001, Hulth et al. 2002, Hannides et al. 2005, Stahl et al. 2006, Zhu et al. 2006).

Hediste diversicolor (O.F. Müller) is a common and abundant polychaete in temperate coastal and estuarine sediments (Miron & Kristensen 1993, Riisgaard et al. 1996, Hansen and Kristensen 1997). Densities vary between 300-6000 ind. m^{-2}, with population maxima dominated by juvenile specimens during spring, but with fewer and larger specimens in autumn and winter (Henriksen et al. 1983, Kristensen 1988, Rysgaard et al. 1995, Riisgaard et al. 1996). Typical population densities in muddy, shallow sediments are around 600 m^{-2} (Banta et al. 1999, Christensen et al. 2000). *Hediste diversicolor* is generally anticipated to live in more- or less U-shaped burrows extending about 2-8 cm into the sediment. By undulating body movements they can irrigate the burrow with oxic water containing food particles that are caught in an excreted mucus web and consumed (Riisgaard 1991). However, suspension feeding can be supplemented with active foraging on

the sediment surface (Thede 1973, Vedel 1998, Christensen et al. 2000). Mass balances and incubation measurements have shown that the burrow of *H. diversicolor* can get anoxic over shorter or longer time intervals during resting periods of the polychaete (Wells and Dales 1951, Thede et al. 1973, Kristensen 1983a). Respiration and ventilation patterns of *H. diversicolor* have been studied on specimens placed in plastic tubes mimicking a defined burrow system (Kristensen 1983a, Nielsen et al. 1995), but extrapolation to *in situ* activities is problematic (Kristensen, 1983b) and associated O_2 dynamics in the burrow are poorly represented. Furthermore, more complex borrow systems with blind ends and additional galleys may evolve in natural systems (Davey 1994).

Bioturbation in sediments has been visualized by applying inverted periscopes equipped with camera systems (Rhoads and Germano 1982, Nilsson and Rosenberg 2000), resin casts, and CT or x-ray imaging of burrow systems (Davey 1994, Furukawa et al. 2001, Rosenberg et al. 2007). Also, a number of models describing solute dynamics and mineralization in bioturbated sediments have been proposed (e.g. Aller 1982, 2001, Furukawa et al. 2001). However, experimental verification of models and detailed quantitative studies on the biogeochemical importance of the secondary interfaces have been hampered by a lack of techniques, that can resolve the pronounced spatial and temporal heterogeneity in burrow systems. Microsensors have been used to map the oxic zone around burrows (e.g. Fenchel 1996), but in practice such measurements are limited to a few point measurements and essentially represent a one-dimensional approach for describing the O_2 distribution in burrows with variable O_2 concentrations. Consequently, the extrapolation of a few microsensor data to the complex nature of the O_2 dynamics around burrows is difficult. Recently, planar optode based O_2 imaging approaches have allowed a more detailed insight in the O_2 dynamics of

natural burrow systems (Wenzhöfer and Glud 2004, Polerecky et al. 2006, Timmerman et al. 2006).

Natural burrow systems are difficult to exploit as their detailed geometry may not always be approached by a simple geometric form (Polerecky et al. 2006). In this study we present an easy method to construct artificial burrow systems with a known geometry in stabilized sediments. By concerted application of planar optodes and flow-thermistors we studied the irrigation behavior in natural and artificial burrow systems of *H. diversicolor* and evaluated the associated O_2 dynamics. The measurements allowed us to establish a detailed budget for the O_2 consuming processes in the burrow.

5.2. Materials and methods

5.2.1. Sampling

Small specimens (0.08-0.15 g w/w) of *Hediste diversicolor* were collected during April-June in Helsingør Harbor, Denmark. The water depth at the sampling site was ~0.5 m, the temperature 10-15ºC, and the salinity S=26. Due to extensive mixing, the surface sediment showed no clear depth dependence in porosity or total organic carbon (TOC) (Fenchel 1996). The average porosity for the upper 5 cm amounted to 0.9±0.1 vol/vol (n=28) and the TOC content was 0.7±0.3% dw (n=25).

After sampling, the polychaetes were kept in an aquarium with sieved and homogenized sediment devoid of any other macrofauna. The aquarium was continuously flushed by flow-through system of sea water (~15ºC and S=30).

During storage, acclimation, and experiments, *H. diversicolor* was fed every second day with aliquots from a dense culture of microalgae (*Rhodomonas* sp.). The specimens were on average kept for 3 weeks prior to any experiments.

5.2.2. Experimental setup

Experiments were conducted with individual specimens transferred to a narrow glass aquarium (Depth=38 mm, width=4mm, length=100 mm) equipped with planar optodes along one of the two large windows. The light dark cycle (12:12 h) from the pre-incubation was maintained. During acclimatization, the aquaria sides were covered with black plastic to eliminate microalgal growth on the semi-transparent planar optode inserted in the sediment. The experimental aquarium was partially filled with either sediment or an agar-mud mixture (see below) (Fig. 1). The planar optode was positioned so that it was covered by sediment and only the upper 3 mm of the optode extended into the water. A steady flow (0.1 cm s^{-1}) of aerated water (100% air saturation) through the aquarium was maintained by connecting the experimental aquarium to a re-circulating water pump immersed in a 5 l reservoir of constantly aerated seawater. The water pump was equipped with a three-way connector, which allowed for re-circulation of a constant water volume (~18 ml) through the sealed chamber to quantify the total benthic oxygen uptake (see below). The average flow velocity through the chamber was determined by collecting the water passing the chamber in a defined time interval and measuring the cross-sectional area of the water column above the sediment. The animals were allowed to acclimatize to the experimental condition for 2 days prior to any measurements.

For the set-up with naturally formed burrows the experimental aquarium was filled with sieved sediment (Fig. 1). Individual polychaetes were transferred to the experimental aquaria; they immediately dug into the sediment and created a natural burrow system. A series of 10 aquaria was established, but in most cases the animals established their burrow systems at some distance form the planar optode and these chambers were discarded. In 3 instances burrows formed along

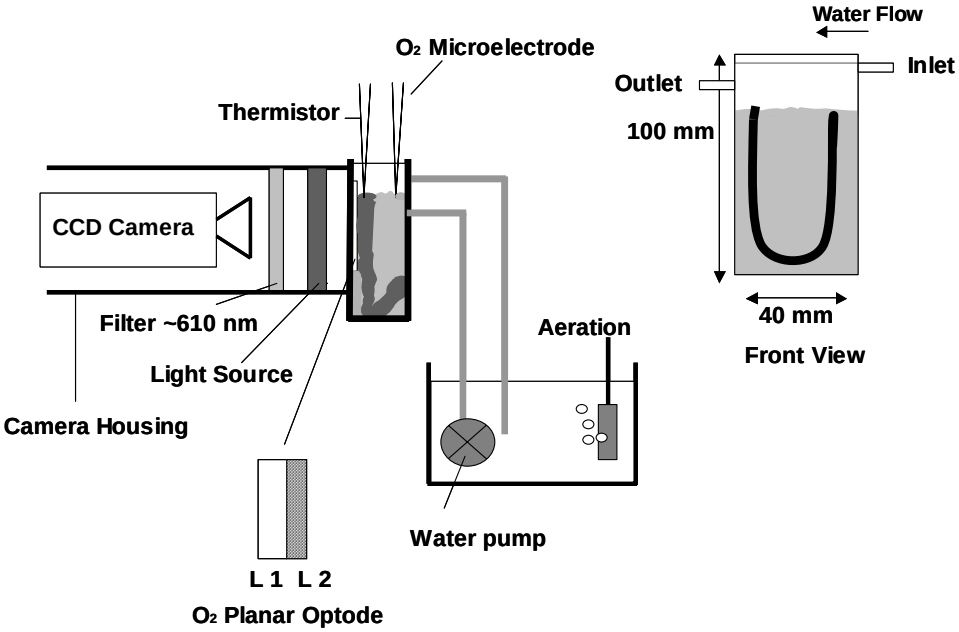

Figure 5-1. Schematic drawing of experimental setup. A planar O_2 optode consisting of a 120 µm thick transparent supporting foil, L1, and a ~10 µm thick semi-transparent oxygen sensitive layer was immobilized on the inside of a narrow aquarium (38 x 4 x 100 mm) containing ~15 ml sediment and 4.5 ml seawater. The aquarium was flushed with aerated seawater from a reservoir via circulation pump. Blue LED's (430-470 nm; Nichia Corp., Japan) connected to a fiber-optic ring light excited the luminescent oxygen indicator in the foil. The distribution of luminescence intensity and lifetime over the foil was recorded with a sensitive fast gate-able CCD camera (PCO Sensimod, PCO GmbH, Kelheim, Germany) equipped with a 35 mm macro lens (Tevidon, F1.6) and a 610 nm long-pass filter. A PC controlled the modulation of excitation LED's and the camera image acquisition via custom made software (see Holst et al. 1998 and Holst and Grunwald 2001 for more details on the luminescence lifetime measuring system and calibration procedures).

the planar optode equipped aquarium wall. All three were used for O_2 imaging and qualitative observations, but only one aquarium was used for TOU measurements.

Geometrically well-defined artificial burrow systems were constructed by placing a PVC-tubing (outer diameter 2 mm) in a U-shape and along the aquarium wall covered with a planar optode. A mixture of fluid 40-45 ºC warm, 3% w/w agar based on 30 ‰ seawater and homogenized sediment was filled into the aquaria. After cooling and solidification of the sediment-agar mixture, the tubing was carefully removed leaving a well-defined artificial burrow along the planar optode. The final porosity of the sediment-agar mixture was 0.9 vol/vol. The chamber was carefully rinsed with seawater and connected to the flow through system as described above. After addition, polychaetes immediately occupied the artificial burrow. Here they were allowed to acclimatize for half a day before any measurements. A series of 5 aquaria were established and 4 aquaria were selected for the experiments described below. However, long-term experiments and TOU measurements were only performed in one aquarium.

5.2.3. Flow measurements

The irrigation activities of *H. diversicolor* were monitored by a custom-made flow-thermistor system (LaBarbera and Vogel 1976). The flow meter measures the temperature change at the sensor tip due to the water flow, which is independent of the current direction (La Barbera and Vogel 1976). Calibration measurements were performed under experimental conditions. The sensor tip was mounted in the center of the experiment chamber a few millimeter above the sediment surface. The water flow through the aquarium was step wise increased and the flow rate was determined by collecting the water passing through the aquarium during a

defined time interval. The corresponding current of the flow-meter was recorded and a calibration curve was established. The sensor signal increased logarithmically with flow in the range of 0.1 to 10 cm s^{-1}.

5.2.4. Oxygen microsensor measurements

Oxygen concentration microprofiles across the primary sediment-water interface were measured with Clark-type oxygen microelectrodes (tip diameters <20 µm, t_{90} response time <1 s, stirring sensitivity <1%) (Revsbech 1989, Glud et al. 2000). Microelectrodes were mounted in a manual micromanipulator (Märtzhäuser, Wetzlar, Germany) and were vertically inserted into the sediment of the experimental aquarium in increments of 25 µm. The sensor signals in each depth horizon were recorded on a strip-chart recorder and were later linearly calibrated against microsensor signals obtained at anoxia and at 100% air-saturation.

The O_2 microelectrodes were also used to measure the total oxygen uptake (TOU). Here the microelectrode tip was positioned in the overlying water, while the water pump was switched to a re-circulating mode channeling water through the sealed chamber (see above). Thereby, the same flow regime could be maintained during microprofile and TOU measurements. Oxygen was never allowed to decrease more than 20% from the initial oxygen level, and control experiments showed an insignificant oxygen consumption in the circulating water or in biofilms establishing on surfaces of the incubation system. In parallel to the incubations, the two-dimensional distribution of O_2 above and within the sediment was imaged by the planar optode set-up (see below).

5.2.5. Two-dimensional mapping of oxygen

Planar O_2 optodes were used to map the two-dimensional O_2 distribution around *H. diversicolor* burrows. The optodes consisted of a thin semi-transparent layer of an oxygen sensitive dye (Ru(II)-tris-4,7-diphenyl–1,10-phenantroline perchlorate) immobilized together with light scattering TiO_2 particles in a matrix of organically modified sol-gel on top of a transparent 120 µm thick supporting foil (Mylar, Goodfellow) (König et al. 2005). The t_{90} response time of the sensor foils was <2 s, and the foils had a homogeneous response to oxygen over several cm^2. More details about construction, characterization, and calibration of the semi transparent sensor foils are presented elsewhere (König et al. 2005).

The optical measuring principle used with O_2 optodes is based on the dynamic luminescence quenching of the ruthenium dye by oxygen (Stern and Volmer 1919, Kautsky 1938). The quenching affects the luminescence decay time, τ, of the immobilized indicator dye. The dependency on the oxygen concentration, c, can be described by a modified Stern-Volmer equation (Carraway et al. 1991):

$$\frac{\tau_c}{\tau_0} = \left[\frac{\alpha}{(1 + cK_{SV})} + (1 - \alpha) \right] \quad (1)$$

where K_{SV} is the sensor specific quenching efficiency of the immobilized dye, α (here 0.95) is the quenchable fraction of the luminescence, τ_0 is the luminescence decay time at zero oxygen and τ_c denotes luminescence decay time at a given oxygen concentration, c.

The distribution of the oxygen dependent luminescence from the planar optode was recorded by a luminescence lifetime imaging system described in detail by Holst et al. (1998, 1999). The system allows the calculation of a 24 bit floating point number image of the luminescence decay time from a set of two (or three) background corrected 12 bit images of the luminescence recorded at two (or

three) different times relative to the eclipse of the blue LED excitation source. The calculation assumes a mono-exponential decay of the luminescence over time and was done with custom routines written in IDL 5.2 (Research Systems Inc., Boulder, USA). Decay time images were then converted to images of oxygen distribution by help of the calibration images and Eq. 1 (more details in Holst and Grunwald 2001).

In the present study, the optical system was adjusted to cover an area of 2.5x3 cm, yielding a pixel resolution of ~50 µm (640x480 pixels per picture). Prior to the introduction of sediment, a two-point pixel by pixel calibration of the immobilized sensor foil inside the experimental aquarium was performed at the experimental salinity and temperature by flushing sea water in the aquarium with air and N_2, respectively. Marker points on the planar optode and the flow chamber allowed re-alignment of acquired images in case slight shifts occurred during the experiments. The semi-transparent planar optode allowed us to record images of the sediment surface and the burrow structure position by recording normal intensity images, while applying intense white light from a fiber-optic halogen lamp (KL1500, Schott, Germany) towards the sediment-foil interface.

5.2.6. Calculations

Assuming zero-order kinetics, the volume specific O_2 consumption at the sediment surface, R_P, (in units of mol O_2 m^{-3} d^{-1}) was calculated from averaged (n=30) vertical microprofiles extracted from steady-state O_2 images according to Bouldin (1968)

$$R_P = 2c_0D_s/(z_0 - z_B) \quad (2)$$

where c_0 is the O_2 concentration at the depth (z_0) having the steepest concentration slope below the sediment surface, D_s is the tortuosity, temperature, and salinity corrected diffusion coefficient for O_2 in the sediment (Ullman and Aller 1982, Broecker and Peng 1976, Li and Gregory 1974), and z_B is the depth where the O_2 concentration reaches zero. The depth of the steepest slope (z_0) was determined from polynomial fits to the extracted O_2 profiles as the tangential turning point.

The volume specific O_2 consumption around the burrow, R_B can be approximated by: $\delta c/\delta t = D_s(\delta^2 c/\delta x^2 + \delta^2 c/\delta y^2 + \delta^2 c/\delta z^2)$ where c denotes the O_2 concentration at a given time, t. Provided that the gradients along the directions of z and y (vertically, and perpendicular to the aquarium wall, respectively) can be ignored, the equation simplifies to (Polerecky et al. 2005, Franke et al. 2006, Polerecky et al. 2006):

$$R_B \approx D_s \delta^2 c/\delta x^2 - \delta c/\delta t \qquad (3)$$

The concentration change over time ($\Box c/\Box t$) at the point of the steepest concentration slope in the sediment was determined from the series of calibrated images. The diffusion term ($D_s\delta^2 c/\delta x^2$) was determined by applying the second deviation of the polynomial fit to the horizontal profile across the burrow.

Knowing the volume specific O_2 consumption, R_B, the rate of the oxygen uptake (OUB in μmol d^{-1}) across the sediment burrow surface can be calculated as

$$OUB = R_B * V_{oxic} \qquad (4)$$

where V_{oxic} is the volume of oxygenated sediment. To account for the conditions at the burrow inlet and outlet, the total OUB is approximated as the average of OUB_{in} and OUB_{out}. The oxygenated sediment volume, V_{oxic}, can be written as the product of the cross-section area of the oxygenated sediment, A_{oxic}, and the length, Z: $V_{oxic} = ZA_{oxic}$.

Our planar optode measurements have some inherent geometric constraints affecting the measured solute distribution, as illustrated in Fig. 2. In an undisturbed burrow system, O_2 will diffuse radially away form the burrow, oxygenating the area B (with radius r_B). With the planar optode directly attached to the burrow wall (Fig. 2) the area M is discarded. The impact on the oxic zone can be approximated by adding the missing sediment area, M', to the oxic sediment, B. Hereby the planar optode detects an enhanced oxygen penetration depth L_B compared to r_B (Frederiksen & Glud 2006). Thus A_{oxic} can be approximated as (Polerecky et al. 2006):

$$A_{oxic} = B + M - \pi r^2 = (r + d)L_B - \pi r^2 + ((r + d)^2 + L_B^2)(\pi - \arctan(L_B/(r + d))) \quad (5)$$

where r represents the burrow radius (Fig. 2) and d is the distance between the planar optode and burrow wall.

The total oxygen uptake (in µmol O_2 d^{-1}) within the experimental aquaria was calculated from the O_2 concentration depletion rate, d, after sealing the aquarium and the total volume of re-circulating water, V, as TOU = *d* x V.

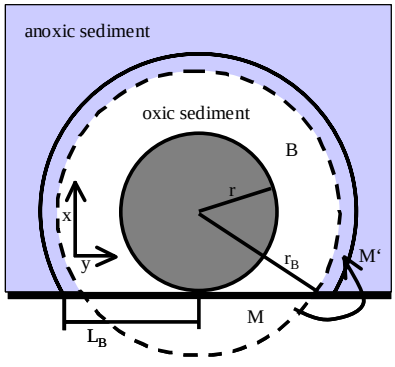

Figure 5-2. Schematic drawing of the horizontal cross section of a cylindrical burrow with radius r. The burrow wall touches the planar optode, thus deforming the radial diffusion geometry. The area (M) is leveled by an enhanced O_2 penetration into the sediment and the planar optode derived O_2 penetration depth (L_B).

5.3. Results

Naturally formed burrows - Initially, the oxygen distribution was measured around *H. diversicolor* burrows as they evolved in natural sediment. In general the burrow structures remained relatively stable for 3 to 6 days, but the sediment surface was continuously reworked due to deposit feeding of polychaetes extending out of their burrows. The burrow structure was often irregular and poorly defined and additional galleries and cross-connections between burrow tubes were observed (not shown) Fig. 3A is a representative image from a series of experiments performed with a specimen of 0.15 g (w/w). Along with the fact that natural burrows extended into the centre of the experimental aquaria, away from the planar optode, the sediment reworking complicated any quantitative assessment of the O_2 consumption of the burrow.

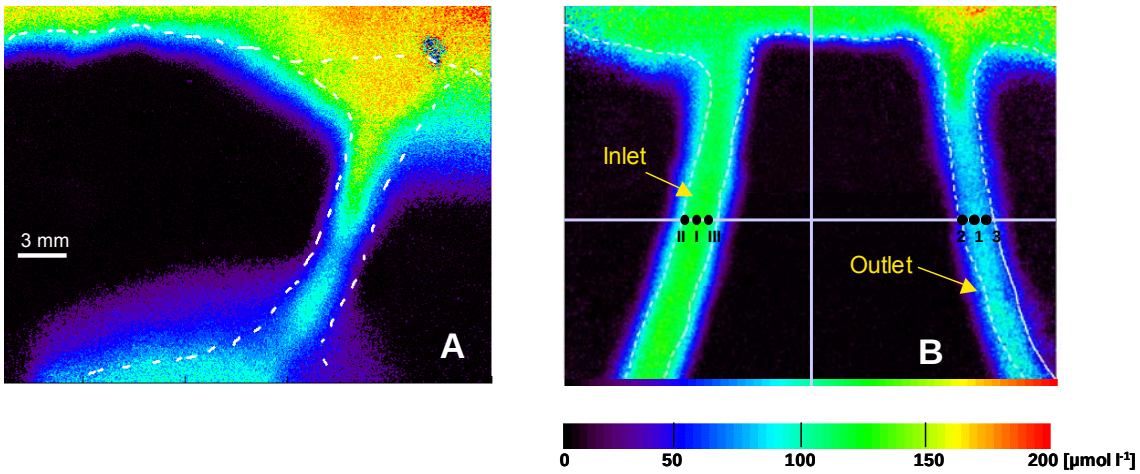

Figure 5-3. Oxygen images recorded along a burrow established in natural sediment (A) and a agar-solidified U-shaped burrow (B) inhabited by two specimens of *H. diversicolor* of 0.15 g and 0.18 g wet-weight, respectively. The O_2 concentration [µmol l^{-1}] is expressed on a 8-bit color scale. Dashed lines outline the primary sediment surface and the secondary burrow-sediment interface. Lines in panel B indicate the position of extracted horizontal (see Fig. 4) and vertical (see Fig. 6) O_2 profiles.

TABLE 1. Oxygen budgets for a burrow system of Hediste diversicolor in natural and artificial sediment. For the artificial sediment O2 budgets at 3 different times are provided.

Symbol [unit]	Definition	Natural system	Artificial system		
			t=0 (n=6)	22.5 h (n=10)	43 h (n=10)
	Irrigation activity (% during 60 min)	60 ± 6 (n=2)	61	60 ± 7 (n=3)	62 ± 10 (n=3)
[ml min^{-1}]	Average ventilation rate	5.4 ± 2.90	4.5 ± 1.4	6.9 ± 2.0	8.5 ± 1.7
Wt w [g]	*H. diversicolor* wet weight	0.15	0.18	0.18	0.18
	sediment-water (primary) interface				
R_P [mmol m^{-3} d^{-1}]	Volume specific O_2 consumption	6.1 ± 2.4	6.1 ± 1.9	6.8 ± 1.9	6.8 ± 2.6
DOE_P [mmol m^{-2} d^{-1}]	Diffusive O_2 exchange	9.2 ± 1.8	(5.2 ± 1.3)	(7.4 ± 0.8)	(7.1 ± 2.2)
L_P [mm]	Vertical O_2 penetration depth	1.5 - 4.5	0.9 ± 0.2	1.1 ± 0.1	1.1 ± 0.3
A_P [cm^2]	Area of primary sediment surface	1.52	1.52	1.52	1.52
OUP [µmol d^{-1}]	Total O_2 uptake of the sediment surface	1.4 ± 0.2	0.8 ± 0.2	1.1 ± 0.1	1.1 ± 0.3
	burrow inlet				
$R_{B,in}$ [mmol m^{-3} d^{-1}]	Volume specific O_2 consumption	-	3.8 ± 0.5	5.67± 2.0	13.7 ± 2.1
$L_{B,in}$ [mm]	Radial O_2 penetration depth	1.0 – 4.0	1.7 ± 0.2	-	-
OUB_{in} [µmol d^{-1}]	O_2 uptake around the burrow	-	3.0 ± 1.7	-	-
R_B*	OUB* / V^*_{oxic}	-	-	26.5 ± 7.2	32.4 ± 10.2
OUB*	TOU-W_{calc}-OUP	7.4 ± 3.2	-	25.0 ± 0.1	32.4 ± 7.1
OUB [µmol d^{-1}]	Total O_2 uptake around the burrow = OUB_{in} + OUB_{out}	-	4.9 ± 2.8	-	-
W_{calc} [µmol d^{-1}]	O_2 consumption rate of *H. diversicolor* as calculated from wet weight (see Banta et al. 1999)	13.2	15.4	15.4	15.4
TOU [µmol d^{-1}]	Total O_2 uptake	21.6 ± 3.2 (n=2)	-	41.5 (n=1)	48.9 ± 7.1 (n=3)

Generally the irrigation patterns reflected a continuous ventilation rate of 5.4±2.9 ml min-1 occasionally interrupted by brief resting periods. Non-filter feeding activity (Kristensen 2000) was characterized by intermittent ventilation, interrupted by periods of rest in unrhythmic fashion (Fig. 4A and 5A). The burrows were irrigated during 60% of the observation time (Table 1). Parallel to the measurements of the ventilation rate, O2 images were recorded at time intervals of 2, 5, and 15 min for up to 12 hour periods. The data showed a clear positive correlation between irrigation activity and O2 levels within the burrows and the burrow walls (data not shown).

The oxygen distribution along the constantly changing primary sediment-water interface was highly variable (Fig. 3A) and the oxygen penetration depth varied from 1.0 to 1.5 mm, with an exceptional value of 4.5 mm (Fig. 3A right side). In the latter case, the sediment was removed by *H. diversicolor* during foraging from the plane of the planar optode. The volume specific O_2 consumption (R_P) was also variable but on average amounted to 6.1±2.4 mmol O_2 m^{-3} d^{-1} (n=30 vertical profiles). Taking the surface area of the primary interface (1.52 cm^2) into account, these rates transfer into a daily O_2 uptake of the sediment surface (OUP) of 1.0±0.3 µmol O_2 d^{-1} (Table 1). The measured daily total oxygen uptake (TOU) was 21.6±3.2 µmol O_2 d^{-1} (n=2, Tab. 1). The difference between TOU and OUP (20.6±3.0 µmol O_2 d^{-1}) is ascribed to the burrow uptake and the respiration of *H. diversicolor,* and was equivalent to 95% of TOU. The oxygen respiration of individual *H. diversicolor* specimen, W_{calc}, could be calculated from their wet weight using empirical formula (Banta et al. 1999, Nielsen et al. 1995) and the total daily O_2 uptake across the burrow wall, OUB*, was estimated as OUB* = (TOU - OUP) – W_{calc} (Table 1). The O_2 consumption by *H. diversicolor* and the burrow wall amounted to 61% and 34% of the total daily oxygen consumption, respectively. As

the burrow geometry (and thus the burrow area) was poorly defined it was difficult to compare the volume specific O_2 consumption rate along the burrow lining to that of the primary interface. In general the irregular shape of the natural burrows extending away from the plane of the O_2 images confounded any detailed quantitative investigations of the O_2 dynamic of the burrow.

Artificial burrows – Specimens added to chambers containing agar-solidified sediment quickly established them self in the confined U-shaped borrows. The well-defined system reflected a gradual O_2 depletion in the water passing through the burrow reaching a minimal O_2 concentration of 55 µM in the lumen of the outlet

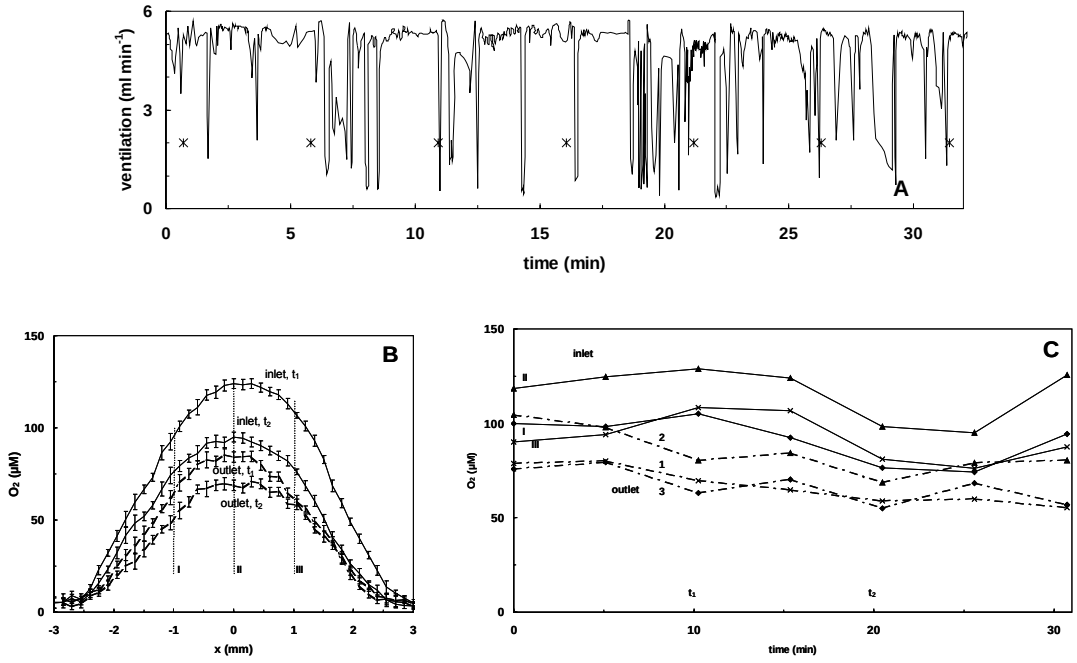

Figure 5-4. (A) Burrow ventilation rate as a function of time measured just above the burrow inlet. The image in Fig. 3B was acquired at the 4th mark (∗) in panel A. The extracted horizontal O_2 concentration profiles (as indicated in Fig 3B) of the inlet and outlet of the burrow are presented in panel B. The variation of oxygen concentration in the burrow inlet (solid lines) and outlet (dashed lines) in selected pixel extracted from image series are provided in panel C. Numbers on curves refer to pixels indicated in Fig. 3B and 4B.

(Fig. 3B and 4C). The radial O_2 distribution reflected the outline of the artificial burrow (Fig. 3B). The O_2 penetration depth of the inlet and outlet amounted to 1.7±0.2 and 1.5±0.3 mm, respectively. Initially (0–1 hours) the burrow was ventilated 61% of the observation time with an average ventilation rate of 4.5±1.4 ml min^{-1} (Table 1). The irregular ventilation pattern with ventilation strokes of various size and length suggested non-filter feeding (Fig. 4A). As for the natural burrows, the oxygen concentration of the burrow lumen correlated with the irrigation activity of *H. diversicolor* (Fig. 4A and C). The dynamic was reflected by the variations in averaged horizontal burrow-profiles (n=30) and selected image points in the lumen and burrow wall (Fig. 3B and 4B). Oxygen levels in the respective positions varied over time with higher levels in the inlet (74-125 µM) than in the outlet (55-104 µM) of the burrow (Fig. 4B and C). On the average oxygen concentration in the lumen of the inlet and outlet differed by 29±12 µM.

Knowing the stable geometry of the burrow and the relative position in relation to the planar optode we could establish an accurate O_2 budget for the burrow (Tab. 1). Applying Eqs 3 and 5 (d=0), revealed a local volume specific O_2 consumption, R_B, in the borrow inlet and outlet of 3.8±0.5 mmol O_2 m^{-3} d^{-1} and 2.0±0.4 mmol O_2 m^{-3} d^{-1}, respectively. The integrated oxygen uptake of the burrow sediment, OUB, amounted to 4.9±2.8 µmol O_2 d^{-1}. This value is lower, but in the same range as compared to the calculated OUB* of the natural system (Table 1).

The burrow walls were quickly colonized by a microbial community and the apparent O_2 concentration as resolved by the planar optode thus declined (Fig. 6A). The O_2 depletion took place within the original outlines of the burrow structure within 20-22 h after animal addition as the mucus film gradually was colonized by bacteria (Fig. 5B to 4E). This enhanced O_2 consumption along the burrow strongly indicates that the burrow lining of mature *Hediste diversicolor* borrows can act as

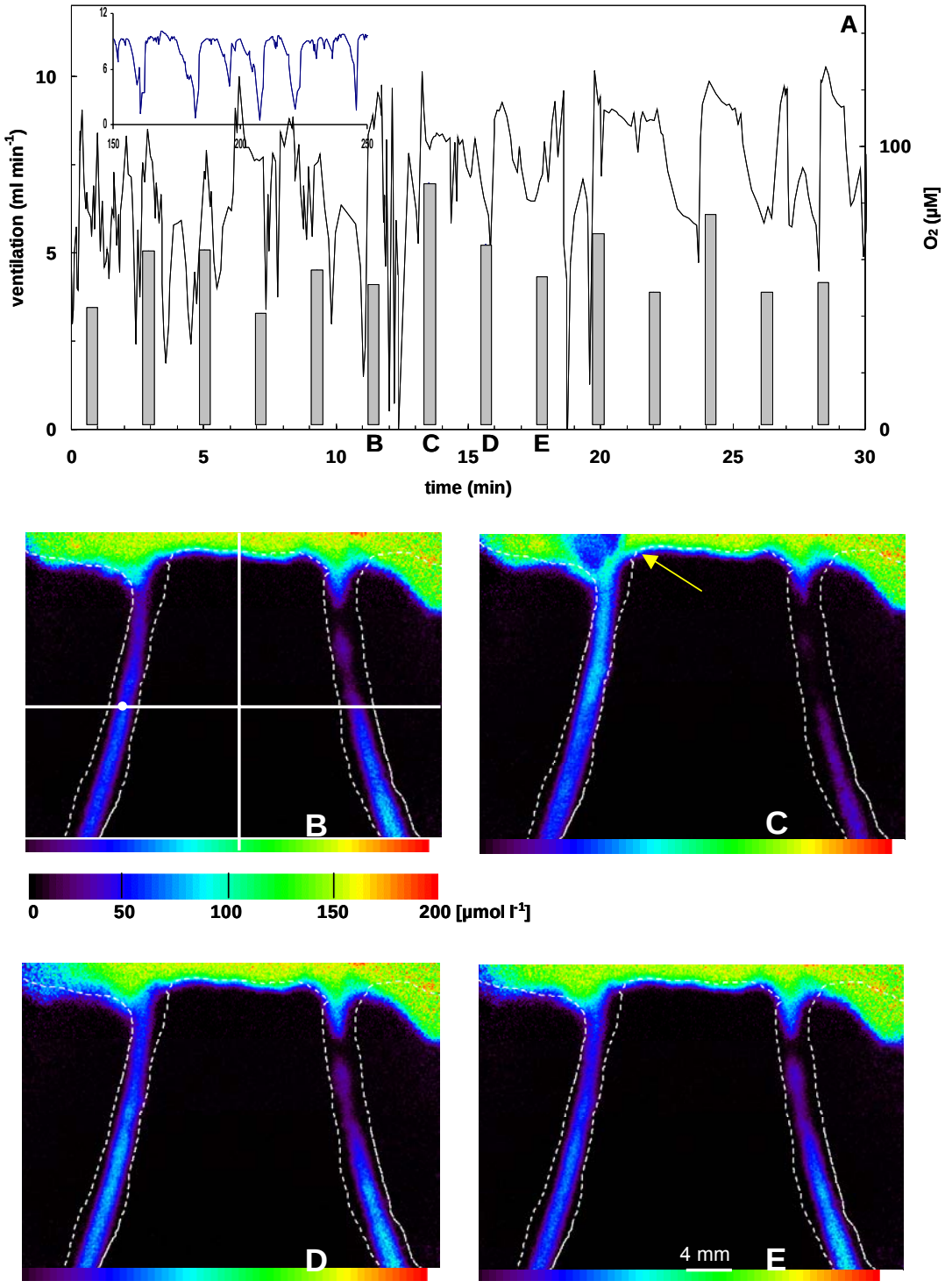

Figure 5-5. Ventilation rates of a *H. diversicolor* (0.18 g w/w) as measured 22.5 h after the animal occupied the artificial burrow system. Letters indicate time points at which the O_2 images were obtained. The right ordinate indicates the O_2 concentration as recorded by the planar optode at the dot in panel B. An example for filter feeding ventilation pattern is provided in the inset of panel A. An arrow in panel C indicates an outburst of oxygen depleted water when ventilation commenced after a resting period. Dashed lines outline the primary sediment surface and the secondary burrow-sediment interface. The O_2 concentration in µmol l^{-1} is expressed on a 8-bit color scale.

diagenetic hot spot. However, the O_2 images still reflected the irrigation activity of the animal (Fig. 5). The lowest O_2 concentration was still found in the borrow outlet and sections of the burrow apparently became almost anoxic as ventilation rates ceased (Fig. 5B). When ventilation resumed, a plume of water with low O_2 content was expelled from the burrow outlet into the overlaying water (Fig. 5C). In some cases the inlet and outlet tube shifted as the animal changed orientation after extensive deposit feeding at the surface (Fig. 5).

The burrow $R_{B,in}$ at $t_{22.5h}$ increased to 5.7±2.0 mmol O_2 m^{-3} d^{-1} and further to 13.7±2.1 mmol O_2 m^{-3} d^{-1} at t_{43h}. A robust evaluation of the burrow outlet was not possible as the polynomial fit to the extracted microprofiles in the heavily colonized section, characterized by low O_2 concentrations, became highly inaccurate. Total oxygen uptake measurements performed at $t_{22.5h}$ and t_{43h} amounted to in 41.5 µmol O_2 d^{-1} (n=1) and 48.9±7.1 µmol O_2 d^{-1} (n=3), respectively.

In contrast to the O_2 profiles of the borrow (Fig. 6A), the vertical O_2 profiles along the primary interface remained almost unaffected during the entire experiment (Fig. 6B) with an average O_2 penetration depth of 1.0±0.3 mm. Based on these profiles we calculated a constant, average R_P for the primary sediment surface of 6.6±2.1 mmol O_2 m^{-3} d^{-1} (Table 1). The results of R_P were 7% higher, but within the same range as the value found for the natural system. The average total uptake at the primary interface, OUP, was accordingly estimated to 1.0±0.4 µmol O_2 d^{-1}.

Microprofiles measured by microelectrodes in the interior of the aquarium filled with natural sediment provided R_P-values of 7.0±2.4 mol m^{-3} d^{-1} and O_2 penetrations depths of 1.0±0.3 mm. This aligned well with the above results from the planar optode measurements at the chamber wall (Tab. 1) and both techniques thus provided similar results.

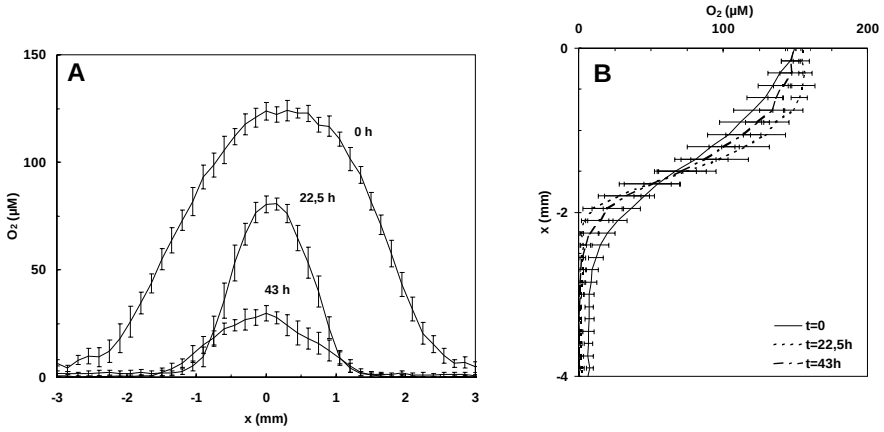

Figure 5-6. O_2 microprofiles extracted from planar optodes at the primary interface (A) and across the burrow 0, 22.5 and 43 h after the animal had occupied the agar solidified burrow system.

The irrigation activity remained constant at 61±12% during the entire experiment, while the ventilation rate increased to 6.9±2.0 ml min^{-1} ($t_{22.5h}$) and 8.5±1.7 ml min^{-1} (t_{43h}). The ventilation pattern suggested infrequent changes between non-filter and filter feeding, the latter being reflected by continuous ventilation with regular ventilation strokes of similar length and size at high rates only interrupted by brief rest periods (Fig. 5A inset).

5.4. Discussion

The dynamic nature and irregularities of natural burrow systems of *H. diversicolor* limited the quantitative insight that could be gained from studying conditions in natural sediments. In contrast, the construction of regular, agar-solidified burrows enabled a much more detailed study of the O_2 dynamics within the burrow. The

artificial burrows had a length of 12 cm, which range with literature values of 9-20 cm for specimens in the range of 0.2-0.4 g w/w. (Davey 1994, Christensen et al. 2000). The ventilation patterns of the natural and the artificial burrow systems were comparable (Tab. 1). Both systems reflected periods of non-filter feeding, and for the artificial system also filter feeding periods were observed as defined by Kristensen (2000). However, a shift in ventilation was not always triggered by feeding with algal suspensions.

Over time the ventilation rate in the artificial system almost doubled (Table 1). Presumably, this was partly caused by a gradual reduction in the burrow diameter as the mucus lining developed. Assuming that the amount of water passing through the burrow remained constant, the increase in ventilation rate at (t_{43h}) would corresponded to a reduction in the burrow diameter from 1.0 to 0.7 mm. The increase in ventilation rate could also partly be ascribed to more intense ventilation in order to sustain the metabolic O_2 requirement in an environment with gradual O_2 depletion. However, this would be expected to result in an increased irrigation activity, which actually remained constant (Table 1).

Changes in irrigation activity and ventilation rate on diel time scales were not considered, and all measurements were performed during daytime. The irrigation activity and the ventilation rates measured in the artificial burrows aligned well with previous measurements in natural systems, where typical ventilation rates of 2-6 ml min^{-1} and irrigation activities during 66–85% of the time have been reported (Kristensen 1983a, b, Christensen et al. 2000, Tang & Kristensen in press). The shift in animal orientation leading to shifts in the burrow inlet and outlet has also previously been observed in natural *H. diversicolor* burrows (Tang & Kristensen in press). The artificial burrow system thus appears to be an ideal set-up for studying natural animal behavior and associated O_2 dynamics quantitatively.

The volume of the overlaying re-circulating water in the aquarium was small (~ 4.5 ml) and the average water flow was modest (0.1 cm s^{-1}). Thus flushing of the burrow lumen after resting periods occasionally induced O_2 depletion in the overlying water. This is not a natural situation where a large water reservoir will buffer such fluctuations. Images obtained during such periods where therefore not included for the mass balance calculations discussed below.

Vertical profiles at the primary interface, as extracted from the O_2 images in natural and artificial systems, where similar and revealed an O_2 penetration depth ranging form 0.9-1.5 mm in both systems.

It has previously been suggested that the mucus lining established in *H. diversicolor* burrows promotes bacterial growth (Riisgard 1991). This was also experienced in our burrows. For instance, the $R_{B,in}$ of the artificial burrows within a few days increased from 3.8±0.5 mmol m^{-3} d^{-1} to 13.7±2.1 mmol m^{-3} d^{-1}, reflecting an intensified microbial activity in the burrow lining. This, however, also complicated simple geometric calculations of the planar optode images. The mucus lining and bacteria created a new interface inside the burrow resulting in a smaller burrow diameter. As the mucus layer also covered the planar optode, images no longer reflected conditions in the lumen and the oxygenated zone around the burrow, and the total O_2 uptake around the burrow could not be determined. However, the R_B could still be derived from the temporal O_2 dynamics using (Eq. 3) and amounted to 13.6±7.9 mmol m^{-3} d^{-1} at t_{43h}.

From simple mass balance calculations it was estimated that the initial TOU of the agar solidified system amounted to (21.1±2.8 µmol O_2 d^{-1}), which aligns well with the measured TOU for the natural system (21.6±3.2 µmol O_2 d^{-1}). Unfortunately, we did not measure the initial TOU of the artificial burrow system but the TOU at $t_{22.5h}$ and t_{43h} amounted to 41.5 µmol O_2 d^{-1} (n=1) and 48.9±7.1

µmol O_2 d^{-1} (n=3), respectively. Assuming a constant polychaete respiration and knowing the OUP, the O_2 uptake by the burrow could be estimated as OUB* = TOU – OUP – W_{clac} and accounted for 25.0±0.1 µmol d^{-1} ($t_{22.5h}$) and 32.4±7.1 µmol d^{-1} (t_{43h}). Thus the oxygen uptake of the burrow was 6.7 times higher after 43 hours.

With the knowledge of A_{oixc} and the burrow radius at time t_{0h}, r, it was possible to calculate the oxygen penetration depth, r_B, from the centre of the burrow when solely surrounded by sediment (Fig. 2):

$$r_B = \sqrt{((A_{oxic}/\pi) + r^2)} \quad (6)$$

From the calculated values for r_B, the oxygen penetration depth was derived (1.3 mm). The ratio between the measured and the calculated oxygen penetration depth $(L_B – r)/(r_B – r)$ was 1.3 and this ratio expresses the enlargement of the oxic zone induced by the presence of the planar optode relative to a situation of undisturbed sediment. This calculation could not be done for the later stages of the experiments when the planar optode in the burrow was covered by a mucus biofilm. A general view on the development of the ratio L_B/r_B relative to the location between burrow lumen and planar optode, d, is presented in Fig. 7 where r_B and r (1 and 2 mm) were set constant. With increasing d the ratio L_B/r_B decreased as the oxygen penetration depth L_B decreased.

In our experimental set-up, the artificial burrow enhanced the total sediment-water interface 5-fold, while the calculated oxic volume at t_{0h} was enhanced 14 times. As a result the O_2 uptake of the artificial burrow wall at t_{0h} was 6 times higher than the total O_2 uptake along the primary interface. Thereby, the fauna mediated uptake including animal respiration, W_{calc}, and the O_2 uptake of the burrow lining, OUB, accounted for 96% of the total O_2 consumption in the experimental aquarium. The respiration accounted for 73% while 23% of the total

burrow consumption could be ascribed to the burrow uptake. After 43 hours, the OUB had increased to 66%.

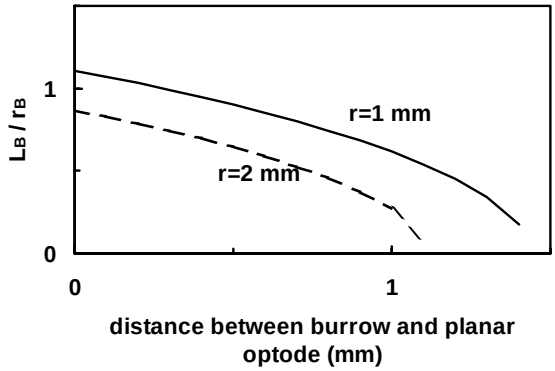

Figure 5-7. Development of the ratio of O_2 penetration depth seen by the planar optode, LB, and the O_2 penetration depth of the undisturbed sediment, r_B, relative to the position of the burrow lumen to the planar optode, d, for burrow radius of 1 and 2 mm.

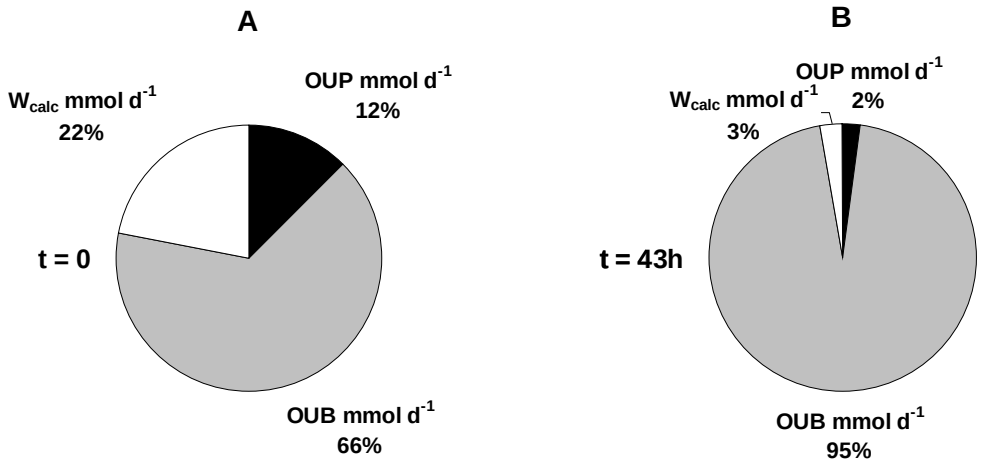

Figure 5-8. The relative importance of the respective O_2 consuming processes at t_{0h} (A) and t_{43h} (B) after the animal had occupied the agar solidified burrow system. Estimates of OUB, OUP, and W_{calc} are given in % of the TOU and are extrapolated to a density of 600 individuals m^{-2}.

Extrapolating the O_2 budgets of the artificial burrow to an average population density of 600 ind. m^{-2}, the fauna mediated O_2 uptake at t_{0h} amounted to 88% (37±2 mmol m^{-2} d^{-1}) of the TOU, divided into 66% for OUB and 22% for the polychaete respiration (Fig. 8A). After 43 hours the fauna mediated O_2 uptake had increased to 98% (319±47 mmol m^{-2} d^{-1}) with 95% being related to the burrow uptake and only 3% to the polychaete respiration (Fig. 8B). These values underscore that burrow walls of *H. diversicolor* represent zones of intensified diagenetic activity. The relative importance of the O_2 consumption due to the polychaete respiration compare to *in situ* reports of 6–25% (Wenzhöfer and Glud 2004) and lab based feeding experiments 15-30% (Christensen et al. 2000).

The high O_2 dynamic around a natural and artificial burrow of *H. diversicolor* were investigated in close detail with the planar optode technique. For the artificial burrow system the volume specific O_2 consumption (R_P and R_B) and the total O_2 uptake (OUP and OUB) at the primary sediment surface and along the burrow wall could be calculated in good precision and correlated with the behaviour of *H. diversicolor*.

Our study shows how the combination of planar optodes and agar-solidified artificial burrows can be used to gain insight to the behavior and associated O_2 dynamics of bottom dwelling invertebrates. The presented procedure can in principle be used for more complex burrow systems and other species of importance for benthic biogeochemistry.

5.5. Acknowledgments

This study was financed by the Max-Planck Society (Germany), the Carlsberg Foundation (Denmark), and the Danish Natural Science Research Council. Gerhard Holst and Björn Grunwald are thanked for help when applying their imaging system described in Holst and Grunwald (2001). Anni Glud is thanked for excellent technical assistance.

5.6. Literature Cited

Aller RC (1982) The effects of macrobenthos on chemical properties of marine sediment and overlying water. In McCall PL, Tevesz MJS (eds) Animal-sediment relations. Plenum, p 53-102

Aller RC (1988) Benthic fauna and biogeochemical processes in marine sediments: the role of burrow structures. In Blackburn TH, Sørensen J (eds) Nitrogen cycling in coastal marine environments. Wiley, p 301-338

Aller RC (2001) Transport and reactions in the bioirrigated zone. In Boudreau BP, Jørgensen BB (eds) The Benthic Boundary Layer: Transport processes and biogeochemistry. Oxford, p.269-301

Aller JY, Aller RC (1986) Evidence for localized enhancement of biological activitiy associated with tube and burrow structures in deep-sea sediments at HEBBLE sie western North Atlantic. Deep-Sea Res. I 33: 755-790

Banta GT, Holmer M, Jensen MH, Kristensen E (1999) Effects of two polychaete worms, Nereis diversicolor and Arenicola marina, on aerobic and anaerobic decomposition in a sandy marine sediment. Aq Microb Ecol 19: 189-204

Bouldin DR (1968) Models for describting the diffusion of oxygen and other mobile constituents across the mud-water interface. J Ecol 56: 77-87

Broecker WS, Peng TH (1974) Gas exchange rates between air and sea. Tellus 26: 21-35

Carraway ER, Demas JN, DeGreef A, Bacon B (1991) Photophysics and the photochemistry of oxygen sensors based on luminescent transition-metal complexes. Anal Chem 63: 337-342

Christensen B, Vedel A, Kristensen E (2000) Carbon and nitrogen fluxes in sediment inhabited by suspension-feeding (Nereis diversicolor) and non-suspension-feeding (N. virens) polychaetes. Mar Ecol Progr Ser 192: 203-217

Davey, JT (1994) The architecture of the burrow of Hediste diversicolor and its quantification in relation to sediment-water exchange. J Exp Mar Biol Ecol 179: 115-129

Fenchel T (1996) Worm burrows and oxic microniches in marine sediments. 1. Spatial and temporal scales. Mar Biol 127: 289-295

Forster S (1996) Spatial and temporal distribution of oxidation events occurring below the sediment-water interface. P.S.Z.N.I. Mar Ecol 17: 309-319

Franke U, Polerecky L, Precht E, Hüttel M (2006) Wave tank study of particulate organic matter degradation in permeable sediments. Limnol Oceanogr 51: 1084-1096

Furukawa Y, Bentley SJ, Lavoie DL (2001) Bioirrigation modeling in experimental benthic mesocosms. J Mar Res 59: 417-452

Frederiksen MS, Glud RN (2006) Oxygen dynamixs in the rhizosphere of Zostera marina: A two-dimensional planar optode study. Limnol Oceanogr 51: 1072-1083

Glud RN, Gundersen JK, Røy H, Jørgensen BB (2003) Seasonal dynamics of benthic O2 uptake in a semienclosed bay: Importance of diffusion and faunal activity. Limnol Oceanogr 41: 1265-1276

Glud RN, Gundersen JK, Ramsing NB (2000) Electrochemical and optical oxygen microsensors for in situ measurements, in Buffle J, Horvai G (eds) In situ monitoring of systems: Chemical analysis and speciation. Wiley, p 19-72

Glud RN, Ramsing NB, Gundersen JK, Klimant I (1996) Planar optrodes: a new tool for fine scale measurements of two-dimensional O2 distribution in benthic communities. Mar Ecol Progr Ser 140: 217-226

Glud RN, Tengberg A, Kühl M, Hall POJ, Klimant I, Holst G (2001) An in situ instrument for planar O2 optode measurements at benthic interfaces. Limnol Oceanogr 46: 2073-2080

Hannides, AK, Dunn SM; Aller RC (2005) Diffusion of organic and inorganic solutes through macrofaunal mucus secretions and tube linings in marine sediments. J Mar Res 63: 957-981

Hansen K, Kristensen E, (1997) Impact of macrofaunal recolonization on benthic metabolism and nutrient fluxes in a shallow marine sediment previously overgrown with macroalgal mats. Estuar Coas Shelf Science 45: 613-628

Henriksen K, Rasmussen MB, Jensen A (1983) Effect of bioturbation on microbial nitrogen transformation in the sediment and fluxes of ammonium and nitrate to the overlying water. Ecol. Bull. 35: 193-205

Holst G, Grunwald B (2001) Luminescence lifetime imaging with transparent oxygen optodes. Sens Act B 74: 78-90

Holst G, Kohls O, Klimant I, König B, Kühl M, Richter T (1998) A modular luminescence lifetime imaging system for mapping oxygen distribution in biological samples. Sens Act B 51: 163-170

Holst G, Grunwald B, Klimant I, Kühl M (1999) A luminescent lifetime imaging system using imaging fibres to measure the 2D distribution of O2 in biological samples. Proc SPIE 3860:154-163

Hulth S, Aller RC, Engström P, Selander E (2002) A pH plate fluorosensor (optode) for early diagenetic studies of marine sediments. Limnol Ocenaogr 47: 212-220

Kautsky H (1938) Quenching of luminescence by oxygen. Faraday Soc 35: 216-219

Klimant I (1993) Entwicklung optischer Sauerstoffsensoren auf der Basis luminiezierender Übergangsmetallkomplexe, PhD thesis, Universitiy of Graz, Austria

Klimant I, Meyer V, Kühl M (1995) Fibre-optic oxygen microsensors, a new tool in aquatic biology. Limnol Oceanogr 40: 1159-1165

Kristensen E (1983a) Ventilation and oxygen uptake by three species of Nereis (Annelida: Polychaeta). I. Effects of hypoxia. Mar Ecol Progr Ser 12: 289-297

Kristensen E (1983b) Ventilation and oxygen uptake by three species of Nereis (Annelida: Polychaeta). II. Effects of temperature and salinity changes. Mar Ecol Progr Ser 12: 299-306

Kristensen E (1988) Factors influencing the distribution of Nereid polychaetes in Danish coastal waters. Ophelia 29: 127-140

Kristensen E (2000) Organic matter diagenesis at the oxic/anoxic interface in coastal marine sediments, with emphasis on the role of burrowing animals. Hydrobiologia 426: 1-24

König B, Kohl O, Holst G, Glud, RN, Kühl M (2005) Fabrication and test of sol-gel based planar oxygen optodes for use in aquatic sediments. Marine Chemistry 97: 262-276

LaBarbera M, Vogel S (1976) An inexpensive thermistor flowmeter for aquatic biology. Limnol Oceanogr 21: 750-756

Li YH, Gregory S (1974) Diffusion of ions in sea water and in deep-sea sediments. Geochim Cosmochim Acta 38: 703-714

Miron G, Kristensen E (1993) Factors influencing the distribution of Nereid polychaetes: the sulfide aspect. Mar Ecol Prog Ser 93:143-153

Nielsen AM, Eriksen NT, Iversen JJL, Riisgard HU (1995) Feeding, growth and respiration in the polychaetes Nereis diversicolor (facultative filter-feeder) and N. virens (omnivorous) – a comparative study. Mar Ecol Prog Ser 125: 149-158

Nilsson HC, Rosenberg R (2000) Succession in marine benthic habitats and fauna in response to oxygen deficiency: analyzed by sediment profiling-imaging and grab samples. Mar Ecol Progr Ser 197: 139-149

Polerecky L, Franke U, Werner U, Grunwald B, de Beer D (2005) High spatial resolutions measurements of oxygen consumption rates in permeable sediments. Limnol Oceanogr Meth 3:75-85

Polerecky L, Volkenborn N, Stief P (2006) High temporal resolution oxygen imaging in bioirrigated sediments. Environ Sci & Technol 40: 5763-5769

Revsbech NP (1989). An oxygen microelectrode with a guard cathode. Limnol Oceanogr 34:474-478

Rhoads DC, Germano JD (1982) Characterization of organism-sediment relations using sediment profile imaging: an efficient method of remote ecological

monitoring of the seafloor (RemotsTM systems). Mar Ecol Progr Ser 8: 115-128

Riisgaard HU (1991) Suspension feeding in the polychaete Nereis diversicolor. Mar Ecol Progr Ser 70: 29-37

Riisgaard HU, Poulsen L, Larsen PS (1996) Phytoplankton reduction in near-bottom water caused by filter-feeding Hediste diversicolor: implications for worm growth and population grazing impact. Mar Ecol Progr Ser 141: 47-54

Rosenberg R, Davey E, Gunnarsson J, Norling K, Frank M (2007) Application of computer-aided tomography to visualize and quantify biogenic structures in marine sediments. Mar Ecol Progr Ser 331: 23-34

Rysgaard S, Christensen PB, Nielsen LP (1995) Seasonal variation in nitrification and denitrification in estuarine sediment colonized by benthic microalgae and bioturbation infauna. Mar Ecol Progr Ser 126: 11-21

Stern O, Volmer M (1919) Über die Abklingzeit der Fluoreszenz. Physik. Zeitschr. 20: 183-188

Stahl H, Glud A, Schröder CR, Klimant I, Tengberg, A, Glud RN (2006) Time-resolved pH imaging in marine sediments with a luminescent planar optode. Limnol Oceanogr Methods 4: 336-345

Tang M, Kristenesen E (in press) Impact of microphytobenthos and macrofauna on temporal variation of benthic metabolism in shallow coastal sediments.

Thede H, Scahudinn J, Saffe F (1973) Ecophysiological studies on four Nereis species of the Kiel Bay. Oikos 15: 246-252

Timmerman K, Banta GT, Glud RN (2006) Linking Arenicola marina irrigation behavior to oxygen transport and dynamics in sandy sediments. Jour Mar Res 64: 915-938

Ullman WJ, Aller RC (1982) Diffusion coefficients in near shore marine sediments. Limnol Oceanogr 27: 552-556

Vedel A (1998) Phytoplankton depletion in the benthic boundary layer caused by suspension-feeding Nereis diversicolor (Polychaeta): grazing impact and effect of temperature. Mar Ecol Progr Ser 163: 125-132

Wells GP, Dales RP (1951) Spontaneous activity patterns in animal behavior: the irrigation of the burrow in the polychaetes Chaetopterus variopedatus Renier and Nereis diversicolor O.F. Müller. J Mar Biol Ass UK 29: 661-680

Wenzhöfer F, Glud RN (2004) Small-scale spatial and temporal variability in coastal benthic O2 dynamics: Effects of fauna activity Limnol Oceanogr 49: 1471-1481

Yingst JY, Rhoads DC (1980) The role of bioturbation in the enhancement of microbial turnover rates in marine sediments, In Tenore KR, Coull BC (eds) Marine Benthic Dynamics. Univ South Carolina Press, p 407-422

Zhu, Q, Aller RC, Fan Y (2006) A new ratiometric, planar fluorosensor for measuring high resolution, two-dimensional pCO_2 distributions in marine sediments. Marine Chemistry 101: 40-53

Chapter 6

6. Summary

First, the technical developments of sensors, camera systems and applications of the imaging techniques were reviewed. Since the first more primitive approaches, more sophisticated systems have been developed, in which both fluorescence intensity and fluorescence lifetime imaging was possible in one as well as two dimensions (planar optodes). The oxygen distributions were visualized by the use of planar sensor foils with an oxygen sensitive fluorophore layer, containing a photostable ruthenium complex, that was reversibly quenched by oxygen. The planar optodes were fabricated of organically modified sol-gel (ORMOSIL). All sensor foils were based on the use of ruthenium(II)-tris-(4,7-diphenyl-1,10-phenantrolin)-perchlorate, which was a fluorescent dye quenched dynamically by oxygen. Sensors made with different sol-gel immobilization matrices, different concentrations of precursors and indicator dye, as well as different types of scattering particles co-immobilized in the sensor foil were investigated systematically. Optimal sensor performance was obtained with dye concentrations of 2-10 mmol/kg in an immobilization matrix made of diphenyldiethoxy-silan and phenyltriethoxy-silan precursors with addition of organically coated TiO_2 particles. The sensors exhibited a good mechanical stability and a high sensitivity from 0 to 100% oxygen, which remained constant over at least 36 days.

The recording system was optimized for modular luminescence lifetime imaging (MOLLI). The central parts of the system were a CCD-camera with a fast electronic shutter and gated LED (light emitting diode) or Xe excitation light sources. A personal computer controlled the gating and image acquisition via a pulse delay generator.

The planar optodes were used to investigate 2-dimensional O_2 dynamics in burrow systems inhabited by *Hediste diversicolor.* Natural burrows often deviated

from the classic U-shape and changed over time. This complicated quantitative assessment of the O_2 dynamics of the burrow. Therefore, a stable U-shaped burrow was established surrounded by agar-solidified sediment. Visual inspection and measured ventilation patterns indicated similar behavior of polychaetes in natural and artificial systems. The volume specific O_2 consumption, R_P, along the primary interface in the two systems were identical. Planar optode and microelectrode measurements gave similar results along the primary sediment-water interface. The radial diffusion of O_2 around a burrow was disturbed by the presence of the planar optode directly attached to the burrow wall causing an enhanced oxygen penetration depth compared to the undisturbed system. With the known geometry of the burrow system the effect could be corrected. Microbial colonization along the burrow lining increased the volume specific O_2 consumption, R_B, from 3.8$\pm$0.5 to 13.7$\pm$2.1 mol m^{-3} d^{-1} within two days reflecting that the burrow lining of *H. diversicolor* acts as a zone of intensified diagenetic activity. Extrapolated to natural densities in coastal sediments (600 m^{-2}) the findings indicate that 88 % of the benthic O_2 uptake is associated to worm burrows and that the major fraction hereof (66 %) is related to microbial activity in the burrow lining, while 22 % can be ascribed to fauna respiration.

Chapter 7

7. List of publications

Contributions of (co-)authors to the manuscripts presented in this thesis

Imaging of oxygen distributions at benthic interfaces: A brief review

B. König, G. Holst, R. N. Glud, and M. Kühl

Concept by B. König, R. N. Glud and M. Kühl, preparation of planar optodes and measurements by B. König with assistance of G. Holst, writing of manuscript by B. König with editorial help of R. Glud.

Fabrication and test of sol-gel based planar oxygen optodes for use in aquatic sediments

B. König, O. Kohls, G. Holst and M. Kühl

Concept by B. König, O. Kohls, and M. Kühl, preparation of planar optodes and measurements by B. König with assistance of G. Holst, writing of manuscript by B. König with editorial help of M. Kühl.

A modular luminescent lifetime imaging system for mapping oxygen distribution in biological samples

G. Holst, O. Kohls, I. Klimant, B. König, M. Kühl, T. Richter

Concept by G. Holst, B. König, M. Kühl, and T. Richter, preparation of optodes by B. König, I. Klimant, and O. Kohls measurements by G. Holst and T. Richter with assistance of B. König, writing of manuscript by G. Holst.

Behavior and associated benthic oxygen dynamics in artificial burrow systems of *H. diversicolor*

B. König, M. Kühl, R. N. Glud

Concept by B. König, R. N. Glud, and M. Kühl, preparation of planar optodes and measurements by B. König, writing of manuscript by B. König with editorial help of R. N. Glud and M. Kühl.

Paper not included in this thesis

Earth life support for aquatic organisms, system and technical aspects

B. König, M. Dünne and K. Slenzka

Concept by B. König, and K. Slenzka, preparation of planar optodes and measurements by B. König supported by M. Dünne, writing of manuscript by B. König with editorial help of K. Slenzka.

Danksagung

Mein erster Dank gilt Prof. Bo Barker Jørgensen für die Begutachtung dieser Arbeit. Sein Engagement hat wesentlich zum Gelingen dieser Arbeit beigetragen. Ganz herzlich möchte ich mich bei meinen Betreuern Michael Kühl und Ronnie N. Glud bedanken, die über die ganzen Jahre nicht müde wurden mich mit Rat und Diskussion zu unterstützen und mir gleichzeitig viel Freiraum in der Durchführung meiner Promotionsarbeit ließen. Besonders danke ich ihnen für ihre Unterstützung in der Fertigstellung dieser Arbeit. Außerdem möchte ich mich bei Oliver Kohls und Gerhard Holst für die freundliche Aufnahme in die 'Optoden Arbeitsgruppe' bedanken.
Für die freundliche und herzliche Atmosphäre in der Mikrosensorgruppe am Max-Planck Institut Bremen und am Marine Biological Laboratory in Helsingør danke ich allen, die in dieser Zeit dazu beigetragen haben. Besonders bedanken möchte ich mich bei meinen ehemaligen Kollegen am MPI Frank Wenzhöfer und Andrea Wieland, die für anhaltend gute Laune gesorgt haben; in Helsingør bei Roland Thar für die tollen Diskussionen, bei Anni Glud und N. Blackburn die mir immer mit einem guten Rat zur Seite standen.
In der Endphase dieser Arbeit waren es meine Arbeitskollegen bei OHB, insbesondere aber Oliver Romberg, der mit beharrlichen Ermunterungen dafür gesorgt hat, dass ich diese Arbeit doch noch zu Ende gebracht habe.
Ein herzliches Dankeschön geht an meinen Bruder Matthias und an all die lieben Menschen, die mit guter Laune, Geduld und Trost für die notwendige Ablenkung und Unterstützung gesorgt haben.
Diese Arbeit wäre ohne die wunderbare Unterstützung und die Geduld meiner Eltern in den Jahren des Studiums und bis heute nicht möglich gewesen. Dafür möchte ich auch euch von Herzen Danke sagen!